



CZECH TECHNICAL UNIVERSITY IN PRAGUE

Faculty of Civil Engineering

Department of Mechanics

Modular-Topology Optimization of Truss Structures Composed of Wang Tiles

Modulárně-topologická optimalizace příhradových konstrukcí tvořených Wangovými dlaždicemi

Diploma Thesis

Study Program:	Civil Engineering
Branch of Study:	Building Structures
Supervisor:	Dr. Jan Zeman

Marek Tyburec

Prague 2017



ZADÁNÍ DIPLOMOVÉ PRÁCE

I. OSOBNÍ A STUDIJNÍ ÚDAJE

Příjmení: Tyburec

Jméno: Marek

Osobní číslo: 396 479

Zadávací katedra: Katedra mechaniky

Studijní program: Stavební inženýrství

Studijní obor: Konstrukce pozemních staveb

II. ÚDAJE K DIPLOMOVÉ PRÁCI

Název diplomové práce: Modulárně-topologická optimalizace příhradových konstrukcí tvořených Wangovými dlaždicemi

Název diplomové práce anglicky: Modular-topology optimization of truss structures composed of Wang tiles

Pokyny pro vypracování:

V rámci diplomové práce se student seznámí s postupy a metodami topologické optimalizace příhradových konstrukcí. Ty následně rozšíří na návrh konstrukcí, které se skládají z omezeného počtu modulů, provede implementaci výsledného algoritmu pro rovinné příhrady, a využije ho na řešení vybraných typových úloh. Vlastní parametrizace návrhu bude založena na teorii neperiodických Wangových dlažďení.

Seznam doporučené literatury:


- [1] M. P. BENDSOE AND O. SIGMUND, Topology optimization: Theory, methods and applications, Springer-Verlag, Berlin, Heidelberg, second ed., 2003.
- [2] A. LAGAE AND P. DUTRÉ, An alternative for Wang tiles: Colored edges versus colored corners, ACM Transactions on Graphics, 25 (2006), pp. 1442–1459.
- [3] A. TUGILIMANA, A. P. THRALL, B. DESCAMPS, AND R. F. COELHO, Spatial orientation and topology optimization of modular trusses, Structural and Multidisciplinary Optimization, (2016), pp. 1–18. doi:10.1007/s00158-016-1501-7.

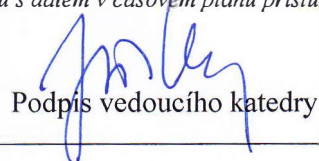
Jméno vedoucího diplomové práce: Jan Zeman

Datum zadání diplomové práce: 5.10.2016

Termín odevzdání diplomové práce: 8.1.2017

Údaj uveďte v souladu s datem v časovém plánu příslušného ak. roku


Podpis vedoucího práce


Podpis vedoucího katedry

III. PŘEVZETÍ ZADÁNÍ

Beru na vědomí, že jsem povinen vypracovat diplomovou práci samostatně, bez cizí pomoci, s výjimkou poskytnutých konzultací. Seznam použité literatury, jiných pramenů a jmen konzultantů je nutné uvést v diplomové práci a při citování postupovat v souladu s metodickou příručkou ČVUT „Jak psát vysokoškolské závěrečné práce“ a metodickým pokynem ČVUT „O dodržování etických principů při přípravě vysokoškolských závěrečných prací“.

5. 10. 2016

Datum převzetí zadání


Podpis studenta(ky)

SPECIFIKACE ZADÁNÍ

Jméno diplomanta: Marek Tyburec

Název diplomové práce: Modulárně-topologická optimalizace příhradových konstrukcí tvořených Wangovými dlaždicemi

Základní část: Modulárně-topologická optimalizace podíl: 100 %

Formulace úkolů: V rámci diplomové práce se student seznámí s postupy a metodami topologické optimalizace příhradových konstrukcí. Ty následně rozšíří na návrh konstrukcí, které se skládají z omezeného počtu modulů, provede implementaci výsledného algoritmu pro rovinné příhrady a využije ho na řešení vybraných typových úloh. Vlastní parametrizace návrhu bude založena na teorii neperiodických Wangových dlaždění.

Podpis vedoucího DP: 

Datum: 20.12.2016

Případné další části diplomové práce (části a jejich podíl určí vedoucí DP):

2. Část: _____ podíl: _____ %

Konzultant (jméno, katedra): _____

Formulace úkolů: _____

Podpis konzultanta: _____

Datum: _____

3. Část: _____ podíl: _____ %

Konzultant (jméno, katedra): _____

Formulace úkolů: _____

Podpis konzultanta: _____

Datum: _____

4. Část: _____ podíl: _____ %

Konzultant (jméno, katedra): _____

Formulace úkolů: _____

Podpis konzultanta: _____

Datum: _____

Poznámka: Zadání včetně vyplněných specifikací je nedílnou součástí diplomové práce a musí být přiloženo k odevzdané práci (vyplněné specifikace není nutné odevzdat na studijní oddělení spolu s 1.stranou zadání již ve 2.týdnu semestru)

Abstract

Despite vivid interest of researchers, fueled further by recent advances in additive manufacturing, efficient handling of structural modularity remains an unresolved topic in topology optimization. This master thesis presents a unifying bilvel optimization framework that allows for simultaneous optimization of modules topology and their distribution within a structure. The approach combines topology optimization of truss structures, which identifies the optimal distribution of a material within a predefined ground structure, and the formalism of vertex-based Wang tiles, which naturally introduces jigsaw-like compatibility of individual modules and allows for straightforward generation of a compatible assembly plan.

The topology optimization, suitably modified to account for modularity constraints, determines the globally optimal design of the modules for a given assembly plan, while either simulated annealing or the genetic algorithm is used to arrive at the optimal assembly plan. The approach thus couples mathematical programming, namely Second-Order Cone Programming or Semidefinite Programming, with meta-heuristics.

The developed methodology is applied to an illustrative problem of compliance minimization of a simply supported beam and the influence of module size is discussed. The optimal design of modular truss structures can be also seen, in a broader perspective, as a preliminary step to optimal design of non-periodic microstructures, approximated by truss members.

Keywords

Truss Topology Optimization, Modular-Topology Optimization, Assembly Plan Optimization, Bilevel Optimization, Wang tiles, Non-Periodic Microstructures, Mathematical Programming, Meta-Heuristics, Finite Element Method

Abstrakt

I přes značnou pozornost, umocněnou v posledních letech významným rozšířením aditivní výroby, zůstává problém topologické optimalizace modulárních konstrukcí nedostatečně vyřešen. Diplomová práce přispívá k jeho řešení návrhem dvouúrovňové optimalizace, která zároveň řeší optimální topologii jednotlivých modulů a jejich rozmístění v konstrukci. Celý přístup využívá standardní topologické optimalizace příhradových konstrukcí, sloužící jako nástroj pro nalezení optimálního rozložení materiálu v rámci zadané podkladové konstrukce, a formalismu vrcholově definovaných Wangových dlaždic, které umožňují přirozeně formulovat požadavky vzájemné kompatibility jednotlivých modulů, a tím umožňují snadno vytvářet kompatibilní skladebné plány.

Topologická optimalizace, která je upravena tak, aby umožnila zahrnout omezení vyplývající z požadavků kompatibility modulů, je v rámci dvouúrovňové optimalizace použita k návrhu topologie jednotlivých modulů, zatímco nalezení optimálního skladebného plánu je řešeno pomocí simulovaného žíhání a genetického algoritmu. Předkládaný přístup tak kombinuje postupy matematického programování, konkrétně kónické programování druhého řádu nebo semidefinitní programování, a meta-heuristické postupy.

Uvedený postup je aplikován na ilustrativní příklad minimalizace poddajnosti prostě podepřeného příhradového nosníku, u kterého je dále řešena i otázka vlivu velikosti jednotlivých modulů. Vyvinutý postup však není omezen pouze na návrh modulárních příhradových konstrukcí, v širším smyslu jej lze chápat jako optimalizaci neperiodické mikrostruktury materiálu, která je v tomto případě modelována příhradovou konstrukcí.

Klíčová slova

Topologická optimalizace příhradových konstrukcí, Modulárně-topologická optimalizace, Optimalizace skladebného plánu, Dvouúrovňová optimalizace, Wangovo dláždění, Neperiodické mikrostruktury, Matematické programování, Meta-heuristika, Metoda konečných prvků

Statutory Declaration

Herewith I declare that I have written the enclosed master thesis *Modular-Topology Optimization of Truss Structures Composed of Wang Tiles* entirely by myself under professional supervision of Dr. Jan Zeman. I also declare that all used bibliography and data are cited and referenced.

Prague, January 2017

Marek Tyburec

Acknowledgement

First, I would like to express my sincere gratitude to Dr. Jan Zeman for introducing me into such an interesting area of research, and for giving me the opportunity to work under his professional supervision. I also greatly appreciate his friendly approach and several fruitful discussions on the topic we had.

I further extend my sincere thanks to Martin Doškář for introduction to Wang tiling and for providing numerous remarks and comments regarding this thesis. I would also like to acknowledge Dr. Matěj Lepš for his comments and advice concerning the genetic algorithm and the numerical examples. Additionally, I wish to express my gratitude to Dr. Jan Novák and to Dr. Anna Kučerová for providing valuable feedback.

I also sincerely thank to Professor Michal Kočvara from University of Birmingham for his kind introduction to the second-order cone programming and for providing sample codes for conic topology optimization.

Last, I would like to give special thanks to my family, especially to my wife and son, whose patience and love made it possible to accomplish this thesis in the present form.

The author acknowledges financial support from Czech Science Foundation, through project No. 14-00420S, and from Grant Agency of CTU in Prague, through project No. SGS16/037/OHK1/1T/11.

Contents

List of Figures	ix
List of Tables	xi
Nomenclature	xii
1 Introduction	1
1.1 Optimal Design of Modular Truss Structures	1
1.2 Topology Optimization of Microstructures	2
1.3 Objectives and Methodology	2
2 Wang Tiles	3
2.1 Fundamental Terminology	3
2.2 Concept of Wang Tiles	4
2.2.1 Aperiodic Tile Sets	5
2.2.2 Applications of Wang Tiles	5
2.3 Vertex-Based Wang Tiles	6
3 Solution of Trusses by Finite Element Method	8
3.1 A Brief Historical Overview	8
3.2 Problem Statement	9
3.3 Derivation of Truss Element Equations	10
3.3.1 Direct Equilibrium	12
3.3.2 Minimum to the Potential Energy Functional	12
3.4 Transformation to Plane Trusses	16
3.5 Truss Element Equations Assembly	19
3.6 Solution to the Truss Equations	20
3.6.1 Equilibrium Equation	20
3.6.2 Minimum to the Potential Energy Function	20
4 Topology Optimization of Truss Structures	21
4.1 Historical Background	22
4.2 Formulations For Truss Topology Optimization	23
4.2.1 Quadratic Programming Formulation	24
4.2.2 Linear Programming Formulation	26
4.2.3 Second-Order Cone Programming Formulation	28
4.2.4 Semidefinite Programming Formulation	29
5 Extension of Topology Optimization to Modular Trusses	32
5.1 Group Vector and Group Matrix	32
5.1.1 Illustrative Example	33

5.2	Complex Modules	34
5.2.1	Structural Modularity Using Wang Tiles	34
5.3	Generalization of Topology Optimization Formulations	35
5.3.1	Second-Order Cone Programming	35
5.3.2	Semidefinite Programming	36
6	Modular-Topology Optimization	37
6.1	Minimum Compliance Problem Statement	37
6.1.1	Bounds on the Global Optimum	38
6.2	Meta-Heuristic Algorithms	39
6.2.1	Simulated Annealing	39
6.2.2	Genetic Algorithm	40
7	Results	44
7.1	Coarsely Discretized Beam	44
7.1.1	Bounds on the Globally Optimal Compliance	45
7.1.2	Brute-Force Enumeration	45
7.1.3	Bilevel Optimization	46
7.1.4	Relations Between Connectivity Matrix and Design Quality	48
7.2	Finely Discretized Beam	49
7.2.1	Bilevel Optimization	50
8	Summary	53
8.1	Directions For Future Research	54

List of Figures

2.1	Example tiling	3
2.2	Difference between periodic and aperiodic tiling	4
2.3	The complete set of edge-based Wang tiles over two colors	4
2.4	Connectivity information, valid and invalid edge-based Wang tiling	4
2.5	Stochastically generated microstructure of compacted graphite iron	6
2.6	Equivalence of the complete set of vertex-based Wang tiles over two colors with a specific set of edge-based Wang tiles over four colors	7
2.7	Connectivity matrix, valid and invalid vertex-based Wang tiling	7
3.1	Displacement of the truss element	9
3.2	Boundary conditions of the truss element	10
3.3	Linear shape functions of the truss element	11
3.4	Normal stresses in an infinitesimally small section of truss element	13
3.5	In-plane truss element	16
3.6	Transformation of displacements in 2D	16
4.1	Examples of topology and shape optimization	21
4.2	An example of Michell's structure	22
4.3	Fully connected ground structure	22
5.1	Modular truss structure composed of three bars	33
5.2	Partitioning of design domain into modules, associations sets and bars	34
5.3	Division of bars into tile-associated and edge-associated sets	35
6.1	Sample cross-over realisation	42
6.2	Sample mutation realization	43
7.1	Dimensions, discretization, boundary conditions, and ground structure of the coarsely discretized beam	44
7.2	Lower-bound and upper-bound solutions of the coarsely discretized beam	45
7.3	Globally optimal design and the corresponding tile set of the coarsely discretized beam	46
7.4	Distribution of optimal compliances of all the enumerated combinations and of 50 independent runs of the bilevel optimization for the coarsely discretized beam	46
7.5	Convergence of 50 independent runs of the simulated annealing algorithm for the coarsely discretized beam	47
7.6	Convergence of 50 independent runs of the genetic algorithm for the coarsely discretized beam	48
7.7	The best design of the coarsely discretized beam obtained through the genetic algorithm	48

7.8	Compliance as a functional of the number of nonzero elements in symmetric part of \mathbf{C} of the coarsely discretized beam	49
7.9	Compliance as a functional of the number of utilized tiles in the coarsely discretized beam	49
7.10	Dimensions, discretization, boundary conditions, and ground structure of the finely discretized beam	50
7.11	Lower-bound and upper-bound solutions of the finely discretized beam . . .	50
7.12	Convergence of 20 independent runs of modular-topology optimization of the finely discretized beam using simulated annealing	51
7.13	The best design of the finely discretized beam obtained through simulated annealing	51
7.14	The best design of the finely discretized beam obtained through genetic algorithm	51
7.15	Convergence of the best individuals from 20 independent runs of modular-topology optimization of the finely discretized beam using genetic algorithm	52
7.16	Distribution of obtained approximate solutions to the bilevel optimization within 20 independent random runs	52

List of Tables

6.1	Equivalence in terminology of mathematical programming, simulated annealing, and genetic algorithm	39
7.1	Comparison of bilevel optimization approaches for the coarsely discretized beam	48
7.2	Comparison of bilevel optimization approaches for the finely discretized beam	52

Nomenclature

α	Upper bound on the specific strain energy
α^*	Optimal upper bound on the specific strain energy
β	Arbitrary nonzero scalar
ℓ	Column vector containing bar lengths
γ_i	Column vector expressing geometric relation between axial and nodal forces of the i -th bar in global coordinates
μ^*	Column vector of optimal multipliers
τ	Column vector of contribution of individual bars to compliance
ΔE	Energy difference
δ	Current generation number
ℓ_i	Length of the i -th bar
$\hat{\gamma}_i$	Column vector expressing geometric relation between axial and nodal forces of i -th bar in local coordinates
$\hat{\mathbf{f}}^i$	Nodal forces column vector of the i -th bar in local coordinates
$\hat{\mathbf{K}}^i$	Stiffness matrix of the i -th bar in local coordinates
$\hat{\mathbf{u}}^i$	Displacement column vector in local coordinates corresponding to the i -th bar
$\hat{\mathbf{u}}_{\text{KA}}^i$	Kinematically admissible displacements of the i -th bar
\hat{x}_i	Longitudinal axis of the i -th bar
\hat{y}_i	Local axis of the i -th bar, orthogonal to \hat{x}_i
\hat{z}_i	Local axis of the i -th bar, orthogonal to \hat{x}_i
$\bar{\mathbf{f}}$	Column vector of prescribed forces
$\bar{\mathbf{u}}$	Column vector of prescribed displacements
\mathbf{A}	Static matrix
\mathbf{a}	Column vector of cross-sectional areas
\mathbf{a}^*	(Globally) optimal column vector of cross-sectional areas
\mathbf{a}_g	Column vector of unique cross-sectional areas
\mathbf{a}_g^*	Globally optimal column vector of unique cross-sectional areas
\mathbf{B}^i	Strain-displacement matrix of the i -th bar
\mathbf{C}	Connectivity matrix
\mathbf{C}^*	Globally optimal connectivity matrix

\mathbf{C}_T	Trial connectivity matrix
$\mathbf{C}_{e_r, \zeta}$	e_r, ζ -th element of the connectivity matrix \mathbf{C}
\mathbf{e}_r	Vector of random indices
\mathbf{f}	Nodal forces column vector
\mathbf{f}^i	Column vector of nodal forces corresponding to the i -th bar in global coordinates
\mathbf{f}_R	Column vector of unknown forces
\mathbf{f}_S	Column vector of all nodal forces
\mathbf{G}	Group matrix
\mathbf{g}	Group vector
$\mathbf{G}_{i,j}$	i -th row and j -th column of the group matrix
\mathbf{K}	Stiffness matrix
\mathbf{K}^i	Stiffness matrix of the i -th bar in global coordinates
\mathbf{K}_S	Structural stiffness matrix
\mathbf{N}^i	Shape function matrix corresponding to the i -th bar
\mathbf{s}	Column vector of axial forces
\mathbf{s}^+	Column vector of tensional axial forces
\mathbf{s}^-	Column vector of compressional axial forces
\mathbf{u}	Column vector of unknown displacements
\mathbf{u}^*	(Globally) optimal column vector of displacements
\mathbf{u}^i	Column vector of displacements corresponding to the i -th bar in global coordinates
\mathbf{u}_S	Column vector of all displacements
\mathbf{v}	Arbitrary nonzero vector
\mathbf{w}	Arbitrary nonzero vector
\mathcal{D}	Design domain
\mathcal{T}	Tile
μ_i^*	Optimal multiplier corresponding to the i -th bar
$\bar{\sigma}_i$	Bound on admissible longitudinal stress in the i -th bar
\bar{c}	Upper bound on structural compliance
$\overline{f_{\hat{x}_i}}(\hat{x}_i)$	Distributed loading in the i -th bar along axis \hat{x}_i
$\bar{F}_{k, \hat{x}}$	External force in node \textcircled{k} acting in the direction of \hat{x}
$\bar{F}_{k, \hat{y}}$	External force in node \textcircled{k} acting in the direction of \hat{y}
$\bar{F}_{k, x}$	External force in node \textcircled{k} acting in the direction of x
$\bar{F}_{k, y}$	External force in node \textcircled{k} acting in the direction of y
$\bar{u}_{k, \hat{x}}$	Prescribed displacement of node \textcircled{k} in the direction of \hat{x}_i
$\bar{u}_{k, \hat{y}}$	Prescribed displacement of node \textcircled{k} in the direction of \hat{y}_i
\bar{V}	Upper bound on structural volume

Π	Total potential energy
Π_i	Potential energy of the i -th bar
\mathcal{T}	Vector of tiles forming tile set
σ_i	Longitudinal stress within the i -th bar
τ	Doubled compliance
τ_i	Contribution of the i -th bar to compliance
θ_i	Angle between x and \hat{x}_i corresponding to the i -th bar
ε_i	Longitudinal strain of the i -th bar
a_i	Cross-sectional area of the i -th bar
$a_{\mathbf{g},g_i}$	g_i -th element of the vector $\mathbf{a}_{\mathbf{g}}$
$a_{\mathbf{g},j}$	j -th element of the vector $\mathbf{a}_{\mathbf{g}}$
$a_{\min,i}$	Cross-sectional area of the i -th bar corresponding to fully-stressed design
c	Compliance
c^*	Globally optimal compliance
c_{AI}	Anti-ideal compliance
c_{I}	Ideal compliance
c_i	Compliance of the i -th truss element
E	Energy
E_i	Modulus of elasticity of the i -th bar
$e_{\mathbf{r},\zeta}$	ζ -th element of the vector $\mathbf{e}_{\mathbf{r}}$
g_i	g_i -th element of the group vector \mathbf{g}
i	i -th bar
i_{nd}	Rank of an individual to become winner of tournament
i_{ter}	Current iteration number
j	j -th group of unique cross-sectional areas
k	k -th node
n_{b}	Number of bars
n_{c}	Tournament size
n_{dof}	Number of degrees of freedom
n_{gen}	Number of generations
n_{g}	Number of groups, equiv. number of unique cross-sectional areas
n_{lc}	Number of loading conditions
n_{n}	Number of nodes
n_{pop}	Population size
n_{S}	Number of steps within a fixed temperature
n_{T}	Number of temperatures

n_t	Number of tiles in tile set
N_k^i	Shape function of the i -th bar corresponding to the node \textcircled{k}
$n_{t,x}$	Number of tiles in horizontal direction
$n_{t,y}$	Number of tiles in vertical direction
n_{e_r}	Number of elements in \mathbf{e}_r
P	Probability
P_c	Cross-over probability
P_m	Mutation probability
P_t	Tournament probability
s_i^+	Tensional axial force of the i -th bar
s_i^-	Compressional axial force of the i -th bar
s_i	Internal axial force in the i -th bar
T	Temperature
t	Current temperature number
T^i	Transformation matrix of the i -th bar
T_0	Initial temperature
U_i	Internal elastic strain energy of the i -th bar
$u_{\hat{x}_i}(\hat{x}_i)$	Deformation function of the i -th bar along axis \hat{x}_i
$u_{\hat{x}_i}^i(\hat{x}_i)$	Approximate displacement function of the i -th bar along axis \hat{x}_i
u_{k,\hat{x}_i}	Displacement of the node \textcircled{k} in the direction of local axis \hat{x}_i
u_{k,\hat{y}_i}	Displacement of the node \textcircled{k} in the direction of local axis \hat{y}_i
$u_{k,x}$	Displacement of the node \textcircled{k} in the direction of global axis x
$u_{k,y}$	Displacement of the node \textcircled{k} in the direction of global axis y
V_i	Volume of the i -th bar
W_i	Potential energy of external forces corresponding to the i -th bar
x	Global axis
y	Global axis

Chapter 1

Introduction

Finding optimal structures has been a challenging task attracting the interest of many researchers since the turn of the 20th century (Culmann, 1875; Michell, 1904). A comprehensive overview of the most common approaches can be found in the excellent book by Bendsøe and Sigmund (2003). The so-called *structural optimization* commonly aims at achieving one of the following objectives: the structure of minimum weight, the stiffest structure, or the structure as insensitive to instability and buckling as possible (Christensen and Klarbring, 2009).

The objectives, albeit distinct, are all driven by investor's desire for increasing competitiveness of their products and expense savings. In this context, structural modularity is a significant ingredient, especially for mass production. Prefabricated modular products, produced off-site in high-tech facilities, are of superior quality (Mikkola, 2003) and contribute considerably to time savings by a parallel execution of the building phases (Tugilimana et al., 2016).

1.1 Optimal Design of Modular Truss Structures

This thesis focuses on the optimal design of modular truss structures. The *topology optimization* represents one of the most powerful methods for finding optimal distribution of material within truss structures. The approach builds on discretization of the continuous design space into the so-called ground structure (Dorn et al., 1964), defining so a set of feasible nodes and potential bars, in which the material is to be distributed. Typically, design variables of the topology optimization involve the cross-sectional areas of individual bars, allowing for vanishing of unnecessary members.

Modular truss structures contain two inherent levels of details: (i) the *element scale* at the level of individual bars and (ii) the *module scale* covering prefabricated building units, associating several bars into modules. The element scale has been extensively studied in the literature, either in its continuous (Bendsøe et al., 1991; Vandenberghe and Boyd, 1996; Lobo et al., 1998), or in the discrete (Stolpe, 2016) settings. The module scale was handled separately by Zawidzki and Nishinari (2012), who provided a framework for finding the optimal arrangement of modules in pedestrian network design.

We believe that the only study dealing with both the scales simultaneously is the recent article by Tugilimana et al. (2016), whose developed theory permits employment of a single rotatable module. To the best of our knowledge, the general settings of *modular-topology optimization*, allowing for concurrent optimization of topology and arrangement of a set of several modules, remains unresolved.

1.2 Topology Optimization of Microstructures

The problem of the two-scale design of modular trusses closely resembles to the widely studied problem of finding optimal material distribution within the structural *macro scale* subjected to the structural boundary conditions, while concurrently optimizing the design of microstructural cells that constitute the *micro scale*. Within the latter problem, a treatment similar to our can be traced in the work of Sigmund (1996), in which the material distribution within microstructural cells was approximated by truss members.

In the case of microstructures, the two scales are commonly separated due to excessive computational demands (Xia and Breitkopf, 2016) arising when the both levels are treated concurrently, which leads to the micro scale designs being tailored to a specific property (Bendsøe and Kikuchi, 1988) rather than a specific application (Alexandersen and Lazarov, 2015). The separated multi-scale model further lacks the ability to constrain mutual compatibility of adjacent microstructural cells (Alexandersen and Lazarov, 2015), hindering possible industrial applications.

In order to solve the stated mutual compatibility problem, several approaches were proposed. While some relied on post-processing of optimal microstructural cells by smoothening material distribution across the boundaries of adjoining cells (Radman et al., 2012), another made use of a periodic unit cell (Zhang and Sun, 2006), or layered microstructures (Alexandersen and Lazarov, 2015) to build periodic microstructural assemblies. Stromberg et al. (2010) introduced an approach based on gradation of a single microstructural cell along specified paths, leading to its stretching or extension, and, thus, offering more economical and manufacturable designs.

To our knowledge, all the present topology optimization approaches either directly involve microstructural periodicity or rely on fuzzy post-processing to produce manufacturable designs, hence, similarly to the topology optimization of truss structures, do not provide an exact procedure possibly leading to aperiodic materials composed of a limited set of distinct cells, clarifying the actual response of real-world materials (Alkhader and Vural, 2008).

1.3 Objectives and Methodology

In the outlined context the objectives of the thesis address the aforementioned limitations and insufficiently resolved problems of the two-scale modular optimization. The thesis presents an approach that couples topology optimization of a given set of truss modules, or equivalently truss microstructural cells, with a search for their optimal, possibly aperiodic, arrangement, while securing jigsaw-like compatibility of adjoining modules by adaptation of vertex-based Wang tiles (Lagae and Dutré, 2006).

The content of the thesis is structured as follows: The following three chapters review fundamentals of Wang tiling, finite element method, and topology optimization of truss structures, respectively. The stated theory is subsequently used for derivation of convex second-order cone and semidefinite programming formulations for the optimal least-compliant design of modular trusses with predefined assembly plans. The fifth chapter then generalizes both programs to develop bilevel optimization formulations, coupling meta-heuristic and mathematical programming, in order to take the compatibility constraints arising in the modular design into account. Finally, in the sixth chapter, meta-heuristics at the macro scale and the mathematical programming approach employed at the micro scale are coupled, allowing for simultaneous optimization of topology and assembly plan of individual modules. Implementation and applicability of the developed approach is illustrated with an example of simply supported beam in the penultimate chapter. The last chapter summarizes the thesis and outlines possible directions of future work.

Chapter 2

Wang Tiles

Since the birth of human civilization people have tended to create various forms of art, making their lives more pleasing. Therefore, it is impossible to state an exact date denoting the beginning of art. Tiling, one of its initial forms, are no exception (Grünbaum and Shephard, 1986), being used for tens of thousands of years. Tiling probably originated from the need to cover floors and walls of dwellings, palaces, and temples, making them more resistant to wear and climatic conditions. Initially, the first tiling were made of stone. As soon as people could choose from various shapes and colors, aesthetics was brought into focus, marking the onset of mosaics. The most famous examples of tiling can be found in Alhambra (Granada, Spain).

As the vast extent of commonly used tiling is beyond the scope and interest of this thesis, we will further focus on the Wang tiling, formed by squares with colored edges that allow for aperiodic assemblies. The following sections state the fundamental properties of Wang tiles, needed in the following chapters.

2.1 Fundamental Terminology

From the mathematical point of view, tiling can be described in the following way: Let us assume a closed set of $n_t \in \mathbb{Z}_{>0}$ planar tiles denoted by $\mathcal{T} = (\mathcal{T}_1 \dots \mathcal{T}_{n_t})$. Tiling is then a compatible¹ arrangement of the tiles from the set \mathcal{T} that allows for covering the Euclidean plane without gaps and overlaps, each tile being used arbitrary number of times. Example segments of tiling are shown in Fig. 2.1.

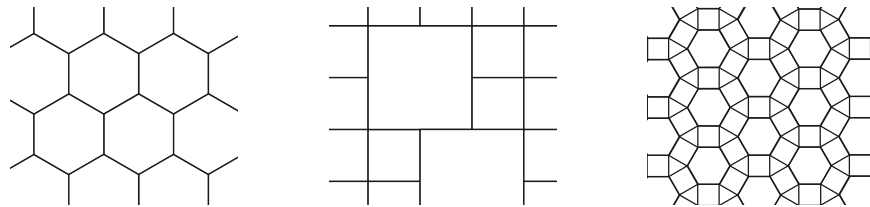


Figure 2.1: Example segments of tiling.

Tiling is said to be *periodic* if and only if there exists a region of the tiling that tiles an infinite plane by translations only in at least two independent directions, i.e. without rotations and reflections. If no such region exists, the tiling is referred to as *aperiodic*. For examples of both the categories, we refer to Fig. 2.2.

¹The compatibility condition is specific to the particular tiling. It can be conveniently represented by enforced color-continuity across neighboring tiles.

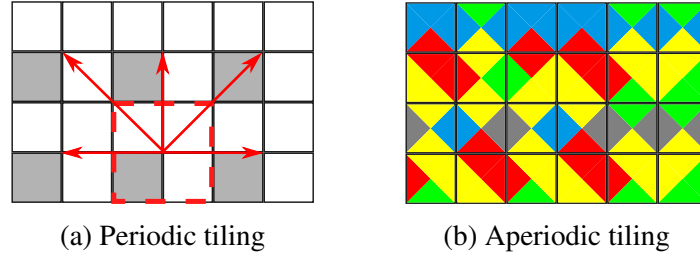


Figure 2.2: Difference between (a) periodic and (b) aperiodic tiling. Note that the tiling (b) adds the constraint that the adjoining edges of neighboring tiles must have the same color.

Further, *aperiodic tile sets* are such tile sets that allow only aperiodic tiling. Tile sets that allow for at least one periodic tiling are named *periodic tile sets*.

2.2 Concept of Wang Tiles

The idea of domino-like Wang tiles was introduced by and is named in honor of Wang (1961), who developed the idea as a tool for studying algorithmic decidability of the predicate calculus first-order-logical problem $\forall\exists\forall$ (Wang, 1962). He demonstrated that the logical problem is equivalent to the so-called *domino problem*: Assume a finite set of equal-sized squares with fixed rotations, later called Wang dominos or Wang tiles, whose edges are assigned specific colors, according to the specific $\forall\exists\forall$ problem. Example Wang tiles over two colors are shown in Fig. 2.3. The objective is then to cover an infinite plane with arbitrary number of copies of dominoes such that their adjoining edges share the same color, for illustration purposes refer to Fig. 2.4b. In the case of feasible objective, the domino problem is said to be solvable, unsolvable otherwise.

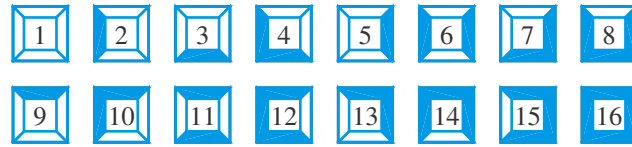


Figure 2.3: The complete set of Wang tiles over two colors.

Wang (1961) straightforwardly concluded in his *fundamental conjecture* that the domino problem is solvable if and only if there exists a rectangular region, such that both its horizontal and vertical edges are identical, respectively, i.e. the tile set being periodic and implying non-existence of the aperiodic tile sets.

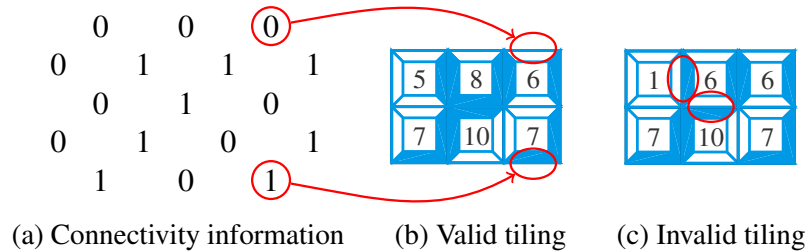


Figure 2.4: Illustration of: (a) connectivity information and its correspondence to valid tiling (b), (c) example of invalid tiling.

Kahr et al. (1962) demonstrated that the origin-constrained domino problem can be reduced to the Turing machine *halting problem* (Turing, 1936; Davis, 1958). Broadly speaking,

the problem consists in determining if an arbitrary algorithm with an arbitrary input will terminate in a finite number of steps. Turing (1936) proved that the halting problem has no solution, as a single Turing machine cannot answer the questions about all possible Turing machines, implying the machine would operate indefinitely. Despite being possible to design a single Turing machine for a specific tile set, halting only if the domino problem is unsolvable (Kahr et al., 1962), i.e. if the tiling does not cover an infinite plane, there is an infinite number of such sets, implying infinite number of the related Turing machines. Consequently, similarly to the halting problem, the domino problem is undecidable and there does not exist an algorithm for general solution to the domino problem in a finite number of steps.

Insolubility of the domino problem was also proved by Wang's student Berger (1966), further providing an aperiodic set of 20426 tiles, contrary to Wang's fundamental conjecture.

2.2.1 Aperiodic Tile Sets

Since Berger, who derived the first aperiodic sets composed of 20426 (Berger, 1966) and 104 (Berger, 1964) tiles, based on the principle of expanding squares (Grünbaum and Shephard, 1986), the size of the smallest aperiodic set gradually decreased. Following the same approach, Knuth (1968) proposed a set of 92 tiles. In 1966, Lauchli sent professor Wang an aperiodic set containing 40 tiles, however the set remained unpublished until (Wang, 1975). Meanwhile, Robinson (1967) found sets of 52 and 56 tiles (Robinson, 1971) and suggested an existence of a set of 35 tiles.

In 1973, following the discovery of a tiling composed of two types of rhombs, Roger Penrose developed even smaller aperiodic set containing 34 tiles. Cooperating with Penrose, Robinson found an aperiodic set of 32 tiles in 1973. A similar method was also used by Grünbaum and Shephard (1986) to produce a set of 24 tiles.

Based on the new approach of Ammann (Grünbaum and Shephard, 1986), Robinson additionally discovered a set of 24 tiles in 1977. In 1978 Ammann developed a set of only 16 tiles, firstly published in (Grünbaum and Shephard, 1986), and subsequently proved its aperiodicity in (Ammann et al., 1992).

Further reductions to the smallest aperiodic tile set waited until 1996, when Kari (1996) introduced a set of 14 tiles. His method was then adopted by Čulík (1996), leading to the tile set of 13 tiles. In 1997, Čulík and Kari (1997) brought up the idea the set of 13 tiles might contain one unnecessary tile and, therefore, there was a possible reduction to 12 tiles. However, they were able to support their observation only for cross bifinite tiling. Their suspicion was proven to be false by Jeandel and Rao (2015), who also presented two aperiodic sets containing 11 tiles over four colors and proved by enumeration that the sets are smallest feasible sets over 4 colors. Additionally, Chen et al. (2014) stated no aperiodic tile set is possible over less than 4 colors.

2.2.2 Applications of Wang Tiles

As mentioned above, the original purpose of establishing Wang tiles was their applicability to automated theorem proving (ATP) (Wang, 1961), due to which Wang was selected to become the first recipient of the milestone prize for ATP (Wang, 1984). In this direction, Wang tiles were then used e.g. for proofs in the cellular automata² theory (Kari, 1990).

Nowadays, Wang tiles are commonly used in computer graphics for texture synthesis, because of their ability to efficiently tile aperiodic and stochastic tile-based textures, refer to (Stam, 1997) and (Cohen et al., 2003). For an example stochastic texture composed of the complete tile set over two colors, see Fig. 2.5.

²Cellular automata are synthetic computing devices similar to human brain (Kari, 2005).

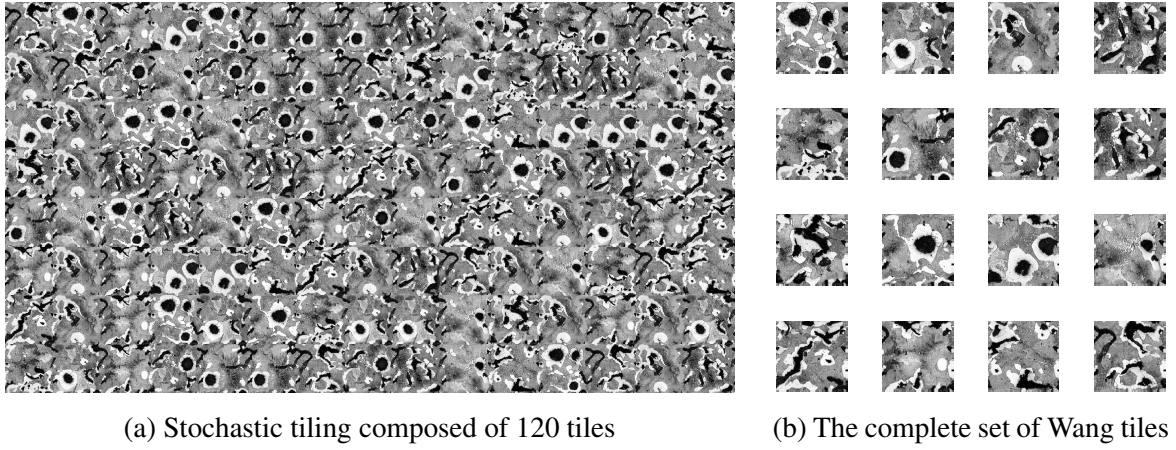


Figure 2.5: (a) Stochastic compacted graphite iron microstructure generated from (b) the complete set of Wang tiles over two colors. Wang tiles were created based on a photograph, courtesy of (Wikimedia Commons, 2009).

Wang tiles are also commonly employed for efficient generation of Poisson disk distributions, refer to (Shade et al., 2000) and (Hiller et al., 2001) for more details. Poisson disk distributions are particularly useful in computer graphics e.g. for object placement (Deussen et al., 1998), anti-aliasing (Yellott, 1982), illumination (Cook, 1986), or for mesh generation (Guo et al., 2016).

Winfree et al. (1998) proposed a molecular realization of Wang tiles, allowing for self-assemblies of biological nanostructures (e.g. DNA) into (a)periodic crystals. Appropriate sets are assembled to perform logical computations or to create complex patterns on the nanoscale (Seeman and Belcher, 2002).

In material engineering, Wang tiles are used for microstructure compression, efficiently representing multiscale material in computations (Novák et al., 2012), and for microstructure reconstruction (Doškář et al., 2014). Doškář and Novák (2016) adopted the concept of Wang tiling to generate large stochastic material samples of the Alporas[®] foam together with its finite element representation. In this thesis it is further aimed at adaptation of Wang tiles to provide pilot results on topology optimization of microstructures.

2.3 Vertex-Based Wang Tiles

Although Wang tiles proved to be useful for compression and construction of complex signals, i.e. textures, some of the sets did not guarantee continuity of stored information near tile corners, because diagonally neighboring tiles were not constrained. In order to solve the so-called *corner problem*, firstly recognized by Cohen et al. (2003), corner tiles were introduced, providing the ability to store the connectivity information in colored corners, instead of edges (Lagae and Dutré, 2006). In order to preserve terminology among dimensions, we further call the corner tiles *vertex-based* Wang tiles.

The vertex-based Wang tiles proved to be superior to the traditional Wang tiles, allowing for a simpler generation of valid tiling, reduced memory requirements, and easier generalization to multiple dimensions (Lagae and Dutré, 2006), while preserving possibility to build aperiodic tiling (Lagae et al., 2006).

The complete set of planar vertex-based Wang tiles over two colors, used throughout the following chapters, contains one vertex-based tile for each possible combination of colors, as shown in Fig. 2.6a. It is easy to see that the set of vertex-based Wang tiles actually defines four distinct types of horizontal and vertical edges, respectively, denoted by the follow-

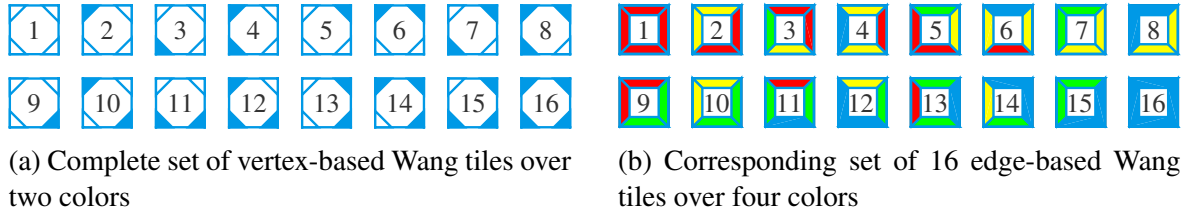


Figure 2.6: Equivalence of (a) the complete set of vertex-based Wang tiles over two colors with (b) a specific set of edge-based Wang tiles over four colors.

ing combinations of vertices: white-white, blue-white, white-blue and blue-blue. Marking the edges by red, yellow, green, and blue, respectively, the vertex-based Wang tiles can be straightforwardly converted to the equivalent set of edge-based Wang tiles, shown in Fig. 2.6b.

In the same manner, any set of vertex-based Wang tiles can be equivalently converted to the set of edge-based Wang tiles. On the contrary, the reverse approach is not generally applicable (Lagae and Dutré, 2006), implying that vertex-based Wang tiles are a subset of the traditional edge-based Wang tiles that is not affected by the corner problem.

In order to create a valid assembly plan of the tiling the vertex-based Wang tiles need to be placed such that the vertex shared by surrounding tiles has the same color, compare Fig. 2.7b and 2.7c. Each color can be marked by an integer value (Lagae and Dutré, 2006), here we use 0 for white and 1 for blue, so that a rectangular tiling is described by a connectivity matrix $\mathbf{C} \in \{0, 1\}^{(n_{t,y}+1) \times (n_{t,x}+1)}$, with $n_{t,y} \in \mathbb{Z}_{>0}$ and $n_{t,x} \in \mathbb{Z}_{>0}$ denoting the count of tiles in vertical and horizontal direction, respectively. The unique equivalence between the connectivity matrix and the assembly plan is illustrated in Fig. 2.7a and 2.7b.

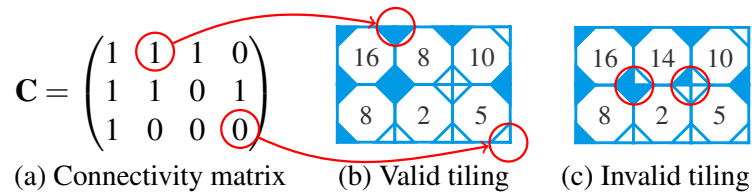


Figure 2.7: Illustration of: (a) connectivity matrix and its correspondence to valid tiling (b), (c) example of invalid tiling.

Utilizing the complete set of vertex-based tiles over a limited set of colors ensure that any connectivity matrix, containing integer values corresponding to the vertex codes of the set, automatically defines a valid tiling from the given set.

Chapter 3

Solution of Trusses by Finite Element Method

In order to understand real-world structural problems one needs to know all the (infinite number of) components a structure consists of and the relations between them. Using an infinite number of infinitesimally small components a continuous formulation, usually in the form of a differential equation with boundary-value conditions, can be obtained.

While for some specific cases an analytical solution to the differential equation can be derived, for more complex cases we are left without the ability to obtain an exact analytical solution. However, based on immense expansion and development of computers, approximate methods for numerical solution of differential equations have been developed in the recent decades. The finite element method then holds a prominent place among the approximate methods.

The key idea of the finite element method consists in *discretization* of the infinite-dimensional continuous model into a discrete finite-dimensional one composed of a finite number of so-called elements. The unknown field is approximated with a so-called *interpolation function* in each element, and *governing equations* describing element properties and behavior are derived. The individual elements are *assembled* according to their shared boundaries (nodes, lines, surfaces etc.), constituting the entire model. Subsequently, solving the differential equation is simplified into a set of ordinary algebraic equations, giving the approximate solution to the original problem.

3.1 A Brief Historical Overview

The origin of the finite element method dates back to 1940s. The idea of discretizing a continuous model with a finite number of elements was firstly adopted by Hrennikoff (1941), specifically, lattice analogy was used to discretize continuous solids by truss-like elements to obtain distribution of stresses.

The first work usually cited in connection with the finite element method is (Courant, 1943), where variational principles were applied to obtain an approximate solution to the traditional Dirichlet problem. The paper also introduced linear shape functions over triangle network.

The actual expansion of the finite element method started in 1950s in the aircraft industry. Argyris (1954) developed a matrix method of structural analysis applicable to structures assembled from discrete elements, facilitating utilization of computers. Turner et al. (1956) then derived truss, beam, triangular, and rectangular plate stiffness matrices. The term finite element was firstly coined in (Clough, 1960).

In (Melosh, 1963), a rigorous variational formulation minimizing the potential energy of the problem was given, resulting in application of the method to non-structural problems, such as fluid flow (H.C.Martin, 1969) or heat conduction (Wilson and Nickell, 1966). In (Szabo and Lee, 1969) the method of weighted residuals was utilized, allowing for a quantitative assessment of the accuracy of the finite element method.

3.2 Problem Statement

Trusses are structures consisting of nodes connected with straight bars. The longitudinal dimension of bars, in the terminology of finite elements called truss elements, is assumed to be much greater compared to the remaining two transverse dimensions, given by the bar cross-sectional area. In our notation the length of an element i will always be aligned with the longitudinal axis \hat{x}_i of the element.

In the subsequent text, we will consider the infinitesimal strain theory and linear elasticity. The truss element is assumed to be prismatic with an infinitely-rigid cross-sectional area $a_i \in \mathbb{R}_{>0}$, remaining planar after deformation. Due to negligible bending and shear stiffness, truss member is subjected only to translations, transmits solely axial forces, and deforms only axially along its local axis \hat{x}_i based on the displacement $u_{\hat{x}_i}(\hat{x}_i)$, see Fig. 3.1.

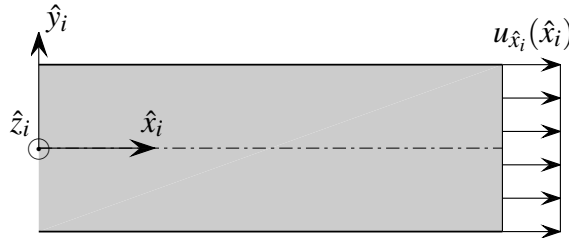


Figure 3.1: Displacement $u_{\hat{x}_i}(\hat{x}_i)$ of the truss element i along local axis \hat{x}_i .

Behavior of the truss element is described by three equations. Based on geometric considerations, we can write the strain-displacement relation as

$$\varepsilon_i(\hat{x}_i) = \frac{du_{\hat{x}_i}(\hat{x}_i)}{d\hat{x}_i}, \quad (3.1)$$

with $\varepsilon_i(\hat{x}_i)$ being the longitudinal strain.

The stress-strain relation, also called a constitutive equation, is expressed with Hooke's law

$$\sigma_i(\hat{x}_i) = E_i \varepsilon_i(\hat{x}_i), \quad (3.2)$$

where E_i denotes the modulus of elasticity of the i -th bar and $\sigma_i(\hat{x}_i)$ stands for the stress within the i -th element.

Finally, the balance equation of an infinitesimal truss section provides us with the condition of the static equilibrium

$$\frac{ds_i(\hat{x}_i)}{d\hat{x}_i} + \overline{f_{\hat{x}_i}}(\hat{x}_i) = 0, \quad \forall \hat{x}_i \in (0, \ell_i), \quad (3.3)$$

where $s_i(\hat{x}_i)$ is an internal axial force in the truss element i , ℓ_i denotes the length of the i -th bar, and $\overline{f_{\hat{x}_i}}(\hat{x}_i)$ is distributed loading. Due to the assumption of trusses being loaded only by external nodal forces, i.e. $\overline{f_{\hat{x}_i}}(\hat{x}_i) = 0$, Eq. (3.3) simplifies to

$$\frac{ds_i(\hat{x}_i)}{d\hat{x}_i} = 0. \quad (3.4)$$

The sum of the stresses $\sigma_i(\hat{x}_i)$ within a cross-sectional area a_i is precisely equal to the axial internal force $s_i(\hat{x}_i)$:

$$s_i(\hat{x}_i) = \int_{a_i} \sigma_i(\hat{x}_i) da_i = \sigma_i(\hat{x}_i) a_i. \quad (3.5)$$

Combining Eqs. (3.1), (3.2), (3.4), and (3.5) a homogeneous differential equation describing the behavior of a single truss element is obtained in the form

$$\frac{d}{d\hat{x}_i} \left(E_i a_i \frac{du_{\hat{x}_i}(\hat{x}_i)}{d\hat{x}_i} \right) = 0. \quad (3.6)$$

Eq. (3.6) has to be supplemented with corresponding kinematic and static boundary conditions, as shown in Fig. 3.2, reflecting the loading of the model.

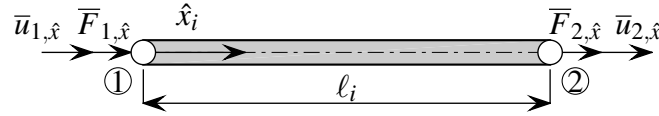


Figure 3.2: Boundary conditions of the truss element i .

Kinematic Dirichlet–boundary conditions are prescribed in the form of displacements $\bar{u}_{1,\hat{x}} \in \mathbb{R}$ and $\bar{u}_{2,\hat{x}} \in \mathbb{R}$:

$$u_{\hat{x}_i}(0) = \bar{u}_{1,\hat{x}} \quad (\text{displacement of node } \textcircled{1}), \quad (3.7a)$$

$$u_{\hat{x}_i}(\ell_i) = \bar{u}_{2,\hat{x}} \quad (\text{displacement of node } \textcircled{2}), \quad (3.7b)$$

and the static Neumann–boundary conditions in the form of external nodal forces $\bar{F}_{1,\hat{x}} \in \mathbb{R}$ and $\bar{F}_{2,\hat{x}} \in \mathbb{R}$:

$$E_i a_i \frac{du_{\hat{x}_i}(0)}{d\hat{x}_i} = -\bar{F}_{1,\hat{x}} \quad (\text{force in node } \textcircled{1}), \quad (3.8a)$$

$$E_i a_i \frac{du_{\hat{x}_i}(\ell_i)}{d\hat{x}_i} = \bar{F}_{2,\hat{x}} \quad (\text{force in node } \textcircled{2}). \quad (3.8b)$$

The convention introduced in Fig. 3.2 directly implies that $\bar{F}_{1,\hat{x}} \in \mathbb{R}_{>0}$ induces compression in the element, and $\bar{F}_{1,\hat{x}} \in \mathbb{R}_{<0}$ tension, hence the negative sign in Eq. (3.8a). On the contrary, $\bar{F}_{2,\hat{x}} \in \mathbb{R}_{>0}$ leads to tension in the element, and $\bar{F}_{2,\hat{x}} \in \mathbb{R}_{<0}$ to compression, which agrees with the sign convention, hence the positive sign in Eq. (3.8b).

In order to uniquely solve the boundary-value problem, two boundary conditions, including at least one kinematic, need to be specified, corresponding to the fact that each node has a single degree of freedom. The solution is, clearly visible from Eq. (3.6), in the form of the displacement function $u_{\hat{x}_i}(\hat{x}_i)$.

3.3 Derivation of Truss Element Equations

The mathematical approach to finite element method is based on approximation of the exact axial displacement function $u_{\hat{x}_i}(\hat{x}_i)$ over the length of the element i by $u_{\hat{x}_i}^i(\hat{x}_i)$, such that

$$u_{\hat{x}_i}(\hat{x}_i) \approx u_{\hat{x}_i}^i(\hat{x}_i). \quad (3.9)$$

Evaluating the truss element, formally stated by Eq. (3.6) with boundary value conditions expressed by Eq. (3.7) and Eq. (3.8) and recognizing that Eq. (3.6) is homogeneous

and the boundary conditions do not state any requirements for the second order derivatives, it is straightforward that the displacement function needs to be only C^0 continuous within the truss element and needs to respect the boundary value conditions. Following the requirements it implies a linear function $u_{\hat{x}_i}^i(\hat{x}_i)$ is sufficient to approximate $u_{\hat{x}_i}(\hat{x}_i)$. It needs to be highlighted, that in the case of the truss element being loaded only by nodal forces, the linear approximation is actually equal to the exact analytical solution.

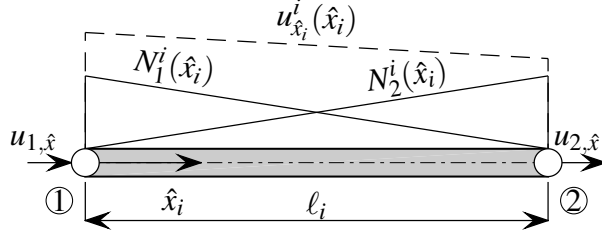


Figure 3.3: Linear shape functions of the truss element i .

Let us now introduce a linear shape (interpolation) function $N_k^i(\hat{x}_i)$, such that

$$N_k^i(\hat{x}_i) = \begin{cases} 1 & \text{in node } \textcircled{k}, \\ 0 & \text{in any other node,} \end{cases} \quad (3.10)$$

so that for a truss element i consisting of nodes $\textcircled{1}$ and $\textcircled{2}$, see Fig. 3.3, the shape functions N_1^i and N_2^i read as

$$N_1^i(\hat{x}_i) = 1 - \frac{\hat{x}_i}{\ell_i}, \quad (3.11a)$$

$$N_2^i(\hat{x}_i) = \frac{\hat{x}_i}{\ell_i}. \quad (3.11b)$$

The displacement $u_{\hat{x}_i}^i(\hat{x}_i)$ is then a linear combination of both the shape functions

$$u_{\hat{x}_i}^i(\hat{x}_i) = N_1^i(\hat{x}_i)u_{1,\hat{x}} + N_2^i(\hat{x}_i)u_{2,\hat{x}}, \quad (3.12)$$

which can be equivalently written in the matrix notation as

$$u_{\hat{x}_i}^i(\hat{x}_i) = \begin{pmatrix} N_1^i(\hat{x}_i) & N_2^i(\hat{x}_i) \end{pmatrix} \begin{Bmatrix} u_{1,\hat{x}} \\ u_{2,\hat{x}} \end{Bmatrix} = \mathbf{N}^i(\hat{x}_i) \hat{\mathbf{u}}^i, \quad (3.13)$$

with $\mathbf{N}^i(\hat{x}_i) \in \mathbb{R}^2$ being the shape function matrix and $\hat{\mathbf{u}}^i \in \mathbb{R}^2$ the displacement column vector of the element i in local coordinates.

From Eq. (3.1), the axial strain field can be expressed through

$$\epsilon_i^i = \begin{pmatrix} \frac{dN_1^i(\hat{x}_i)}{d\hat{x}_i} & \frac{dN_2^i(\hat{x}_i)}{d\hat{x}_i} \end{pmatrix} \begin{Bmatrix} u_{1,\hat{x}} \\ u_{2,\hat{x}} \end{Bmatrix} = \begin{pmatrix} -\frac{1}{\ell_i} & \frac{1}{\ell_i} \end{pmatrix} \begin{Bmatrix} u_{1,\hat{x}} \\ u_{2,\hat{x}} \end{Bmatrix} = \mathbf{B}^i \hat{\mathbf{u}}^i, \quad (3.14)$$

where $\mathbf{B}^i \in \mathbb{R}^2$ is the strain-displacement matrix of the i -th element. Note that the axial strain is constant within the truss element.

In the following sections the truss governing equations are to be derived by two different approaches, showing various perspectives. While direct equilibrium approach is the most straightforward, the method based on minimizing the potential energy functional will prove to be convenient in the subsequent chapters.

3.3.1 Direct Equilibrium

Because the axial strain is constant within the truss element, recall Eq. (3.14), the longitudinal stress is also constant over its length, and based on Eq. (3.2) equals to

$$\sigma_i = E_i \mathbf{B}^i \hat{\mathbf{u}}^i. \quad (3.15)$$

Similarly, the axial internal force after substituting Eq. (3.15) into Eq. (3.5) reads as

$$s_i = E_i a_i \mathbf{B}^i \hat{\mathbf{u}}^i. \quad (3.16)$$

Again, it should be noted that the axial internal force s_i is constant within the truss element.

Let us now return to Fig. 3.2 and the boundary conditions, as defined by Eqs. (3.7) and (3.8). From the static equilibrium on the element i it implies that the axial force s_i has to be equal to $-\bar{F}_{1,\hat{x}}$ and also to $\bar{F}_{2,\hat{x}}$, therefore it stands that

$$\begin{pmatrix} -1 \\ 1 \end{pmatrix} \{s_i\} = \begin{pmatrix} \bar{F}_{1,\hat{x}} \\ \bar{F}_{2,\hat{x}} \end{pmatrix}, \quad (3.17)$$

which is equivalently in matrix notation

$$\hat{\boldsymbol{\gamma}}_i s_i = \hat{\mathbf{f}}^i, \quad (3.18)$$

with $\hat{\boldsymbol{\gamma}}_i \in \mathbb{R}^2$ being a column vector expressing geometric relation between axial and nodal forces in local coordinates and $\hat{\mathbf{f}}^i \in \mathbb{R}^2$ standing for nodal forces column vector of the element i , respectively. Note that it further stands that

$$\mathbf{B}^i = \frac{1}{\ell_i} (\hat{\boldsymbol{\gamma}}_i)^T. \quad (3.19)$$

Combination of Eq. (3.17) with Eq. (3.16) then leads to the relation

$$\frac{E_i a_i}{\ell_i} \begin{pmatrix} 1 & -1 \\ -1 & 1 \end{pmatrix} \begin{Bmatrix} u_{1,\hat{x}} \\ u_{2,\hat{x}} \end{Bmatrix} = \begin{Bmatrix} \bar{F}_{1,\hat{x}} \\ \bar{F}_{2,\hat{x}} \end{Bmatrix}, \quad (3.20)$$

which is in matrix notation

$$\hat{\mathbf{K}}^i \hat{\mathbf{u}}^i = \hat{\mathbf{f}}^i, \quad (3.21)$$

with the stiffness matrix of the element i in local coordinates $\hat{\mathbf{K}}^i \in \mathbb{R}^{2 \times 2}$ defined as

$$\hat{\mathbf{K}}^i = \frac{E_i a_i}{\ell_i} \begin{pmatrix} 1 & -1 \\ -1 & 1 \end{pmatrix} = (\mathbf{B}^i)^T E_i a_i \ell_i \mathbf{B}^i = \hat{\boldsymbol{\gamma}}_i \frac{E_i a_i}{\ell_i} (\hat{\boldsymbol{\gamma}}_i)^T. \quad (3.22)$$

Note that the element stiffness matrix is symmetric and positive definite for an arbitrary cross-sectional area $a_i > 0$ and can be expressed in the form of a dyadic product.

3.3.2 Minimum to the Potential Energy Functional

Solution of trusses can also be seen from the perspective of a search for the natural structural state that minimizes the total energy. Let us, therefore, define the potential energy functional of the i -th element Π_i as the sum of internal elastic strain energy U_i and the potential energy of external forces W_i

$$\Pi_i = U_i + W_i. \quad (3.23)$$

Internal Elastic Strain Energy

For derivation of the internal elastic strain energy U_i an infinitesimally small section of the truss element is considered. Due to the already stated assumption of bars transmitting only the axial forces, resulting in the stress field σ_i , the section is consequently elongated from its initial length $d\hat{x}_i$ to $d\hat{x}_i(1 + d\epsilon_i)$, with $d\hat{x}_i d\epsilon_i$ denoting the actual differential elongation, as shown in Fig. 3.4.

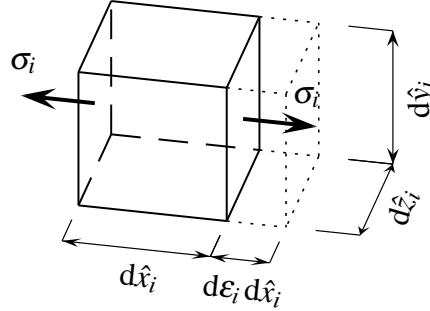


Figure 3.4: Normal stresses in an infinitesimally small section of the truss element i .

The differential internal work, corresponding to the infinitesimally small section of the truss element and denoting the work done by internal forces on displacements, then reads as

$$dU_i = s_i du_{\hat{x}_i}(\hat{x}_i), \quad (3.24)$$

which can be based on Eq. (3.5) rewritten as

$$dU_i = \sigma_i d\hat{y}_i d\hat{z}_i d\epsilon_i d\hat{x}_i \quad (3.25)$$

and finally as

$$dU_i = \sigma_i d\epsilon_i dV_i, \quad (3.26)$$

where $dV_i = d\hat{x}_i d\hat{y}_i d\hat{z}_i$ corresponds to the volume of the infinitesimally small section of the truss element.

By integration of Eq. (3.26) over the strains, to obtain displacements, and over the volume, the internal elastic strain energy of the whole truss element

$$U_i = \int_{V_i} \left(\int_0^{\epsilon_i} \sigma_i d\epsilon_i \right) dV_i \quad (3.27)$$

is obtained. After integration over the strains we get

$$U_i = \frac{1}{2} \int_{V_i} \sigma_i \epsilon_i dV_i, \quad (3.28)$$

which reads after expressing σ_i from Eq. (3.5) and after substituting into Eq. (3.28) as

$$U_i = \frac{1}{2} \int_{\hat{x}_i} \int_{\hat{y}_i} \int_{\hat{z}_i} \frac{s_i}{a_i} \epsilon_i d\hat{z}_i d\hat{y}_i d\hat{x}_i \quad (3.29)$$

and equivalently as

$$U_i = \frac{1}{2} \int_0^{\ell_i} s_i \epsilon_i d\hat{x}_i. \quad (3.30)$$

Finally, insertion of Eq. (3.1) and Eq. (3.5) into Eq. (3.30) leads to

$$U_i = \frac{1}{2} \int_0^{\ell_i} \frac{du_{\hat{x}_i}(\hat{x}_i)}{d\hat{x}_i} E_i a_i \frac{du_{\hat{x}_i}(\hat{x}_i)}{d\hat{x}_i} d\hat{x}_i. \quad (3.31)$$

Potential Energy of External Forces

The potential energy of external forces is the external work done by external forces on nodal displacements. Using the notation from Fig. 3.2 we can write

$$W_i = - \begin{pmatrix} u_{\hat{x}_i}(0) & u_{\hat{x}_i}(\ell_i) \end{pmatrix} \begin{pmatrix} \bar{F}_{1,\hat{x}} \\ \bar{F}_{2,\hat{x}} \end{pmatrix}, \quad (3.32)$$

with the negative sign implying the loss of energy when the force acts in the displaced direction.

Potential Energy Function

Insertion of the derived relations for the internal elastic strain energy (3.31) and for the potential energy of external forces (3.32) into Eq. (3.23) leads us to the formula

$$\Pi_i(u_{\hat{x}_i}(\hat{x}_i)) = \frac{1}{2} \int_0^{\ell_i} \frac{du_{\hat{x}_i}(\hat{x}_i)}{d\hat{x}_i} E_i a_i \frac{du_{\hat{x}_i}(\hat{x}_i)}{d\hat{x}_i} d\hat{x}_i - \bar{F}_{1,\hat{x}} u_{\hat{x}_i}(0) - \bar{F}_{2,\hat{x}} u_{\hat{x}_i}(\ell_i) \quad (3.33)$$

that can be equivalently rewritten in matrix notation as

$$\Pi_i(\hat{\mathbf{u}}^i) = \frac{1}{2} \int_0^{\ell_i} (\hat{\mathbf{u}}^i)^T (\mathbf{B}^i)^T E_i a_i \mathbf{B}^i \hat{\mathbf{u}}^i d\hat{x}_i - (\hat{\mathbf{u}}^i)^T \hat{\mathbf{f}}^i \quad (3.34)$$

and after integration as

$$\Pi_i(\hat{\mathbf{u}}^i) = \frac{1}{2} (\hat{\mathbf{u}}^i)^T (\mathbf{B}^i)^T E_i a_i \ell_i \mathbf{B}^i \hat{\mathbf{u}}^i - (\hat{\mathbf{u}}^i)^T \hat{\mathbf{f}}^i, \quad (3.35)$$

that is a convex quadratic function *only* in terms of $\hat{\mathbf{u}}^i$.

Proposition 1. *Minimum to the potential energy function Π_i automatically satisfies Eq. (3.21).*

Proof. Expanding Eq. (3.35) leads to

$$\Pi_i(\hat{\mathbf{u}}^i) = \frac{1}{2} E_i a_i \ell_i \begin{Bmatrix} u_{1,\hat{x}} \\ u_{2,\hat{x}} \end{Bmatrix} \begin{pmatrix} -\frac{1}{\ell_i} \\ \frac{1}{\ell_i} \end{pmatrix} \begin{pmatrix} -\frac{1}{\ell_i} & \frac{1}{\ell_i} \end{pmatrix} \begin{Bmatrix} u_{1,\hat{x}} \\ u_{2,\hat{x}} \end{Bmatrix} - \begin{Bmatrix} u_{1,\hat{x}} & u_{2,\hat{x}} \end{Bmatrix} \begin{pmatrix} \bar{F}_{1,\hat{x}} \\ \bar{F}_{2,\hat{x}} \end{pmatrix}, \quad (3.36)$$

which after multiplication equals to

$$\Pi_i(\hat{\mathbf{u}}^i) = \frac{1}{2} E_i a_i \ell_i \left(\frac{1}{\ell_i^2} u_{1,\hat{x}}^2 - \frac{2}{\ell_i^2} u_{1,\hat{x}} u_{2,\hat{x}} + \frac{1}{\ell_i^2} u_{2,\hat{x}}^2 \right) - \bar{F}_{1,\hat{x}} u_{1,\hat{x}} - \bar{F}_{2,\hat{x}} u_{2,\hat{x}}, \quad (3.37)$$

and also to

$$\Pi_i(\hat{\mathbf{u}}^i) = \frac{1}{2} \frac{E_i a_i}{\ell_i} (u_{1,\hat{x}}^2 - 2u_{1,\hat{x}} u_{2,\hat{x}} + u_{2,\hat{x}}^2) - \bar{F}_{1,\hat{x}} u_{1,\hat{x}} - \bar{F}_{2,\hat{x}} u_{2,\hat{x}}. \quad (3.38)$$

Due to the function Π_i being convex, its minimum clearly requires only a stationary to the potential energy function, such that

$$\frac{\partial \Pi_i(\hat{\mathbf{u}}^i)}{\partial u_{1,\hat{x}}} = 0, \quad (3.39a)$$

$$\frac{\partial \Pi_i(\hat{\mathbf{u}}^i)}{\partial u_{2,\hat{x}}} = 0. \quad (3.39b)$$

The derivative in Eq. (3.39a) leads us directly to

$$\frac{\partial \Pi_i(\hat{\mathbf{u}}^i)}{\partial u_{1,\hat{x}}} = \frac{1}{2} \frac{E_i a_i}{\ell_i} (2u_{1,\hat{x}} - 2u_{2,\hat{x}}) - \bar{F}_{1,\hat{x}} = 0, \quad (3.40)$$

and similarly, the derivative in Eq. (3.39b) equals to

$$\frac{\partial \Pi_i(\hat{\mathbf{u}}^i)}{\partial u_{2,\hat{x}}} = \frac{1}{2} \frac{E_i a_i}{\ell_i} (-2u_{1,\hat{x}} + 2u_{2,\hat{x}}) - \bar{F}_{2,\hat{x}} = 0. \quad (3.41)$$

Finally, Eqs. (3.40) and (3.41) rewritten into matrix notation denote the requirements of the minimum

$$\frac{\partial \Pi_i(\hat{\mathbf{u}}^i)}{\partial \hat{\mathbf{u}}^i} = \frac{E_i a_i}{\ell_i} \begin{pmatrix} 1 & -1 \\ -1 & 1 \end{pmatrix} \begin{Bmatrix} u_{1,\hat{x}} \\ u_{2,\hat{x}} \end{Bmatrix} - \begin{Bmatrix} \bar{F}_{1,\hat{x}} \\ \bar{F}_{2,\hat{x}} \end{Bmatrix} = 0, \quad (3.42)$$

which is exactly

$$\hat{\mathbf{K}}^i \hat{\mathbf{u}}^i = \hat{\mathbf{f}}^i, \quad (3.43)$$

and we are done. \square

Compliance of the Truss Element

Let $\hat{\mathbf{u}}_{\text{KA}}^i \in \mathbb{R}^2$ denote a vector of kinematically admissible displacements, satisfying the boundary conditions. The quadratic potential energy function from Eq. (3.35) can then be written as

$$\Pi_i(\hat{\mathbf{u}}_{\text{KA}}^i) = \frac{1}{2} (\hat{\mathbf{u}}_{\text{KA}}^i)^T \hat{\mathbf{K}}^i \hat{\mathbf{u}}_{\text{KA}}^i - (\hat{\mathbf{u}}_{\text{KA}}^i)^T \hat{\mathbf{f}}^i \quad (3.44)$$

and further as

$$\Pi_i(\hat{\mathbf{u}}_{\text{KA}}^i) = (\hat{\mathbf{u}}_{\text{KA}}^i)^T \left(\frac{1}{2} \hat{\mathbf{K}}^i \hat{\mathbf{u}}_{\text{KA}}^i - \hat{\mathbf{f}}^i \right). \quad (3.45)$$

Now, we search its minimum over all admissible displacements:

$$\min_{\forall \hat{\mathbf{u}}_{\text{KA}}^i \in \mathbb{R}^2} \left[(\hat{\mathbf{u}}_{\text{KA}}^i)^T \left(\frac{1}{2} \hat{\mathbf{K}}^i \hat{\mathbf{u}}_{\text{KA}}^i - \hat{\mathbf{f}}^i \right) \right]. \quad (3.46)$$

Because Eq. (3.21) is satisfied at the minimum to the potential energy function, recall Proposition 1, $\hat{\mathbf{u}}^i$ is clearly a minimizer to Eq. (3.46). Subsequently, the term $\hat{\mathbf{K}}^i \hat{\mathbf{u}}^i$ can be substituted by $\hat{\mathbf{f}}^i$, implying the minimum to potential energy function equals to

$$\min_{\forall \hat{\mathbf{u}}_{\text{KA}}^i \in \mathbb{R}^2} (\Pi_i(\hat{\mathbf{u}}_{\text{KA}}^i)) = (\hat{\mathbf{u}}^i)^T \left(\frac{1}{2} \hat{\mathbf{f}}^i - \hat{\mathbf{f}}^i \right) = -\frac{1}{2} (\hat{\mathbf{u}}^i)^T \hat{\mathbf{f}}^i = -\frac{1}{2} (\hat{\mathbf{f}}^i)^T \hat{\mathbf{u}}^i, \quad (3.47)$$

where

$$c_i = \frac{1}{2} (\hat{\mathbf{f}}^i)^T \hat{\mathbf{u}}^i, \quad (3.48)$$

$c_i \in \mathbb{R}_{>0}$ is called compliance of the i -th truss element. Compliance represents one half of the work done by external forces, recall Eq. (3.32), and measures the stiffness of the truss with respect to specified nodal forces. The lower the compliance, the stiffer the truss element.

3.4 Transformation to Plane Trusses

Let us consider a Cartesian coordinate system defined by orthogonal axes x and y , forming plane, with the truss element i placed between arbitrary located nodes ① and ②, see Fig. 3.5. Let the angle between x and the longitudinal axis of the element \hat{x}_i be measured counterclockwise and denoted by $\theta_i \in [0, 2\pi)$.

Because truss elements do not possess shear and bending stiffness, each node of the in-plane truss element is associated with two degrees of freedom. Subsequently, the element is assigned four degrees of freedom, specified by displacements u_{1,\hat{x}_i} and u_{2,\hat{x}_i} in the direction of \hat{x}_i and displacements u_{1,\hat{y}_i} and u_{2,\hat{y}_i} in the direction of \hat{y}_i , respectively.

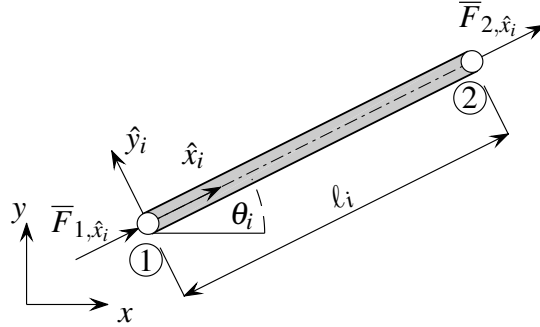


Figure 3.5: In-plane truss element i .

For a truss structure consisting of several arbitrary truss members it is of great importance to treat all degrees of freedom, denoted by local displacements, within a single unifying framework, denoted by the global-coordinates displacements $u_{1,x}$, $u_{2,x}$ in the direction of x , and $u_{1,y}$ and $u_{2,y}$ in the direction of y .

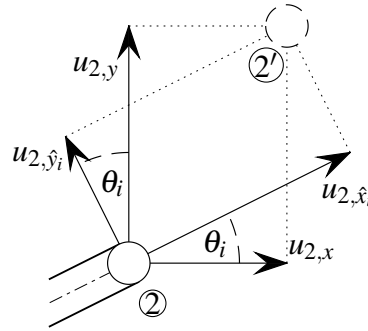


Figure 3.6: Transformation of displacements between local and global coordinates.

Let us begin with a sample node ② of a truss element being displaced to the position ②', as shown in Fig. 3.6. Then, based on geometrical properties of the problem, we can write relations between the local displacements u_{2,\hat{x}_i} and u_{2,\hat{y}_i} and the global displacements $u_{2,x}$ and $u_{2,y}$ as

$$u_{2,\hat{x}_i} = u_{2,x} \cos(\theta_i) + u_{2,y} \sin(\theta_i) \quad (3.49)$$

and

$$u_{2,\hat{y}_i} = u_{2,x} \sin(\theta_i) + u_{2,y} \cos(\theta_i), \quad (3.50)$$

that is in matrix notation

$$\begin{Bmatrix} u_{2,\hat{x}_i} \\ u_{2,\hat{y}_i} \end{Bmatrix} = \begin{pmatrix} \cos(\theta_i) & \sin(\theta_i) \\ \sin(\theta_i) & \cos(\theta_i) \end{pmatrix} \begin{Bmatrix} u_{2,x} \\ u_{2,y} \end{Bmatrix}. \quad (3.51)$$

Similarly, for the whole truss element consisting of nodes ① and ② it is straightforward to write

$$\begin{Bmatrix} u_{1,\hat{x}_i} \\ u_{1,\hat{y}_i} \\ u_{2,\hat{x}_i} \\ u_{2,\hat{y}_i} \end{Bmatrix} = \begin{pmatrix} \cos(\theta_i) & \sin(\theta_i) & 0 & 0 \\ \sin(\theta_i) & \cos(\theta_i) & 0 & 0 \\ 0 & 0 & \cos(\theta_i) & \sin(\theta_i) \\ 0 & 0 & \sin(\theta_i) & \cos(\theta_i) \end{pmatrix} \begin{Bmatrix} u_{1,x} \\ u_{1,y} \\ u_{2,x} \\ u_{2,y} \end{Bmatrix}, \quad (3.52)$$

or, equivalently

$$\hat{\mathbf{u}}^i = \mathbf{T}^i \mathbf{u}^i. \quad (3.53)$$

Here, $\hat{\mathbf{u}}^i \in \mathbb{R}^4$ denotes the column vector of displacements along local axes \hat{x}_i and \hat{y}_i , $\mathbf{u}^i \in \mathbb{R}^4$ standing for a column vector of displacements along global axes x and y , and the transformation matrix of the i -th element $\mathbf{T}^i \in \mathbb{R}^{4 \times 4}$ stands for

$$\mathbf{T}^i = \begin{pmatrix} \cos(\theta_i) & \sin(\theta_i) & 0 & 0 \\ \sin(\theta_i) & \cos(\theta_i) & 0 & 0 \\ 0 & 0 & \cos(\theta_i) & \sin(\theta_i) \\ 0 & 0 & \sin(\theta_i) & \cos(\theta_i) \end{pmatrix}. \quad (3.54)$$

Note that the transformation matrix is actually a rotation matrix, and it is therefore orthogonal.

Similarly to the displacements, the linear transformation can be applied on local forces column vector $\hat{\mathbf{f}}^i \in \mathbb{R}^4$, such that

$$\begin{Bmatrix} \bar{F}_{1,\hat{x}} \\ \bar{F}_{1,\hat{y}} \\ \bar{F}_{2,\hat{x}} \\ \bar{F}_{2,\hat{y}} \end{Bmatrix} = \begin{pmatrix} \cos(\theta_i) & \sin(\theta_i) & 0 & 0 \\ \sin(\theta_i) & \cos(\theta_i) & 0 & 0 \\ 0 & 0 & \cos(\theta_i) & \sin(\theta_i) \\ 0 & 0 & \sin(\theta_i) & \cos(\theta_i) \end{pmatrix} \begin{Bmatrix} \bar{F}_{1,x} \\ \bar{F}_{1,y} \\ \bar{F}_{2,x} \\ \bar{F}_{2,y} \end{Bmatrix}, \quad (3.55)$$

or, equivalently

$$\hat{\mathbf{f}}^i = \mathbf{T}^i \mathbf{f}^i \quad (3.56)$$

with $\hat{\mathbf{f}}^i \in \mathbb{R}^4$ being a column vector of nodal forces in local coordinates and $\mathbf{f}^i \in \mathbb{R}^4$ standing for a column vector of nodal forces in global coordinates.

Stress-Displacement Relation

The axial stress-displacement relation in local coordinates is based on Eq. (3.15), and reads as

$$\sigma_i = E_i \mathbf{B}^i \hat{\mathbf{u}}^i = E_i \begin{pmatrix} -\frac{1}{\ell_i} & 0 & \frac{1}{\ell_i} & 0 \end{pmatrix} \begin{Bmatrix} u_{1,\hat{x}_i} \\ u_{1,\hat{y}_i} \\ u_{2,\hat{x}_i} \\ u_{2,\hat{y}_i} \end{Bmatrix}, \quad (3.57)$$

which can be equivalently rewritten into global coordinates:

$$\sigma_i = E_i \mathbf{B}^i \mathbf{T}^i \mathbf{u}^i = E_i \begin{pmatrix} -\frac{1}{\ell_i} & 0 & \frac{1}{\ell_i} & 0 \end{pmatrix} \begin{pmatrix} \cos(\theta_i) & \sin(\theta_i) & 0 & 0 \\ \sin(\theta_i) & \cos(\theta_i) & 0 & 0 \\ 0 & 0 & \cos(\theta_i) & \sin(\theta_i) \\ 0 & 0 & \sin(\theta_i) & \cos(\theta_i) \end{pmatrix} \begin{Bmatrix} u_{1,x} \\ u_{1,y} \\ u_{2,x} \\ u_{2,y} \end{Bmatrix}. \quad (3.58)$$

After expanding the matrix multiplications, the previous relation simplifies into

$$\sigma_i = \frac{E_i}{\ell_i} \begin{pmatrix} -\cos(\theta_i) & -\sin(\theta_i) & \cos(\theta_i) & \sin(\theta_i) \end{pmatrix} \begin{Bmatrix} u_{1,x} \\ u_{1,y} \\ u_{2,x} \\ u_{2,y} \end{Bmatrix}, \quad (3.59)$$

with the matrix form

$$\sigma_i = \frac{E_i}{\ell_i} \boldsymbol{\gamma}_i^T \mathbf{u}^i \quad (3.60)$$

where $\boldsymbol{\gamma}_i \in \mathbb{R}^4$ stands for a column vector expressing geometric relation between axial and nodal forces, so that it holds

$$\boldsymbol{\gamma}_i s_i = \mathbf{f}^i. \quad (3.61)$$

The axial force equals to

$$s_i = E_i a_i \mathbf{B}^i \hat{\mathbf{u}}^i = E_i a_i \mathbf{B}^i \mathbf{T}^i \mathbf{u}^i = \frac{E_i a_i}{\ell_i} \boldsymbol{\gamma}_i^T \mathbf{u}^i. \quad (3.62)$$

Equilibrium Equation

In order to state the equilibrium equation in global coordinates, we will firstly recall the local-coordinates version:

$$\hat{\mathbf{K}}^i \hat{\mathbf{u}}^i = \hat{\mathbf{f}}^i. \quad (3.63)$$

Inserting Eq. (3.53) and Eq. (3.56) into Eq. (3.63) leads to

$$\hat{\mathbf{K}}^i \mathbf{T}^i \mathbf{u}^i = \mathbf{T}^i \mathbf{f}^i, \quad (3.64)$$

which is equivalent to

$$(\mathbf{T}^i)^{-1} \hat{\mathbf{K}}^i \mathbf{T}^i \mathbf{u}^i = \mathbf{f}^i. \quad (3.65)$$

Because the transformation matrix is orthogonal we have $(\mathbf{T}^i)^{-1} = (\mathbf{T}^i)^T$. Subsequently, we can write

$$(\mathbf{T}^i)^T \hat{\mathbf{K}}^i \mathbf{T}^i \mathbf{u}^i = \mathbf{f}^i. \quad (3.66)$$

The global stiffness matrix $\mathbf{K}^i \in \mathbb{R}^{4 \times 4}$ of i -th element then equals to

$$\mathbf{K}^i = (\mathbf{T}^i)^T \hat{\mathbf{K}}^i \mathbf{T}^i = (\mathbf{T}^i)^T (\mathbf{B}^i)^T E_i a_i \ell_i \mathbf{B}^i \mathbf{T}^i = \boldsymbol{\gamma}_i \frac{E_i a_i}{\ell_i} (\boldsymbol{\gamma}_i)^T, \quad (3.67)$$

and specifically to

$$\mathbf{K}^i = \frac{E_i a_i}{\ell_i} \begin{pmatrix} \cos(\theta_i)^2 & \cos(\theta_i) \sin(\theta_i) & -\cos(\theta_i)^2 & -\cos(\theta_i) \sin(\theta_i) \\ \cos(\theta_i) \sin(\theta_i) & \sin(\theta_i)^2 & -\cos(\theta_i) \sin(\theta_i) & -\sin(\theta_i)^2 \\ -\cos(\theta_i)^2 & -\cos(\theta_i) \sin(\theta_i) & \cos(\theta_i)^2 & \cos(\theta_i) \sin(\theta_i) \\ -\cos(\theta_i) \sin(\theta_i) & -\sin(\theta_i)^2 & \cos(\theta_i) \sin(\theta_i) & \sin(\theta_i)^2 \end{pmatrix}. \quad (3.68)$$

Finally, the global-coordinates equilibrium equation reads as

$$\mathbf{K}^i \mathbf{u}^i = \mathbf{f}^i. \quad (3.69)$$

Potential Energy Function

Similarly, let us recall the equation for the potential energy function in local coordinates:

$$\Pi_i(\hat{\mathbf{u}}^i) = \frac{1}{2} (\hat{\mathbf{u}}^i)^T \hat{\mathbf{K}}^i \hat{\mathbf{u}}^i - (\hat{\mathbf{u}}^i)^T \hat{\mathbf{f}}^i. \quad (3.70)$$

After substituting Eq. (3.53) and Eq. (3.56) into Eq. (3.70), we obtain

$$\Pi_i(\mathbf{u}^i) = \frac{1}{2} (\mathbf{T}^i \mathbf{u}^i)^T \hat{\mathbf{K}}^i \mathbf{T}^i \mathbf{u}^i - (\mathbf{T}^i \mathbf{u}^i)^T \mathbf{T}^i \mathbf{f}^i, \quad (3.71)$$

which is equivalently

$$\Pi_i(\mathbf{u}^i) = \frac{1}{2} (\mathbf{u}^i)^T (\mathbf{T}^i)^T \hat{\mathbf{K}}^i \mathbf{T}^i \mathbf{u}^i - (\mathbf{u}^i)^T (\mathbf{T}^i)^T \mathbf{T}^i \mathbf{f}^i. \quad (3.72)$$

Exploiting orthogonality of the transformation matrix and substituting \mathbf{K}^i from Eq. (3.67), we are led to the final relation in the global coordinates

$$\Pi_i(\mathbf{u}^i) = \frac{1}{2} (\mathbf{u}^i)^T \mathbf{K}^i \mathbf{u}^i - (\mathbf{u}^i)^T \mathbf{f}^i. \quad (3.73)$$

3.5 Truss Element Equations Assembly

Consider a general truss structure consisting of $n_b \in \mathbb{Z}_{>0}$ truss members. In order to provide a unified framework coupling all truss elements, their equations need to be expressed in dependence on the structural displacement field column vector $\mathbf{u}_S \in \mathbb{R}^{2n_n}$, defined as

$$\mathbf{u}_S = \begin{pmatrix} u_{1,x} \\ u_{1,y} \\ \vdots \\ u_{n_n,x} \\ u_{n_n,y} \end{pmatrix}, \quad (3.74)$$

where $n_n \in \mathbb{Z}_{>0}$ denotes the number of nodes the truss structure contains.

In this spirit, the structural stiffness matrix $\mathbf{K}_S \in \mathbb{R}^{2n_n \times 2n_n}$, relating global forces with global displacements, is defined as the sum of the contributions of all bars

$$\mathbf{K}_S = \sum_{i=1}^{n_b} \mathbf{K}^i, \quad (3.75)$$

where the element stiffness matrices are added to such rows and columns that correspond to the coincidence of variables in \mathbf{u}_S and \mathbf{u}^i . Note that it follows from the developments in Section 3.3 that the structural stiffness matrix \mathbf{K}_S is square, symmetric, singular, and positive semidefinite.

A similar approach is also applicable to the assembly of the nodal forces column vector $\mathbf{f}_S \in \mathbb{R}^{2n_n}$, defined as the sum of nodal forces within all truss elements

$$\mathbf{f}_S = \sum_{i=1}^{n_b} \mathbf{f}^i = \begin{pmatrix} \bar{F}_{1,x} \\ \bar{F}_{1,y} \\ \vdots \\ \bar{F}_{n_n,x} \\ \bar{F}_{n_n,y} \end{pmatrix}. \quad (3.76)$$

The total potential energy function $\Pi(\mathbf{u}_S) : \mathbb{R}^{2n_n} \rightarrow \mathbb{R}$ is composed from contributions of individual members:

$$\Pi(\mathbf{u}_S) = \sum_{i=1}^{n_b} \Pi_i(\mathbf{u}_S) = \sum_{i=1}^{n_b} \left(\frac{1}{2} (\mathbf{u}^i)^T \mathbf{K}^i \mathbf{u}^i - (\mathbf{u}^i)^T \mathbf{f}^i \right), \quad (3.77)$$

which is equivalent to

$$\Pi(\mathbf{u}_S) = \frac{1}{2} (\mathbf{u}_S)^T \mathbf{K}_S \mathbf{u}_S - (\mathbf{u}_S)^T \mathbf{f}_S. \quad (3.78)$$

The structural static matrix $\mathbf{A}_S \in \mathbb{R}^{2n_n \times n_b}$ can be assembled as

$$\mathbf{A}_S = \sum_{i=1}^{n_b} \boldsymbol{\gamma}_i, \quad (3.79)$$

with $\boldsymbol{\gamma}_i \in \mathbb{R}^{n_n}$ being added to the i -th column and to the rows corresponding to the coincidence of variables in \mathbf{u}_S and \mathbf{u}^i .

3.6 Solution to the Truss Equations

In Section 3.2, we have already stated that we will consider only two types of boundary conditions: prescribed nodal forces $\bar{\mathbf{f}} \in \mathbb{R}^{n_{\text{dof}}}$ (Neumann-type boundary conditions) and prescribed displacements $\bar{\mathbf{u}} \in \mathbb{R}^{2n_n - n_{\text{dof}}}$ (Dirichlet-type boundary conditions), with n_{dof} denoting the number of degrees of freedom, corresponding to the unconstrained displacements. Note that also the unknowns are of two kinds: the reactions $\mathbf{f}_R \in \mathbb{R}^{2n_n - n_{\text{dof}}}$ acting at the prescribed displacements, and, on the contrary, the displacement field $\mathbf{u} \in \mathbb{R}^{n_{\text{dof}}}$ for Neumann data.

3.6.1 Equilibrium Equation

Without loss of generality, the equilibrium equations

$$\mathbf{K}_S \mathbf{u}_S = \mathbf{f}_S \quad (3.80)$$

can be reordered and decomposed into smaller parts, corresponding to the boundary conditions, such that

$$\begin{pmatrix} \mathbf{K} & \mathbf{K}_{uR} \\ \mathbf{K}_{Ru} & \mathbf{K}_{RR} \end{pmatrix} \begin{Bmatrix} \mathbf{u} \\ \bar{\mathbf{u}} \end{Bmatrix} = \begin{Bmatrix} \bar{\mathbf{f}} \\ \mathbf{f}_R \end{Bmatrix}. \quad (3.81)$$

Subsequently, the unknown displacement field \mathbf{u} is solved first from

$$\mathbf{u} = \mathbf{K}^{-1} \mathbf{f}, \quad (3.82)$$

where

$$\mathbf{f} = \bar{\mathbf{f}} - \mathbf{K}_{uR} \bar{\mathbf{u}}. \quad (3.83)$$

3.6.2 Minimum to the Potential Energy Function

Based on the boundary conditions, the total potential energy function can be expressed as

$$\Pi(\mathbf{u}) = \frac{1}{2} (\mathbf{u})^T \mathbf{K} \mathbf{u} - (\mathbf{u})^T \mathbf{f}. \quad (3.84)$$

Following Proposition 1, the unknown displacement field is the minimizer of the convex quadratic function with the minimum of $-c$, where

$$c = \frac{1}{2} \mathbf{f}^T \mathbf{u} \quad (3.85)$$

is, again, the so-called compliance.

Chapter 4

Topology Optimization of Truss Structures

Finding optimal structures has always been a challenging task in interest of many researchers, see e.g. (Michell, 1904), (Dorn et al., 1964) and (Bendsøe and Sigmund, 2003); and the references herein. The so-called structural optimization usually aims at achieving one of the following objectives: the structure of minimum weight, the most stiff structure, or the structure as insensitive to instability and buckling as possible (Christensen and Klarbring, 2009).

To narrow the wide range of possibilities in structural optimization, we further focus entirely on optimization of truss structures. Based on employed design variables, optimization of truss structures is, generally, being divided into the following classes: *sizing optimization*, searching for positive cross-sectional areas of fixed truss elements; *shape optimization*, assuming fixed nodal connectivity and optimizing solely position of nodes, hence exploring optimal structural shape, see Fig 4.1c for an example, and *topology optimization*. The latter is in focus of this thesis, and resembles the sizing optimization, but additionally permits the cross-sectional areas to become zero, implying some bars might vanish, see Fig. 4.1b.

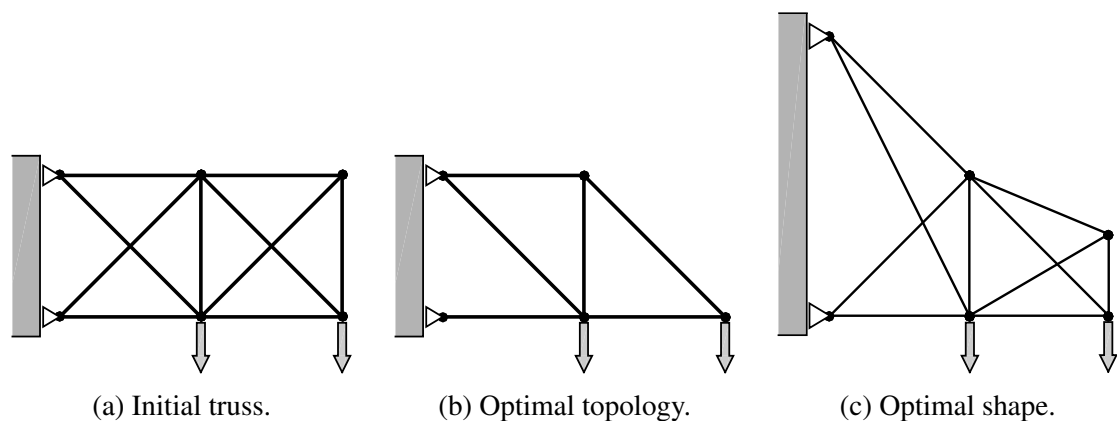


Figure 4.1: Optimization of truss structures. Assuming (a) the initial truss, sample results of (b) topology optimization and (c) shape optimization are displayed.

Albeit differently, both the topology and the shape optimization offer a designer a way to acquire optimal geometry, subsequently both are collectively referred to as *geometry optimization*. Simultaneous optimization of shape and topology is named *layout optimization*.

4.1 Historical Background

Topology optimization of truss structures with continuous design variables has significantly evolved in the recent century, tightly following advances in optimization techniques and algorithms.

Culmann (1875) was probably the first one, who addressed layout optimization of trusses (Prager, 1974). Fundamental properties of optimal grid-like structures were stated by Michell (1904), who derived optimality conditions for least weight trusses subjected to stress constraints and a single loading condition. The developed approach, however, often led to designs containing infinite number of bars, see Fig. 4.2 for an example, making the approach impractical (Prager, 1974).

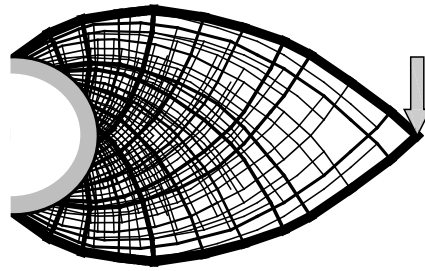


Figure 4.2: An example of Michell's structure.

An approximate solution to the original Michell's approach was introduced by Dorn et al. (1964), who discretized the continuous structural universe (Kirsch, 1989) into a finite-dimensional design domain \mathcal{D} , the so-called ground structure, specifying a finite set of fixed admissible nodes and a finite set of their admissible connections (Bendsøe and Sigmund, 2003), consequently also avoiding the possibility of infinite number of bars; see Fig. 4.3 for an example. Since then, the ground structure method have become the cornerstone of the truss topology optimization.

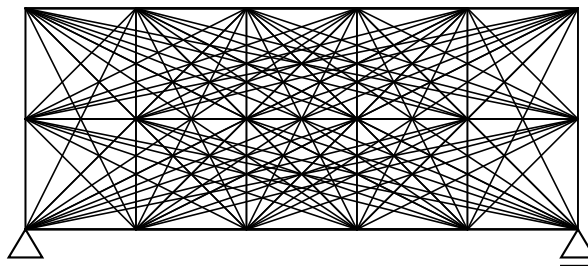


Figure 4.3: Fully connected ground structure.

Following developments in mathematical programming and rise of computers, the minimum-weight design of trusses subjected to a single loading condition was stated as a linear program (Hemp, 1973), efficiently solvable by the simplex method. Because the formulation omits compatibility conditions, the resulting optimal design is also referred to as the plastic design.

In the subsequent years, several trials were made towards an elastic formulation that would be suitable for multiple loading conditions and would permit constraining cross-sectional areas. Majority of attempts, however, relied on nonconvex or heuristic techniques applicable only to small-scale problems, see, e.g., (Kirsch, 1989) for an overview.

The problem of optimal elastic design had remained unsolved until the early 90s, when the originally non-convex elastic formulation was reformulated into a convex quadratic opti-

mization problem solvable by interior-point methods, see (Bendsøe et al., 1991), (Achtziger et al., 1992) and (Ben-Tal and Bendsøe, 1993).

Further, Vandenberghe and Boyd (1996) developed a linear semidefinite programming formulation, allowing straightforward addition of constraints on global buckling (Ben-Tal and Nemirovski, 1997) or free-vibrations (Ohsaki et al., 1999). Finally, Lobo et al. (1998) and Ben-Tal and Nemirovski (2001) introduced second-order cone programming formulation, that is, together with the semidefinite programming formulation, used in this thesis.

4.2 Formulations For Truss Topology Optimization

For historical reasons the existing formulations are traditionally divided into the plastic design, which disregards the compatibility conditions, is applicable only to problems with a single loading condition, and does not allow for constraints on cross-sectional areas; and the elastic design. In the following sections, however, we are going to show that all the common formulations for truss topology optimization are built on the same basis, in particular, and they are special cases of the traditional elastic minimum-compliance formulation

$$\min_{\mathbf{a} \in \mathbb{R}_{\geq 0}^{n_b}, \mathbf{u} \in \mathbb{R}^{n_{\text{dof}}}} \frac{1}{2} \mathbf{f}^T \mathbf{u} \quad (4.1a)$$

$$\text{s.t.} \quad \mathbf{K}(\mathbf{a}) \mathbf{u} = \mathbf{f}, \quad (4.1b)$$

$$\boldsymbol{\ell}^T \mathbf{a} \leq \bar{V}, \quad (4.1c)$$

$$\mathbf{a} \geq \mathbf{0}, \quad (4.1d)$$

or the minimum-volume (weight) formulation

$$\min_{\mathbf{a} \in \mathbb{R}_{\geq 0}^{n_b}, \mathbf{u} \in \mathbb{R}^{n_{\text{dof}}}} \boldsymbol{\ell}^T \mathbf{a} \quad (4.2a)$$

$$\text{s.t.} \quad \mathbf{K}(\mathbf{a}) \mathbf{u} = \mathbf{f}, \quad (4.2b)$$

$$\frac{1}{2} \mathbf{f}^T \mathbf{u} \leq \bar{c}, \quad (4.2c)$$

$$\mathbf{a} \geq \mathbf{0}, \quad (4.2d)$$

where $\mathbf{a} \in \mathbb{R}_{\geq 0}^{n_b}$, $\mathbf{a} = (a_1 \ \dots \ a_{n_b})^T$, denotes a column vector of cross-sectional areas, $\boldsymbol{\ell} \in \mathbb{R}_{> 0}^{n_b}$, $\boldsymbol{\ell} = (\ell_1 \ \dots \ \ell_{n_b})^T$, stands for a column vector containing bar lengths, $\bar{V} \in \mathbb{R}_{> 0}$ is the upper bound on structural volume, and $\bar{c} \in \mathbb{R}_{> 0}$ denotes the upper bound on structural compliance.

The formulation (4.1) searches a minimum-compliant design, compare the objective (4.1a) with Eq. (3.85), subjected to the compatibility conditions (4.1b), volume constraint (4.1c), and non-negativity of cross-sectional areas (4.1d). Similarly, the formulation (4.2) searches a minimum-volume (4.2a) design subjected to the compatibility conditions (4.2b), the bound on structural compliance (4.2c), and non-negativity of cross-sectional areas (4.2d).

It should be noted that the (globally) optimal solution \mathbf{a}^* and \mathbf{u}^* to (4.1) is also (globally) optimal to (4.2) if $\bar{c} = \frac{1}{2} \mathbf{f}^T \mathbf{u}^*$, and conversely (globally) optimal solution \mathbf{a}^* and \mathbf{u}^* to (4.2) is also (globally) optimal to (4.1) if $\bar{V} = \boldsymbol{\ell}^T \mathbf{a}^*$.

Both the formulations (4.1) and (4.2) would be convex and could be solved in the space of cross-sectional areas only, if a positive lower bound had been imposed on \mathbf{a} . In that case $\mathbf{K}(\mathbf{a})$ would have been positive definite and thus \mathbf{u} could be uniquely determined from Eq. (4.1b) or (4.2b) (Svanberg, 1981). However, imposing a lower bound on \mathbf{a} leads to a sizing optimization problem and prohibits any member to vanish, which is the key idea of

the topology optimization. For the truss topology optimization the matrix $\mathbf{K}(\mathbf{a})$ is positive semidefinite, making the formulations non-convex (Bendsøe and Sigmund, 2003) and hard to solve even for small-scale problems (Kočvara and Outrata, 2006).

In the following sections, the initial non-convex problem will be reformulated into equivalent *convex* formulations, providing also globally optimal solution \mathbf{a}^* and \mathbf{u}^* to both the original formulations (4.1) and (4.2).

4.2.1 Quadratic Programming Formulation

Solution to the non-convex optimization problem (4.1) to proven global optimality had been a challenging task until its reformulation to a convex quadratic programming problem, developed by Bendsøe et al. (1991). In the following text the quadratic formulation will be derived, following the approach of (Ben-Tal and Bendsøe, 1993), (Achtziger et al., 1992), and (Kočvara and Zowe, 1996).

Let us firstly recall the potential energy function from Section 3.6.2:

$$\Pi(\mathbf{u}) = \frac{1}{2} \mathbf{u}^T \mathbf{K}(\mathbf{a}) \mathbf{u} - \mathbf{f}^T \mathbf{u}, \quad (4.3)$$

which allows us to rewrite Eq. (4.1) as

$$- \max_{\mathbf{a} \in \mathbb{R}_{\geq 0}^{n_b} \wedge \mathcal{L}^T \mathbf{a} = \bar{\mathbf{V}}} \left[\min_{\mathbf{u} \in \mathbb{R}^{n_{\text{dof}}}} \left(\frac{1}{2} \mathbf{u}^T \mathbf{K}(\mathbf{a}) \mathbf{u} - \mathbf{f}^T \mathbf{u} \right) \right]. \quad (4.4)$$

As already derived, the quadratic potential energy function is convex in \mathbf{u} and thus bounded from below, by negative compliance $-\frac{1}{2} \mathbf{f}^T \mathbf{u}$, recall Eq. (3.47). In order to make the objective positive and equal to (4.1a), negative sign is imposed at the beginning of Eq. (4.4). At the minimum of the quadratic function the compatibility conditions are automatically satisfied, recall Proposition 1, therefore satisfying (4.1b). The max operator is then linear in \mathbf{a} and constrained to satisfy (4.1c) and (4.1d), making the entire problem (4.4) concave-convex and equivalent to (4.1).

Rewriting Eq. (4.4) to remove the leading negative sign, we obtain

$$\min_{\mathbf{a} \in \mathbb{R}_{\geq 0}^{n_b} \wedge \mathcal{L}^T \mathbf{a} = \bar{\mathbf{V}}} \left[\max_{\mathbf{u} \in \mathbb{R}^{n_{\text{dof}}}} \left(\mathbf{f}^T \mathbf{u} - \frac{1}{2} \mathbf{u}^T \mathbf{K}(\mathbf{a}) \mathbf{u} \right) \right], \quad (4.5)$$

that is a convex-concave problem, for which the saddle-point exists and the min and max operators can be conveniently interchanged (Rockafellar, 1997, pp. 393), subsequently leading to

$$\max_{\mathbf{u} \in \mathbb{R}^{n_{\text{dof}}}} \left[\min_{\mathbf{a} \in \mathbb{R}_{\geq 0}^{n_b} \wedge \mathcal{L}^T \mathbf{a} = \bar{\mathbf{V}}} \left(\mathbf{f}^T \mathbf{u} - \frac{1}{2} \mathbf{u}^T \mathbf{K}(\mathbf{a}) \mathbf{u} \right) \right] \quad (4.6)$$

or, in the expanded form,

$$\max_{\mathbf{u} \in \mathbb{R}^{n_{\text{dof}}}} \left[\min_{\mathbf{a} \in \mathbb{R}_{\geq 0}^{n_b} \wedge \mathcal{L}^T \mathbf{a} = \bar{\mathbf{V}}} \left(\mathbf{f}^T \mathbf{u} - \left(\frac{1}{2} \mathbf{u}^T \boldsymbol{\gamma}_1 \frac{E_1}{\ell_1} \boldsymbol{\gamma}_1^T \mathbf{u} \quad \dots \quad \frac{1}{2} \mathbf{u}^T \boldsymbol{\gamma}_{n_b} \frac{E_{n_b}}{\ell_{n_b}} \boldsymbol{\gamma}_{n_b}^T \mathbf{u} \right) \begin{Bmatrix} a_1 \\ \vdots \\ a_{n_b} \end{Bmatrix} \right) \right] \quad (4.7)$$

with the inner part (with fixed \mathbf{u}) being a linear program in terms of \mathbf{a} . Although the stiffness matrix has been expanded into dyadic products, which cannot be done for multiple loading conditions, the following procedure is valid also for the general multiple loading cases, up to minor changes in notation.

The feasible space of the linear program is, from its nature, a polyhedron, implying we need to find its extreme vertex. Due to $\mathbf{f}^T \mathbf{u}$ being fixed for all $i \in \{1 \dots n_b\}$ and $\frac{1}{2} \mathbf{u}^T \boldsymbol{\gamma}_i \frac{E_i}{\ell_i} \boldsymbol{\gamma}_i^T \mathbf{u}$ being a scalar for any $i \in \{1 \dots n_b\}$, the linear program is minimized by assigning all the available material \bar{V} to the member(s) with the maximum specific strain energy $\frac{1}{2} \mathbf{u}^T \boldsymbol{\gamma}_i \frac{E_i}{\ell_i} \boldsymbol{\gamma}_i^T \mathbf{u}$, allowing us to rewrite Eq. (4.7) as

$$\max_{\mathbf{u} \in \mathbb{R}^{n_{\text{dof}}}} \left[\mathbf{f}^T \mathbf{u} - \frac{\bar{V}}{2} \max_{i \in \{1 \dots n_b\}} \left(\mathbf{u}^T \boldsymbol{\gamma}_i \frac{E_i}{\ell_i^2} \boldsymbol{\gamma}_i^T \mathbf{u} \right) \right], \quad (4.8)$$

which is a non-smooth concave quadratic problem (Bendsøe et al., 1994) only in terms of \mathbf{u} . Although the quadratic program (4.8) can be directly treated by non-smooth algorithms (Achtziger et al., 1992), it is more convenient to denote an upper bound on the specific strain energy by $\alpha \in \mathbb{R}_{>0}$, so that

$$\frac{\bar{V}}{2} \mathbf{u}^T \boldsymbol{\gamma}_i \frac{E_i}{\ell_i^2} \boldsymbol{\gamma}_i^T \mathbf{u} \leq \alpha, \quad \forall i \in \{1 \dots n_b\}, \quad (4.9)$$

consequently transforming the problem (4.8) into an equivalent smooth concave linear program with quadratic constraints (Achtziger et al., 1992)

$$\max_{\mathbf{u} \in \mathbb{R}^{n_{\text{dof}}}, \alpha \in \mathbb{R}_{>0}} \mathbf{f}^T \mathbf{u} - \alpha \quad (4.10a)$$

$$\text{s.t.} \quad \frac{\bar{V}}{2} \mathbf{u}^T \boldsymbol{\gamma}_i \frac{E_i}{\ell_i^2} \boldsymbol{\gamma}_i^T \mathbf{u} - \alpha \leq 0, \quad \forall i \in \{1 \dots n_b\}, \quad (4.10b)$$

efficiently solvable by interior-point methods (Jarre et al., 1998).

Theorem 1. *The pair \mathbf{u}^* and α^* solve (4.10) if and only if there exist multipliers $\boldsymbol{\mu}^* \in \mathbb{R}_{\geq 0}^{n_b}$, $\boldsymbol{\mu}^* = (\mu_1 \dots \mu_{n_b})^T$, such that*

$$\mu_i^* = \frac{a_i^* \ell_i}{\bar{V}}, \quad \forall i \in \{1 \dots n_b\}. \quad (4.11)$$

Proof. From the Karush-Kuhn-Tucker conditions we have

$$\boldsymbol{\mu}^* \geq \mathbf{0}, \quad (4.12a)$$

$$-1 = -\sum_{i=1}^{n_b} \mu_i^*, \quad (4.12b)$$

$$\mathbf{f} = \sum_{i=1}^{n_b} \mu_i^* \bar{V} \boldsymbol{\gamma}_i \frac{E_i}{\ell_i^2} \boldsymbol{\gamma}_i^T \mathbf{u}^*. \quad (4.12c)$$

Substituting μ_i^* from Eq. (4.11) into Eq. (4.12) we obtain

$$\frac{a_i^* \ell_i}{\bar{V}} \geq 0, \quad \forall i \in \{1 \dots n_b\}, \quad (4.13a)$$

$$\sum_{i=1}^{n_b} \frac{a_i^* \ell_i}{\bar{V}} = 1, \quad (4.13b)$$

$$\mathbf{f} = \sum_{i=1}^{n_b} \frac{a_i^* \ell_i}{\bar{V}} \bar{V} \boldsymbol{\gamma}_i \frac{E_i}{\ell_i^2} \boldsymbol{\gamma}_i^T \mathbf{u}^*, \quad (4.13c)$$

which is equivalent to

$$\mathbf{a}^* \geq \mathbf{0}, \quad (4.14a)$$

$$\boldsymbol{\ell}^T \mathbf{a}^* = \bar{V}, \quad (4.14b)$$

$$\mathbf{K}(\mathbf{a}^*) \mathbf{u}^* = \mathbf{f}, \quad (4.14c)$$

that are exactly the constraints from Eq. (4.1) and we are done. \square

4.2.2 Linear Programming Formulation

For a single loading condition the element stiffness matrices \mathbf{K}^i are expressed in the form of dyadic products¹. The specific strain energies of individual bars are then equal to

$$\mathbf{u}^T \boldsymbol{\gamma}_i \frac{E_i}{\ell_i^2} \boldsymbol{\gamma}_i^T \mathbf{u} = \left(\frac{\sqrt{E_i}}{\ell_i} \boldsymbol{\gamma}_i^T \mathbf{u} \right)^2, \quad \forall i \in \{1 \dots n_b\}. \quad (4.15)$$

Subsequently, the linear program with quadratic constraints (4.10) can be rewritten as

$$\max_{\mathbf{u} \in \mathbb{R}^{n_{\text{dof}}}, \alpha \in \mathbb{R}_{>0}} \quad \mathbf{f}^T \mathbf{u} - \alpha \quad (4.16a)$$

$$\text{s.t.} \quad \frac{\bar{V}}{2} \left(\frac{\sqrt{E_i}}{\ell_i} \boldsymbol{\gamma}_i^T \mathbf{u} \right)^2 - \alpha \leq 0, \quad \forall i \in \{1 \dots n_b\}. \quad (4.16b)$$

The constraint (4.16b) can then be recast into the form

$$-\sqrt{\alpha} \leq \sqrt{\frac{\bar{V} E_i}{2}} \frac{1}{\ell_i} \boldsymbol{\gamma}_i^T \mathbf{u} \leq \sqrt{\alpha}, \quad \forall i \in \{1 \dots n_b\}. \quad (4.17)$$

Fixing $\alpha = 1$ and removing the constant term α from objective, the following linear program is obtained (Achtziger et al., 1992)

$$\max_{\mathbf{u} \in \mathbb{R}^{n_{\text{dof}}}} \quad \mathbf{f}^T \mathbf{u} \quad (4.18a)$$

$$\text{s.t.} \quad -1 \leq \sqrt{\frac{\bar{V} E_i}{2}} \frac{1}{\ell_i} \boldsymbol{\gamma}_i^T \mathbf{u} \leq 1, \quad \forall i \in \{1 \dots n_b\}. \quad (4.18b)$$

Problem (4.18) is, up to scaling (caused by fixed α), equivalent to Eq. (4.10). The actual scaling factors can be found e.g. in (Achtziger et al., 1992). Note that also the objective (4.18a) is only proportional, but not equal, to the compliance.

Now, writing the dual of Eq. (4.18) we obtain

$$\min_{\mathbf{x}^- \in \mathbb{R}_{\geq 0}^{n_b}, \mathbf{x}^+ \in \mathbb{R}_{\geq 0}^{n_b}} \quad \sum_{i=1}^{n_b} x_i^- + x_i^+ \quad (4.19a)$$

$$\text{s.t.} \quad \sqrt{\frac{\bar{V}}{2}} \begin{pmatrix} -\sqrt{E_1} \frac{1}{\ell_1} \boldsymbol{\gamma}_1^T \\ \vdots \\ -\sqrt{E_{n_b}} \frac{1}{\ell_{n_b}} \boldsymbol{\gamma}_{n_b}^T \\ \sqrt{E_1} \frac{1}{\ell_1} \boldsymbol{\gamma}_1^T \\ \vdots \\ \sqrt{E_{n_b}} \frac{1}{\ell_{n_b}} \boldsymbol{\gamma}_{n_b}^T \end{pmatrix}^T \begin{Bmatrix} \mathbf{x}^- \\ \mathbf{x}^+ \end{Bmatrix} = \mathbf{f}, \quad (4.19b)$$

$$\mathbf{x}^-, \mathbf{x}^+ \geq \mathbf{0}, \quad (4.19c)$$

¹For multiple loading conditions, the element stiffness matrices are block-diagonal matrices constructed from the matrices \mathbf{K}_1^i through $\mathbf{K}_{n_{\text{lc}}}^i$, with n_{lc} denoting the number of loading conditions, hence not allowing explicit dyadic product expression.

which is after substitution² $\bar{\sigma}_i = \sqrt{E_i}$, $x_i^- = \sqrt{\frac{2}{V}} \frac{\ell_i s_i^-}{\bar{\sigma}_i}$, and $x_i^+ = \sqrt{\frac{2}{V}} \frac{\ell_i s_i^+}{\bar{\sigma}_i}$ equivalent to

$$\min_{\mathbf{s}^- \in \mathbb{R}_{\geq 0}^{n_b}, \mathbf{s}^+ \in \mathbb{R}_{\geq 0}^{n_b}} \sqrt{\frac{2}{V}} \sum_{i=1}^{n_b} \frac{s_i^- + s_i^+}{\bar{\sigma}_i} \ell_i \quad (4.20a)$$

$$\text{s.t.} \quad (-\mathbf{A} \quad \mathbf{A}) \begin{Bmatrix} \mathbf{s}^- \\ \mathbf{s}^+ \end{Bmatrix} = \mathbf{f}, \quad (4.20b)$$

$$\mathbf{s}^-, \mathbf{s}^+ \geq \mathbf{0}. \quad (4.20c)$$

After removal of the scaling factor $\sqrt{\frac{2}{V}}$ from the objective function, the linear program reads

$$\min_{\mathbf{s}^- \in \mathbb{R}_{\geq 0}^{n_b}, \mathbf{s}^+ \in \mathbb{R}_{\geq 0}^{n_b}} \sum_{i=1}^{n_b} \frac{s_i^- + s_i^+}{\bar{\sigma}_i} \ell_i \quad (4.21a)$$

$$\text{s.t.} \quad (-\mathbf{A} \quad \mathbf{A}) \begin{Bmatrix} \mathbf{s}^- \\ \mathbf{s}^+ \end{Bmatrix} = \mathbf{f}, \quad (4.21b)$$

$$\mathbf{s}^-, \mathbf{s}^+ \geq \mathbf{0}, \quad (4.21c)$$

with $\bar{\sigma}_i$ denoting a bound on admissible longitudinal stress in the i -th bar, $\mathbf{s}^- \in \mathbb{R}_{\geq 0}^{n_b}$, $\mathbf{s}^- = (s_1^- \dots s_{n_b}^-)^T$ and $\mathbf{s}^+ \in \mathbb{R}_{\geq 0}^{n_b}$, $\mathbf{s}^+ = (s_1^+ \dots s_{n_b}^+)^T$ being column vectors of compressional and tensional axial forces, respectively, such that $\mathbf{s} = \mathbf{s}^+ - \mathbf{s}^-$. Also, note that if $s_i^+ > 0$ for some $i \in \{1 \dots n_b\}$, then $s_i^- = 0$ and, similarly, if $s_i^- > 0$ for some $i \in \{1 \dots n_b\}$, then $s_i^+ = 0$.

After substitution $a_i = \frac{s_i^- + s_i^+}{\bar{\sigma}_i}$, $\forall i \in \{1 \dots n_b\}$, we get

$$\min_{\mathbf{a} \in \mathbb{R}_{\geq 0}^{n_b}, \mathbf{s} \in \mathbb{R}^{n_b}} \boldsymbol{\ell}^T \mathbf{a} \quad (4.22a)$$

$$\text{s.t.} \quad \mathbf{A} \mathbf{s} = \mathbf{f}, \quad (4.22b)$$

$$-\bar{\sigma}_i a_i \leq s_i \leq \bar{\sigma}_i a_i, \quad \forall i \in \{1 \dots n_b\}, \quad (4.22c)$$

$$\mathbf{a} \geq \mathbf{0}, \quad (4.22d)$$

which is the traditional minimum-volume (weight) plastic design formulation, see e.g. (Dorn et al., 1964) or (Hemp, 1973).

For the plastic formulation the optimal design is fully stressed and statically determinate, i.e. the optimal-design static matrix \mathbf{A} is regular and the axial forces thus uniquely determined (Rozvany et al., 2014).

Proposition 2. *The least volume truss subjected to stress constraints and a single loading condition is fully-stressed.*

Proof. Let us begin with a contradiction that there exists a truss element i strictly satisfying

$$-\bar{\sigma}_i < \sigma_i < \bar{\sigma}_i, \quad (4.23)$$

with σ_i being the actual stress in the i -th element.

Based on linear elasticity, recall Eq. (3.5), the relation between axial force and stress is stated as

$$a_i = \frac{s_i}{\sigma_i}. \quad (4.24)$$

²Note that the units of the scaled variables from Eq. (4.18b) are also scaled.

Built upon this equation, we can directly state the relation of the lower bound for cross-sectional area a_i on the admissible longitudinal stress bound $\bar{\sigma}$, such that

$$a_{\min,i} = \begin{cases} \frac{-s_i}{\bar{\sigma}_i} & \text{for } s_i \leq 0 \\ \frac{s_i}{\bar{\sigma}_i} & \text{for } s_i \geq 0 \end{cases}. \quad (4.25)$$

If the truss element is in compression, then it holds, based on the contradiction, that

$$\frac{s_i}{\sigma_i} > \frac{-s_i}{\bar{\sigma}_i}, \quad (4.26)$$

which is equivalent to

$$a_i > a_{\min,i}. \quad (4.27)$$

Similarly, if the truss element is in tension, it holds that

$$\frac{s_i}{\sigma_i} > \frac{s_i}{\bar{\sigma}_i}, \quad (4.28)$$

which is equivalent to

$$a_i > a_{\min,i}. \quad (4.29)$$

Due to the cross-sectional areas being constrained only by the stress bounds and their non-negativity, recall Eq. (4.22), the not-fully-stressed truss simply cannot be the least volume, as the cross-sectional area of the i -th element could be further reduced to the corresponding $a_{\min,i}$ value, making the truss lighter. \square

Finally, we conclude that the plastic formulation does not state any compatibility or stress-strain relation, so that the forces are not distributed with respect to individual element stiffnesses. Considering a single loading condition and no constraints on the cross-sectional areas, the plastic formulation leads to fully-stressed statically determinate optimal design, consequently automatically satisfying the compatibility conditions (Bendsøe and Sigmund, 2003). For multiple loading conditions or when another constraints on cross-sectional areas are imposed (positive lower bound, upper bound or their equality), the linear programming formulation cannot be used.

4.2.3 Second-Order Cone Programming Formulation

Second-order cone programming is a field of mathematical programming that covers linear programming, and convex quadratic programming with the addition of second-order cone constraints (Boyd and Vandenberghe, 2004).

The second-order cone formulation for truss topology optimization was firstly derived from a potential energy function in (Ben-Tal and Nemirovski, 2001) and (Lobo et al., 1998), another derivation based on complementary energy was published in (Makrodimopoulos et al., 2010).

In order to derive the second-order cone program, we will firstly modify the linear program with quadratic constraints, recall Eq. (4.10), to

$$\max_{\mathbf{u} \in \mathbb{R}^{n_{\text{dof}}}, \alpha \in \mathbb{R}_{>0}} \mathbf{f}^T \mathbf{u} - \alpha \quad (4.30a)$$

$$\text{s.t.} \quad \left(\frac{\sqrt{2\bar{V}E_i}}{2\ell_i} \boldsymbol{\gamma}_i^T \mathbf{u} \right)^2 - \alpha \leq 0, \quad \forall i \in \{1 \dots n_b\}. \quad (4.30b)$$

Such a formulation can be readily stated as a second-order cone program, because quadratic programming is a subset of second-order cone programming. Based on (Ben-Tal and Nemirovski, 2001, pp. 88) we can write

$$\max_{\mathbf{u} \in \mathbb{R}^{n_{\text{dof}}}, \alpha \in \mathbb{R}_{>0}} \mathbf{f}^T \mathbf{u} - \alpha \quad (4.31a)$$

$$\text{s.t.} \quad \left\| \begin{pmatrix} \frac{\sqrt{2V E_i}}{2\ell_i} \boldsymbol{\gamma}_i^T \mathbf{u} \\ \frac{\alpha - 1}{2} \end{pmatrix} \right\|_2 \leq \frac{\alpha + 1}{2}, \quad \forall i \in \{1 \dots n_b\}, \quad (4.31b)$$

where the notation $\|\cdot\|_2$ denotes the Euclidean norm, so that the constraints (4.31b) form second-order cones.

Now that we have stated the second-order cone program, we state its dual as

$$\min_{\mathbf{a} \in \mathbb{R}_{\geq 0}^{n_b}, \mathbf{w} \in \mathbb{R}_{\geq 0}^{n_b}, \mathbf{s} \in \mathbb{R}^{n_b}} \sum_{i=1}^{n_b} \mathbf{w}_i \quad (4.32a)$$

$$\text{s.t.} \quad \boldsymbol{\ell}^T \mathbf{a} \leq \bar{V}, \quad (4.32b)$$

$$\sum_{i=1}^{n_b} s_i \boldsymbol{\gamma}_i = \mathbf{f}, \quad (4.32c)$$

$$\left\| \begin{pmatrix} w_i - a_i \\ \sqrt{\frac{2\ell_i}{E_i}} s_i \end{pmatrix} \right\|_2 \leq w_i + a_i, \quad \forall i \in \{1 \dots n_b\}, \quad (4.32d)$$

$$\mathbf{a} \geq \mathbf{0}, \quad (4.32e)$$

where the design variables are the cross-sectional areas \mathbf{a} , complementary strain energy $\mathbf{w} \in \mathbb{R}^{n_b}$, $\mathbf{w} = (w_1 \dots w_{n_b})^T$, and the axial forces \mathbf{s} .

Compared to the quadratic programming formulation, the second-order cone program (4.32) explicitly uses the cross-sectional areas as its primal variables, which is very convenient when the cross-sectional areas are subjected to additional constraints.

4.2.4 Semidefinite Programming Formulation

Semidefinite programming is a subset of convex optimization that includes linear, quadratic and conic programming, with addition of semidefinite cones, implying its greater generality. Subsequently, any linear, quadratic or conic program can be equivalently cast as a semidefinite program.

Even the traditional elastic truss topology formulation was reformulated to semidefinite programming. To the author's knowledge, the formulation originates in (Vandenberghe and Boyd, 1996), but commonly (Ben-Tal and Nemirovski, 1997) is being referenced. The reformulation to a convex linear semidefinite program then reads

$$\min_{\mathbf{a} \in \mathbb{R}_{\geq 0}^{n_b}, \tau \in \mathbb{R}_{\geq 0}} \frac{1}{2} \tau \quad (4.33a)$$

$$\text{s.t.} \quad \begin{pmatrix} \tau & -\mathbf{f}^T \\ -\mathbf{f} & \mathbf{K}(\mathbf{a}) \end{pmatrix} \succeq \mathbf{0}, \quad (4.33b)$$

$$\boldsymbol{\ell}^T \mathbf{a} \leq \bar{V}, \quad (4.33c)$$

$$\mathbf{a} \geq \mathbf{0}, \quad (4.33d)$$

where the linear matrix inequality " $\mathbf{X} \succeq \mathbf{0}$ " denotes the requirement of a matrix \mathbf{X} to be positive semidefinite.

Comparing Eq. (4.1) with Eq. (4.33) it is obvious that Eq. (4.1c) equals to Eq. (4.33c) and Eq. (4.1d) is identical to Eq. (4.33d). Subsequently, we only need to prove the following theorem. Similar proof can also be found in (Achtziger and Kočvara, 2008), (Ben-Tal and Nemirovski, 1997) or (Ohsaki et al., 1999).

Theorem 2. Let $\mathbf{a} \in \mathbb{R}_{\geq 0}^{n_b}$ denote a column vector of cross-sectional areas and $\tau \in \mathbb{R}_{\geq 0}$. Then, there exist $\mathbf{u}^* \in \mathbb{R}^{n_{\text{dof}}}$ satisfying $\mathbf{f}^T \mathbf{u}^* \leq \tau$ and $\mathbf{K}(\mathbf{a})\mathbf{u}^* = \mathbf{f}$ if and only if

$$\begin{pmatrix} \tau & -\mathbf{f}^T \\ -\mathbf{f} & \mathbf{K}(\mathbf{a}) \end{pmatrix} \succeq \mathbf{0}. \quad (4.34)$$

Proof. Based on the definition of positive semidefiniteness we can equivalently write

$$\begin{pmatrix} \beta \\ \mathbf{v} \end{pmatrix}^T \begin{pmatrix} \tau & -\mathbf{f}^T \\ -\mathbf{f} & \mathbf{K}(\mathbf{a}) \end{pmatrix} \begin{pmatrix} \beta \\ \mathbf{v} \end{pmatrix} \geq 0, \quad \forall \beta \in \mathbb{R} \setminus 0, \forall \mathbf{v} \in \mathbb{R}^{n_{\text{dof}}} \setminus \mathbf{0}, \quad (4.35)$$

which expands into

$$\beta^2 \tau - 2\beta \mathbf{f}^T \mathbf{v} + \mathbf{v}^T \mathbf{K}(\mathbf{a}) \mathbf{v} \geq 0, \quad \forall \beta \in \mathbb{R} \setminus 0, \forall \mathbf{v} \in \mathbb{R}^{n_{\text{dof}}} \setminus \mathbf{0}. \quad (4.36)$$

Since $\beta \neq 0$ by definition and $\beta^2 > 0$, Eq. (4.36) can be divided by β^2 , leading to

$$\tau - 2\mathbf{f}^T \left(\frac{\mathbf{v}}{\beta} \right) + \left(\frac{\mathbf{v}}{\beta} \right)^T \mathbf{K}(\mathbf{a}) \left(\frac{\mathbf{v}}{\beta} \right) \geq 0, \quad \forall \beta \in \mathbb{R} \setminus 0, \forall \mathbf{v} \in \mathbb{R}^{n_{\text{dof}}} \setminus \mathbf{0}, \quad (4.37)$$

which is after substitution $\mathbf{w} = \frac{\mathbf{v}}{\beta}$ equal to

$$\tau - 2\mathbf{f}^T \mathbf{w} + \mathbf{w}^T \mathbf{K}(\mathbf{a}) \mathbf{w} \geq 0, \quad \forall \mathbf{w} \in \mathbb{R}^{n_{\text{dof}}} \setminus \mathbf{0}. \quad (4.38)$$

In order to make the above inequality (4.38) valid $\forall \mathbf{w} \in \mathbb{R}^{n_{\text{dof}}} \setminus \mathbf{0}$, we actually need that

$$\min_{\mathbf{w} \in \mathbb{R}^{n_{\text{dof}}} \setminus \mathbf{0}} (\tau - 2\mathbf{f}^T \mathbf{w} + \mathbf{w}^T \mathbf{K}(\mathbf{a}) \mathbf{w}) \geq 0, \quad (4.39)$$

which can be equivalently written as

$$\min_{\mathbf{w} \in \mathbb{R}^{n_{\text{dof}}} \setminus \mathbf{0}} \left[\tau + 2 \left(\frac{1}{2} \mathbf{w}^T \mathbf{K}(\mathbf{a}) \mathbf{w} - \mathbf{f}^T \mathbf{w} \right) \right] \geq 0, \quad (4.40)$$

with the potential energy function $\Pi(\mathbf{u})$ being in the parentheses, recall Section 3.6.2. Therefore, Eq. (4.40) is convex, minimized at $\mathbf{K}(\mathbf{a})\mathbf{u}^* = \mathbf{f}$ by $\mathbf{w} = \mathbf{u}^*$ and bounded from below by negative compliance $-\frac{1}{2}\mathbf{f}^T \mathbf{u}^*$. In consequence, this proves that the compatibility conditions (4.1b) are satisfied.

Subsequently, we can further write

$$\tau + 2 \left(-\frac{1}{2} \mathbf{f}^T \mathbf{u}^* \right) \geq 0, \quad (4.41)$$

implying that

$$\tau \geq \mathbf{f}^T \mathbf{u}^*, \quad (4.42)$$

and proving that τ is lower-bounded by doubled compliance $\mathbf{f}^T \mathbf{u}^*$, making the proof complete. \square

Similarly to the minimum compliance formulation, the minimum-volume formulation, see Eq. (4.2), can be also cast as a linear semidefinite program

$$\min_{\mathbf{a} \in \mathbb{R}_{\geq 0}^{n_b}, \tau \in \mathbb{R}_{\geq 0}} \ell^T \mathbf{a} \quad (4.43a)$$

$$\text{s.t.} \quad \begin{pmatrix} \tau & -\mathbf{f}^T \\ -\mathbf{f} & \mathbf{K}(\mathbf{a}) \end{pmatrix} \succeq \mathbf{0}, \quad (4.43b)$$

$$\tau \leq 2\bar{c}, \quad (4.43c)$$

$$\mathbf{a} \geq \mathbf{0}. \quad (4.43d)$$

The advantage of the semidefinite programming reformulations of topology optimization consists in its ability to easily add constraints on fundamental free-vibrations (Achtziger and Kočvara, 2008) and global buckling (Ben-Tal and Nemirovski, 1997), both preserving convexity of the optimization problem.

Chapter 5

Extension of Topology Optimization to Modular Trusses

While there exist several objectives in optimal design of truss structures, recall for example the minimum-compliant or the least-volume design introduced in the previous chapter, they are driven by the same demand—effort of an investor to be economical. Note that these objectives express such a desire only approximately, as the actual optimization problem would be significantly more complex otherwise. Although finding an optimal topology to a given ground structure through any of the already developed formulations significantly reduces the total costs with respect to the material usage, excessive number of present bars (Asadpoure et al., 2015), as well as the multitude of varied cross-sectional areas (Kanno, 2016) also have a considerable influence on the construction economy.

In practice, the established problem is usually solved by designing prefabricated *modular structures*. Modularity represents an approach of partitioning the complex structure into several simpler repeated units, so-called modules, allowing for their independent mass-production in high-controlled facilities (Mikkola, 2003). The controlled manufacturing allows for better quality control and leads to significant time savings in the building phases, as the production and construction can be carried out concurrently (Tugilimana et al., 2016).

Throughout this chapter two of the previously established formulations of truss topology optimization will be enhanced to facilitate partitioning of a given ground structure into a set of (identical) modules. The extension limits the number of unique continuous cross-sectional areas and permits the subsequent development of bilevel modular-topology optimization framework that will be introduced in the following chapter.

5.1 Group Vector and Group Matrix

In order to introduce notation and the theory valid for topology optimization of modular trusses (Pospíšilová and Lepš, 2013), the fundamentals are going to be established for the most simple, yet illustrative, case of each module containing exactly one single bar.

Let us consider a ground structure consisting of $n_b \in \mathbb{Z}_{>0}$ bars and a condition restricting the count of *unique* cross-sectional areas to the number $n_g \in \mathbb{Z}_{>0}$, $n_g \leq n_b$. Further, let $\mathbf{a}_g \in \mathbb{R}_{\geq 0}^{n_g}$ denote a column vector of unique cross-sectional areas. Then, for each bar $i \in \{1 \dots n_b\}$ there exists a number $g_i \in \mathbb{Z}_{>0}$ assigning the g_i -th element of the unique cross-sectional areas column vector \mathbf{a}_g to the bar i , such that

$$1 \leq g_i \leq n_g, \quad \forall i \in \{1 \dots n_b\}. \quad (5.1)$$

Subsequently, the group vector $\mathbf{g} \in \mathbb{Z}_{>0}^{n_b}$ is defined as $\mathbf{g} = (g_1 \dots g_{n_b})^T$.

Following the definition of the group vector, let the group matrix $\mathbf{G} \in \{0,1\}^{n_b \times n_g}$ be defined $\forall i \in \{1 \dots n_b\}$ and $\forall j \in \{1 \dots n_g\}$ as

$$\mathbf{G}_{i,j} = \begin{cases} 0 & \text{for } j \neq g_i, \\ 1 & \text{for } j = g_i, \end{cases} \quad (5.2)$$

with $\mathbf{G}_{i,j}$ denoting i -th row and j -th column of the matrix \mathbf{G} . The group matrix is a linear transformation matrix mapping the space of unique cross-sectional areas $\mathbf{a}_g \in \mathbb{R}_{\geq 0}^{n_g}$ to the space of cross-sectional areas $\mathbf{a} \in \mathbb{R}_{\geq 0}^{n_b}$, so that it holds

$$\mathbf{a} = \mathbf{G}\mathbf{a}_g. \quad (5.3)$$

Note that if $n_g = n_b$ the problem simplifies back to the non-modular design.

5.1.1 Illustrative Example

Let us evaluate a simple truss structure, as shown in Fig. 5.1, to demonstrate the developed approach. The truss is assembled from three bars, n_b thus being equal to 3. While the bars $\boxed{1}$ and $\boxed{3}$ are both being assigned an identical cross-sectional area a_1 , the cross-sectional area of the bar $\boxed{2}$ equals a_2 .

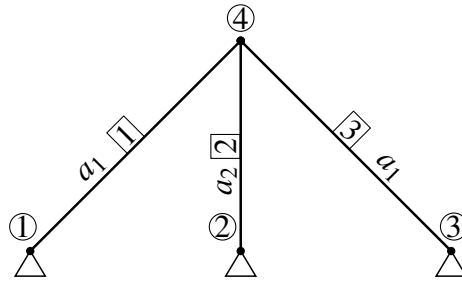


Figure 5.1: Modular truss structure composed of three bars.

For this specific settings $n_g = 2$ and

$$\mathbf{a}_g = \begin{Bmatrix} a_1 \\ a_2 \end{Bmatrix}. \quad (5.4)$$

The group vector then takes the form

$$\mathbf{g} = (1 \quad 2 \quad 1)^T \quad (5.5)$$

and the corresponding group matrix reads

$$\mathbf{G} = \begin{pmatrix} 1 & 0 \\ 0 & 1 \\ 1 & 0 \end{pmatrix}. \quad (5.6)$$

Finally, the original vector of cross-sectional areas is obtained as

$$\mathbf{a} = \mathbf{G}\mathbf{a}_g = \begin{pmatrix} 1 & 0 \\ 0 & 1 \\ 1 & 0 \end{pmatrix} \begin{Bmatrix} a_1 \\ a_2 \end{Bmatrix} = \begin{Bmatrix} a_1 \\ a_2 \\ a_1 \end{Bmatrix}. \quad (5.7)$$

5.2 Complex Modules

Let us assume a fixed structural design domain \mathcal{D} partitioned into square truss modules with fixed orientation, refer to Fig. 5.2a, and let $n_{t,x}$ and $n_{t,y}$ denote the number of modules in horizontal and in vertical direction, respectively. The modularity implies that the number of unique modules n_t needs to be lower than $n_{t,x} \cdot n_{t,y}$. In the following text all adjacent modules are by definition compatible across the corresponding edges, in the sense of constituting a statically admissible ground structure.

In order to secure compatibility of modules, the bars within each module are divided into three sets. The bars located exclusively inside a module, so-called *tile-associated* bars, belong entirely to the specific module, schematically colored by white in Fig. 5.2b and drawn with solid black lines in Fig. 5.2c. The second and the third sets contain bars that overlap module boundaries. In order to preserve constant cross-sectional area of the interdomain bars along their length, they need to belong to multiple modules. The *vertex-associated* bars, coming strictly through a vertex of a module, imply they are bound to all the surrounding modules sharing the same vertex. Common location of such bars is illustrated in the dark gray color in Fig. 5.2b. Finally, the bars that intersect only an edge of a module, so-called *edge associated* bars, belong to both modules sharing the edge, as schematically denoted by the light gray color in Fig. 5.2b and plotted by dashed lines in Fig. 5.2c.

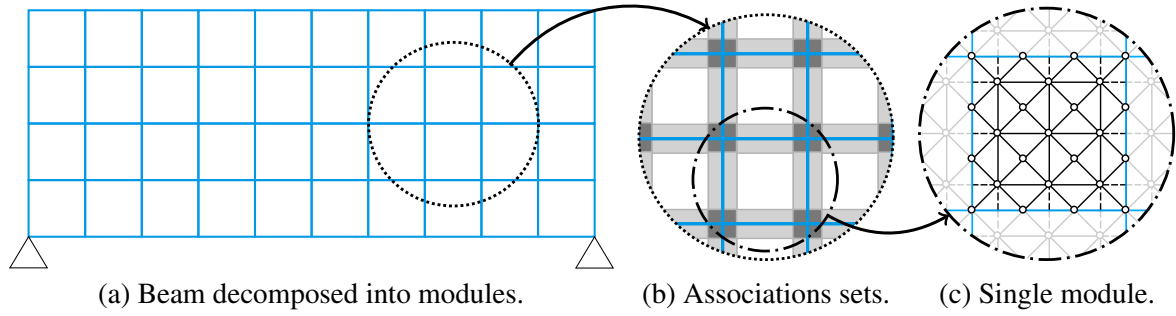


Figure 5.2: (a) Partitioning of design domain into several modules. (c) Bars forming each module are split into (b) three sets—tile-associated, edge-associated and vertex-associated.

5.2.1 Structural Modularity Using Wang Tiles

In the worst-case scenario when each module type is adjacent to all module types, a structure composed of instances from a set of n_t unique modules can contain n_t^2 types of distinct vertical edges, n_t^2 types of various horizontal edges and especially n_t^4 types of particular vertices. The polynomial growth makes handling and, in particular, prefabricating such products impractical.

The outlined difficulty is, however, readily eliminated adopting the concept of vertex-based Wang tiles over two colors, recall Chapter 2, implying $n_t = 16$, constraining the number of unique vertices to 2, and fixing the count of distinct horizontal and vertical edges to 4. Wang tiles then provide jigsaw-like compatibility of tiles (modules), while simultaneously allowing for aperiodic assemblies.

From this moment forth, we will consider all tiles from the complete tile set, recall Fig. 2.6a, having the same *tile ground structure*, depicted in Fig. 5.2c. Following the already described approach, the bars in tile ground structures are divided into the association sets. In this particular case of the tile ground structure, there are only the tile-associated and the edge-associated bars, refer to Fig. 5.3.

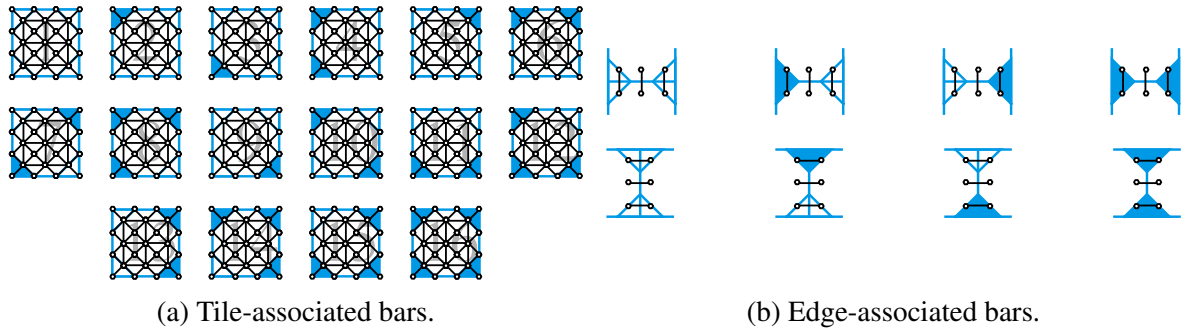


Figure 5.3: Division of bars into (a) tile-associated and (b) edge-associated sets. The scattered points represent nodes.

Assuming a fixed assembly defined by the connectivity matrix $\mathbf{C} \in \{0, 1\}^{(n_{t,y}+1) \times (n_{t,x}+1)}$, we can further assign a group to each bar and, subsequently, assemble the group vector $\mathbf{g}(\mathbf{C})$ and the group matrix $\mathbf{G}(\mathbf{C})$, by a direct analogy to Section 5.1. Each tile from the complete tile set contains 48 tile-associated bars, yielding $16 \times 48 = 768$ groups of tile-associated bars in total, recall Fig. 5.3a. Similarly, each edge, either horizontal or vertical, accommodates 3 edge-associated bars, leading to $8 \times 3 = 24$ groups of edge-associated bars, recall Fig. 5.3b. Consequently, we have $n_g = 792$ for this specific choice of the tile set and the tile ground structure.

5.3 Generalization of Topology Optimization Formulations

In order to provide a framework for topology optimization of modular trusses, the established formulations for topology optimization need to be modified. Modularity is inherently prescribed in terms of constraints on cross-sectional areas. As a result, only formulations with the cross-sectional areas as primal design variables can be straightforwardly modified. It should be further noted that the linear programming *plastic design* prohibits addition of such constraints, because their imposing leads to violating the statical determinacy and the compatibility conditions of the optimal design.

5.3.1 Second-Order Cone Programming

With the cross-sectional areas governed by Eq. (5.3), the volume constraint (4.32b) transforms into

$$\ell^T \mathbf{G}(\mathbf{C}) \mathbf{a}_g \leq \bar{V} \quad (5.8)$$

and the second-order cone constraints (4.32d) then reads as

$$\left\| \begin{pmatrix} w_i - a_{g,g_i(\mathbf{C})} \\ \sqrt{\frac{2\ell_i}{E_i}} s_i \end{pmatrix} \right\|_2 \leq w_i + a_{g,g_i(\mathbf{C})}, \quad \forall i \in \{1 \dots n_b\}, \quad (5.9)$$

with $a_{g,g_i(\mathbf{C})}$ denoting the $g_i(\mathbf{C})$ -th element of the vector \mathbf{a}_g . The final formulation of topology optimization with modular trusses written as second-order cone program is then

$$\min_{\mathbf{a}_g \in \mathbb{R}^{n_g}, \mathbf{w} \in \mathbb{R}^{n_b}, \mathbf{s} \in \mathbb{R}^{n_b}} \sum_{i=1}^{n_b} w_i \quad (5.10a)$$

$$\text{s.t. } \boldsymbol{\ell}^T \mathbf{G}(\mathbf{C}) \mathbf{a}_g \leq \bar{V}, \quad (5.10b)$$

$$\sum_{i=1}^{n_b} s_i \boldsymbol{\gamma}_i = \mathbf{f}, \quad (5.10c)$$

$$\left\| \begin{pmatrix} w_i - a_{g,g_i(\mathbf{C})} \\ \sqrt{\frac{2\ell_i}{E_i}} s_i \end{pmatrix} \right\|_2 \leq w_i + a_{g,g_i(\mathbf{C})}, \quad \forall i \in \{1 \dots n_b\}, \quad (5.10d)$$

$$\mathbf{a}_g \geq \mathbf{0}. \quad (5.10e)$$

5.3.2 Semidefinite Programming

Compared to the second-order cone program, generalization of the semidefinite programming formulation in order to include modularity requires modification of the structural stiffness matrix assembly:

$$\mathbf{K}(\mathbf{a}_g, \mathbf{C}) = \sum_{j=1}^{n_g} \left(\sum_{i=1}^{n_b} \mathbf{K}^i(a_{g,j}) [j = g_i(\mathbf{C})] \right), \quad (5.11)$$

with $a_{g,j}$ denoting the j -th element of the vector \mathbf{a}_g . Consequently, the minimum-compliance semidefinite program (4.33) extended to structural modularity takes the following form:

$$\min_{\mathbf{a}_g \in \mathbb{R}_{\geq 0}^{n_g}, \tau \in \mathbb{R}_{\geq 0}} \frac{1}{2} \tau \quad (5.12a)$$

$$\text{s.t. } \begin{pmatrix} \tau & -\mathbf{f}^T \\ -\mathbf{f} & \mathbf{K}(\mathbf{a}_g, \mathbf{C}) \end{pmatrix} \succeq \mathbf{0}, \quad (5.12b)$$

$$\boldsymbol{\ell}^T \mathbf{G}(\mathbf{C}) \mathbf{a}_g \leq \bar{V}, \quad (5.12c)$$

$$\mathbf{a}_g \geq \mathbf{0}. \quad (5.12d)$$

Similarly, the minimum-volume semidefinite program (4.43) reads as

$$\min_{\mathbf{a}_g \in \mathbb{R}_{\geq 0}^{n_g}, \tau \in \mathbb{R}_{\geq 0}} \boldsymbol{\ell}^T \mathbf{G}(\mathbf{C}) \mathbf{a}_g \quad (5.13a)$$

$$\text{s.t. } \begin{pmatrix} \tau & -\mathbf{f}^T \\ -\mathbf{f} & \mathbf{K}(\mathbf{a}_g, \mathbf{C}) \end{pmatrix} \succeq \mathbf{0}, \quad (5.13b)$$

$$\tau \leq 2\bar{c}, \quad (5.13c)$$

$$\mathbf{a}_g \geq \mathbf{0}. \quad (5.13d)$$

Chapter 6

Modular-Topology Optimization

In the previous chapter two straightforward convex minimum-compliance formulations were developed, allowing for optimization of modular trusses with fixed assembly plan, denoted by the connectivity matrix \mathbf{C} . Because the matrix \mathbf{C} needs to be specified in advance, quality of the optimal solution highly depends on the provided connectivity matrix. Note that the number of all potential connectivity matrices increases exponentially with the size of \mathbf{C} , through so-called combinatorial explosion, making manual specification of a “good” connectivity matrix from scratch extremely problematic.

For these reasons, this chapter introduces bilevel formulation of the *modular-topology* optimization problem, optimizing simultaneously topology of individual modules and the assembly plan. The optimization problem is approximately solved with combination of meta-heuristics and mathematical programming methods, circumventing the need for a priori given connectivity matrix.

6.1 Minimum Compliance Problem Statement

Let \mathbf{C} be gradually fixed for all the $2^{(n_{t,y}+1) \times (n_{t,x}+1)}$ possible combinations of assemblies. Then, the bilevel optimization problem that simultaneously optimizes the assembly and topology of modules, using the second-order cone programming formulation (5.10), reads as

$$\min_{\mathbf{C} \in \{0,1\}^{(n_{t,y}+1) \times (n_{t,x}+1)}} \sum_{i=1}^{n_b} w_i \quad (6.1a)$$

$$\mathbf{w} = \underset{\mathbf{a}_g \in \mathbb{R}_{\geq 0}^{n_g}, \mathbf{w} \in \mathbb{R}_{> 0}^{n_b}, \mathbf{s} \in \mathbb{R}^{n_b}}{\operatorname{argmin}} \sum_{i=1}^{n_b} w_i \quad (6.1b)$$

$$\text{s.t.} \quad \boldsymbol{\ell}^T \mathbf{G}(\mathbf{C}) \mathbf{a}_g \leq \bar{V}, \quad (6.1c)$$

$$\sum_{i=1}^{n_b} s_i \boldsymbol{\gamma}_i = \mathbf{f}, \quad (6.1d)$$

$$\left\| \begin{pmatrix} w_i - a_{g,gi}(\mathbf{C}) \\ \sqrt{\frac{2\ell_i}{E_i}} s_i \end{pmatrix} \right\|_2 \leq w_i + a_{g,gi}(\mathbf{C}), \quad \forall i \in \{1 \dots n_b\}, \quad (6.1e)$$

$$\mathbf{a}_g \geq \mathbf{0}. \quad (6.1f)$$

Equivalently, the optimization problem can be posed using the semidefinite programming formulation (5.12) in the form

$$\min_{\mathbf{C} \in \{0,1\}^{(n_{t,y}+1) \times (n_{t,x}+1)}} \frac{1}{2} \tau \quad (6.2a)$$

$$\tau = \underset{\mathbf{a}_g \in \mathbb{R}_{\geq 0}^{n_g}, \tau \in \mathbb{R}_{>0}}{\operatorname{argmin}} \frac{1}{2} \tau \quad (6.2b)$$

$$\text{s.t. } \ell^T \mathbf{G}(\mathbf{C}) \mathbf{a}_g \leq \bar{V}, \quad (6.2c)$$

$$\begin{pmatrix} \tau & -\mathbf{f}^T \\ -\mathbf{f} & \mathbf{K}(\mathbf{a}_g, \mathbf{C}) \end{pmatrix} \succeq \mathbf{0}, \quad (6.2d)$$

$$\mathbf{a}_g \geq \mathbf{0}. \quad (6.2e)$$

Both (6.1) and (6.2) are NP-hard combinatorial-convex optimization problems, solved with (i) the globally optimal connectivity matrix \mathbf{C}^* and with (ii) the globally optimal vector of unique cross-sectional areas \mathbf{a}_g^* at the globally optimal compliance c^* . Due to the nature of both the problems, there is no deterministic polynomial time algorithm for their solution if $P \neq NP$. Consequently, a direct solution rests on enumeration of the combinations, making the solution challenging even for small-scale problems. Therefore, in the following sections we adopt two popular meta-heuristic approaches—the genetic algorithm (Holland, 1992) and the simulated annealing (Kirkpatrick et al., 1983), (Černý, 1985)—leading to solutions near the global optimum in a reasonable time.

6.1.1 Bounds on the Global Optimum

The structural modularity comes at a price of increase, i.e. worse, compliance compared to the non-modular design (Huang and Xie, 2008). Consequently, the non-modular “ideal” design with compliance $c_1 \in \mathbb{R}_{>0}$ represents a lower bound on the optimal solution c^* for both the bilevel programs (6.1) and (6.2). In the case when all the tiles from the tile set are defined equal tile ground structures, the ideal compliance is stated as the optimum to the non-modular topology optimization, i.e. the quadratically-constrained linear program (4.10), the second-order cone program (4.32) or the semidefinite program (4.33). Otherwise, if the tile ground structures are varied among tile types, a fictitious ideal tile needs to be created, whose tile ground structure is defined as unification of tile ground structures of all the tiles in the complete tile set. Assembling the fictitious ideal tiles, such that the partitioned structural domain is entirely filled, leads to the most complex ground structure virtually feasible. Finally, the ideal compliance is obtained through topology optimization of just defined ground structure without imposing modularity.

Similarly to the ideal compliance, the upper-bound anti-ideal compliance $c_{AI} \in \mathbb{R}_{>0}$ can be straightforwardly obtained when all the tiles in the complete tile set are assigned equal tile ground structure. Then, the upper-bound worst-case compliance is computed by solving topology optimization of the ground structure composed of only one tile type, i.e. the connectivity matrix \mathbf{C} containing all zeros or all ones, through the second-order cone (5.10) or the semidefinite (5.12) program. On the contrary, when the tiles contain distinct tile ground structures, we need a definition of a fictitious anti-ideal tile, whose tile ground structure equals to the intersection of tile ground structures of all tiles from the complete tile set. The least complex ground structure is then composed by assembling the partitioned design domain entirely from the fictitious anti-ideal tile. The upper-bound compliance c_{AI} is finally obtained through solution of the just defined topology optimization problem of a modular truss structure, consisting of a single repeatedly placed module.

The value of the global minimum c^* is thus constrained by

$$c_I \leq c^* \leq c_{AI}. \quad (6.3)$$

6.2 Meta-Heuristic Algorithms

The term *meta-heuristics*, introduced by Glover (1986), covers optimization algorithms, often nature inspired, that provide a master strategy for modification and guiding heuristics towards solutions beyond the scope of local optimality (Glover and Laguna, 1999). Therefore, meta-heuristic algorithms are valuable for their capability of finding sufficiently good solutions to difficult problems with limited computational resources (Bianchi et al., 2009).

In the following sections we briefly review the fundamentals of two standard, widely-used meta-heuristic algorithms, namely the simulated annealing and the genetic algorithm, that are capable of finding solutions near global optimum for the stated bilevel optimization problems. Due to different origin and inspiration, nomenclature of the meta-heuristic algorithms differs from that of mathematical programming, the correspondence between nomenclatures is provided in Table 6.1.

Table 6.1: Equivalence in terminology of mathematical programming, simulated annealing, and genetic algorithm.

Mathematical Programming	Simulated Annealing	Genetic Algorithm
Feasible solution	State	Individual
Objective function	Energy	Fitness function
Optimal solution	Ground state	Best individual
Control parameter	Temperature	Crossover probability Mutation probability

6.2.1 Simulated Annealing

Simulated annealing is a meta-heuristic algorithm developed independently by Kirkpatrick et al. (1983) and Černý (1985). Its main idea is based on an analogy to the physical process of annealing of solids, a thermal procedure used to bring solids into a low-energy state, while improving material properties. The annealing starts with temperature increasing, resulting in melting of the solid and random scatter of the particles the solid is composed of. Through the subsequent process of gradual cooling, the particles are allowed to rearrange into a minimal-energy grid, improving material properties.

Algorithm

Let us take a random connectivity matrix \mathbf{C} , that represents the state and corresponds to the design variables of the outer optimization in (6.1) and (6.2), as input to the simulated annealing algorithm. Also assume three fixed parameters: the initial temperature $T_0 \in \mathbb{R}_{\geq 0}$ stated as

$$T_0 = \frac{c_{AI} - c_I}{25}, \quad (6.4)$$

the number of temperatures $n_T \in \mathbb{Z}_{>0}$ computed by

$$n_T = 32(n_{t,y} + 1)(n_{t,x} + 1), \quad (6.5)$$

and the number of steps within a fixed temperature $n_S \in \mathbb{Z}_{>0}$. Here, we use $n_S = 1$.

For a specified random state \mathbf{C} the algorithm uniquely determines the corresponding energy $E(\mathbf{C})$, i.e. the structural compliance, by solving either (6.1), or (6.2). Note that because the initial state \mathbf{C} was defined to be generated randomly, its energy is (most likely) considerably higher compared to the lower bound c_L .

Subsequently, the state \mathbf{C} enters the main iteration cycle, consisting of $n_T \cdot n_S$ iterations, and permitting gradual cooling after every n_S successive steps accordingly to the predefined cooling schedule

$$T = \left[e^{\left(\frac{640}{n_T} \log(0.99) \right)} \right]^t T_0, \quad t \in \{1 \dots n_T\}, \quad (6.6)$$

where T denotes the actual temperature. In each iteration $i_{\text{ter}} \in \{1 \dots n_T n_S\}$, a trial *neighbor state* \mathbf{C}_T is generated and its energy $E(\mathbf{C}_T)$ compared with the stored energy $E(\mathbf{C})$. If $E(\mathbf{C}_T) \leq E(\mathbf{C})$, the trial state is accepted and substitutes the former one. Otherwise, the trial state is accepted with the probability

$$P = e^{\frac{E(\mathbf{C}) - E(\mathbf{C}_T)}{T}}. \quad (6.7)$$

Initially, when the temperature is high, almost all the worse trial states with higher energies are accepted. Gradually following the decrease of temperature, the probability of accepting states with higher energies diminishes. Therefore, unlike gradient methods, the algorithm avoids being trapped in a local optimum for non-convex problems¹ and, with correct settings, converges to the global optimum (Burke and Kendall, 2014).

Let us now take a closer look on the Neighbor function, permitting to reach a neighbor state. The neighbor function randomly reverts several elements $\mathbf{e}_r = (e_{r,1} \dots e_{r,n_{er}})^T \in \{1 \dots (n_{t,y} + 1)(n_{t,x} + 1)\}^{n_{er}}$, of the connectivity matrix, such that

$$\mathbf{C}_{e_r, \zeta} = 1 - \mathbf{C}_{e_r, \zeta}, \quad \forall \zeta \in \{1 \dots n_{er}\}, \quad (6.8)$$

where $\mathbf{C}_{e_r, \zeta}$ denotes the e_r, ζ -th element of the connectivity matrix \mathbf{C} . The number of inverted elements is picked at random, but constrained by

$$1 \leq n_{er} \leq \max \left\{ \left\lceil \frac{1 - \left\lfloor \frac{(n_{t,y} + 1)(n_{t,x} + 1)}{2} \right\rfloor}{0.9 n_T n_S} i_{\text{ter}} + \left\lfloor \frac{(n_{t,y} + 1)(n_{t,x} + 1)}{2} \right\rfloor \right\rceil, 1 \right\}. \quad (6.9)$$

The algorithm terminates after the prescribed number of iterations. Based on specified control parameters and allowed number of iterations, either a local or global optimum is computed. A pseudo-code of simulated annealing is stated in Algorithm 1.

6.2.2 Genetic Algorithm

Genetic algorithm is a meta-heuristic stochastic optimization algorithm developed by Holland (1992) that simulates the natural process of evolution. The initial population evolves throughout generations, following Darwin's (Darwin, 1859) "survival of the fittest" phrase (Spencer, 1864). The competition among individuals results in dominance of the fittest individuals over the weaker ones, allowing for their reproduction and passing their genetic information on to the next generations, gradually improving quality of the whole population.

Naturally, all living organisms are formed by their genetic information—chromosomes consisting of genes—determining their fitness, properties, capabilities, and ability to succeed. Similarly to the real life, a population of individuals in the genetic algorithm is defined

¹For combinatorial (discrete) optimization generalized (non)convexity can be introduced (Burkard, 2005).

Algorithm 1 Simulated Annealing

```

function SIMULATEDANNEALING( $\mathbf{C}$ ,  $T_0$ ,  $n_T$ ,  $n_S$ )
   $T \leftarrow T_0$                                 ▷ Initial temperature
  for  $t \leftarrow 1, n_T$  do                        ▷ For all the temperatures
    for  $\eta \leftarrow 1, n_S$  do                    ▷ For all the steps within constant temperature
       $\mathbf{C}_T \leftarrow \text{Neighbor}(\mathbf{C})$           ▷ Obtain trial neighbor state
       $\Delta E \leftarrow E(\mathbf{C}_T) - E(\mathbf{C})$         ▷ Compute energy difference
      if  $\Delta E \leq 0$  then                      ▷ If better solution is found ...
         $\mathbf{C} \leftarrow \mathbf{C}_T$                   ▷ ... the state is accepted ...
      else                                       ▷ ... otherwise ...
        if  $\text{rand}(1) \leq \exp(-\Delta E/T)$  then  ▷ ... accepted based on probability
           $\mathbf{C} \leftarrow \mathbf{C}_T$ 
        end if
      end if
    end for
     $T \leftarrow \text{Cooling}(T)$                 ▷ Cool the temperature
  end for
  return  $\mathbf{C}$                                 ▷ Return approximation to  $\mathbf{C}^*$ 
end function

```

by chromosomes, denoted by initially random connectivity matrices \mathbf{C} , allowing for unique determination of the corresponding structural compliances. The lower the compliance, the higher the fitness, since the compliance is to be minimized. Note that chromosomes correspond to the design variable of the outer optimization in (6.1) and in (6.2).

In each step (generation) of the algorithm, the stronger individuals of higher fitness are *selected* to reproduce and establish a new generation, inheriting their parents genetic information through the so-called *cross-over*. Because reproduction represents a complex process of combining two chromosomes, errors can occur in the form of *mutations*, contributing to the population diversity.

After the cross-over and mutation, the old generation passes away except for the *elite* individual with the highest fitness value, who survives within the new generation in order to keep the best chromosome. To extend the search space of the algorithm, *diversity* is enforced by replacing duplicate individuals with random ones.

For the bilevel optimization, the population size $n_{\text{pop}} \in \mathbb{Z}_{>0}$ is heuristically set to be

$$n_{\text{pop}} = \left\lceil 3.6 \sqrt{(n_{t,y} + 1)(n_{t,x} + 1) + \frac{1}{2}} \right\rceil, \quad (6.10)$$

and the number of generations $n_{\text{gen}} \in \mathbb{Z}_{>0}$ equals

$$n_{\text{gen}} = 5 \left\lceil \frac{2.45 n_{\text{pop}}}{5} + \frac{1}{2} \right\rceil. \quad (6.11)$$

Selection

According to Darwin's evolution theory, only the fittest individuals survive, create new offspring, and consequently pass their genes on to the next generation. Currently, there are several ways of defining the selection operator, i.e. controlling mating the fittest individuals to reproductions. The most common approaches are the *roulette-wheel* (DeJong, 1975), *rank* (Baker, 1985), and *tournament* (Brindle, 1981) selection. With respect to the stated

bilevel optimization problem (6.1) or (6.2), the tournament selection proved to be the most advantageous.

The tournament selection consists in randomly choosing $n_c \in \mathbb{Z}_{>0}$ competitors (individuals), with n_c denoting the tournament size. The competitors are then sorted accordingly to their fitness in a descending order and assigned a probability of winning the tournament, such that the probability of the i_{nd} -th individual to become a winner is proportional to

$$P_t (1 - P_t)^{i_{\text{nd}}}, \quad (6.12)$$

where $P_t \in [0, 1]$ denotes the tournament probability control parameter. If $P_t = 1$, the fittest individual is selected and the selection becomes deterministic, while if $P_t = 0$, the winner is selected at random, making the selection purely stochastic. The tournament selection thus facilitates direct possibility to adjust the selection pressure, defining the preference of the fittest individual, through the tournament size and the tournament probability parameters. Note that the winner of a larger tournament have in average higher fitness compared to the winner of a smaller tournament. The winner of the tournament is subsequently inserted into the *mating pool*, grouping the parents of the next generation.

For the bilevel optimization the following parameters were used,

$$n_c = \left\lfloor \frac{4}{3} \sqrt{(n_{t,y} + 1)(n_{t,x} + 1)} + \frac{1}{2} \right\rfloor, \quad (6.13)$$

and

$$P_t = 0.30. \quad (6.14)$$

Cross-Over

The cross-over operator governs mating of the couples from the mating pool, reproduction, i.e. combining their genetic information, and subsequent birth of their offspring. Common cross-over techniques include *single-point*, *two-point*, and *uniform* (Syswerda, 1989) cross-over. However, in the following text, we will consider only the uniform cross-over.

Having two parents to give birth to a new offspring, their fitness can be straightforwardly compared. As the genes of the individual with higher fitness should be preferred, the offspring is created in such a way that it obtains the genetic information from its parents approximately proportionally to the ratio of their fitness. In order to facilitate the described behavior, each single gene, i.e. each element of the connectivity matrix in our case, is inherited with probability defined by the ratio of parents fitness. A sample uniform cross-over realization is displayed in Fig. 6.1, where genes of the fitter parent are written in red.

$$\begin{pmatrix} 0 & 0 & 1 \\ 1 & 0 & 0 \end{pmatrix} \oplus \begin{pmatrix} 1 & 1 & 1 \\ 0 & 1 & 0 \end{pmatrix} \ominus \begin{pmatrix} 1 & 0 & 1 \\ 0 & 0 & 0 \end{pmatrix}$$

Figure 6.1: Sample cross-over realization.

Usually, the cross-over operator is used only to a portion of reproductions, given by the *cross-over probability* $P_c \in [0, 1]$. If $P_c = 1$, all offspring are made by cross-over. On the contrary, if $P_c = 0$, the offspring are exact copies of the parents with higher fitness. In this thesis we use $P_c = 0.94$.

Mutation

Mutation represents an operator that secures diversity of the population and simultaneously enables random exploration of the design space. Mutation affects each individual gene of

the chromosome independently and inverts its value with prescribed *mutation probability* $P_m \in [0, 1]$, which is usually close to 0. For a sample realization of the mutation operator, refer to Fig. 6.2.

$$\begin{pmatrix} 1 & 0 & 1 \\ 0 & 0 & 0 \end{pmatrix} \Rightarrow \begin{pmatrix} 1 & 0 & \mathbf{0} \\ 0 & 0 & 0 \end{pmatrix}$$

Figure 6.2: Sample mutation realization.

In this thesis we have adopted the settings

$$P_m = \frac{1}{(n_{t,y} + 1)(n_{t,x} + 1)}. \quad (6.15)$$

Finally, combining the described theory we can write a psuedo-code of the genetic algorithm, see Algorithm 2, leading to an approximate solution to \mathbf{C}^* .

Algorithm 2 Genetic Algorithm

```

function GENETICALGORITHM( $\mathbf{C}, n_{\text{pop}}, n_{\text{gen}}, n_c, P_t, P_c, P_m$ )
   $population \leftarrow \text{GeneratePopulation}(\mathbf{C}, n_{\text{pop}})$  ▷ Create random population
   $fitness \leftarrow \text{FevalFitness}(population)$  ▷ Evaluate fitness of individuals
  for  $\delta \leftarrow 1, n_{\text{gen}}$  do ▷ For all generations
     $elite \leftarrow \text{BestIndividual}(population)$  ▷ Keep the best individual
     $matingPool \leftarrow \text{Selection}(population, n_c, P_t)$  ▷ Select parents
     $population \leftarrow \text{CrossOver}(matingPool, P_c)$  ▷ Give birth to offspring
     $population \leftarrow \text{Mutation}(population, P_m)$  ▷ Apply mutation
     $population \leftarrow \text{AppendElite}(population, elite)$  ▷ Keep the elite individual
     $population \leftarrow \text{Diversify}(population)$  ▷ Replace duplicates by random  $\mathbf{C}$ 
     $fitness \leftarrow \text{FevalFitness}(population)$  ▷ Evaluate fitness of individuals
  end for
  return  $\mathbf{C} \leftarrow \text{BestIndividual}(population)$  ▷ Return approximation to  $\mathbf{C}^*$ 
end function

```

Chapter 7

Results

The modular-topology optimization approaches developed in the previous chapters have been successfully implemented in MATLAB. In this section, the approach is applied to an illustrative problem of designing a planar hinge-supported beam. In order to assess performance of the proposed bilevel approaches coupling meta-heuristics (the simulated annealing or the genetic algorithm) and mathematical programming (second-order cone or semidefinite programming), a relatively coarse discretization is adopted first, as it allows for obtaining a globally optimal design through brute-force enumeration. Subsequently, we assume also a finer discretization, demonstrating applicability of the developed approach to more difficult problems. Finally, the coarse and fine designs are compared.

All the computations were performed on a Linux workstation with two Intel® Xeon® E5-2630 processors and 128 GB RAM. The second-order cone programs for topology optimization of trusses were solved using the commercial solver Gurobi 7.0 (Gurobi Optimization, Inc., 2016), for the semidefinite programming the state-of-the-art open-source solver SDPA 7.3.9 (Yamashita et al., 2003) was employed. Both the mathematical programming formulations were modeled using YALMIP toolbox (Löfberg, 2004).

7.1 Coarsely Discretized Beam

As an illustrative example, a simple supported planar beam of dimensions 8×3 m is taken, see Fig. 7.1. In the coarse discretization the beam is partitioned into 24 square modules, each of the unit size, and assembled from a complete set of vertex-based Wang tiles. We assume the same tile ground structure, depicted in Fig. 5.2c, for all tiles within the tile

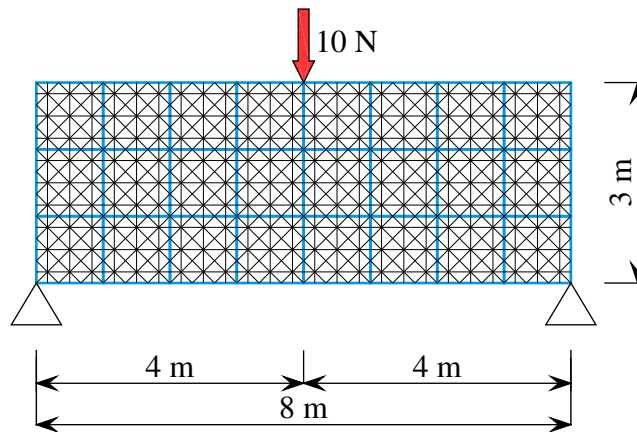


Figure 7.1: Dimensions, discretization, boundary conditions, and ground structure of the evaluated coarsely discretized beam.

set. Young's modulus E of each bar of the ground structure is set to 1 Pa. The beam is supported with two hinges at the very bottom-left and bottom-right corners and loaded with an external force of magnitude 10 N at the midspan of the bent beam. It should be noted that the selected properties do describe neither a specific material nor a realistic situation and have been chosen only to avoid scaling of the optimization problem and ensure numerical stability at the same time.

7.1.1 Bounds on the Globally Optimal Compliance

Following the theory developed in Section 6.1.1 the ideal and anti-ideal compliances can be straightforwardly computed, bounding the range within which the globally optimal compliance is guaranteed to lie. Because all the tiles from the complete tile set are assigned the same tile ground structure, the fictitious ideal and anti-ideal tiles are equal and both are defined by the tile ground structure shown in Fig. 5.2c.

Performing the topology optimization *without* prescribed modularity, recall Eqs. (4.10), (4.32), and (4.33), leads to the lower-bound ideal compliance $c_I = 61.9$ Nm and to the design shown in Fig. 7.2a. Note that the reached objective value cannot be overcome in any modular design, based on the same tile ground structures, but the compliance of the modular design should be as close to the attained lower bound as possible.

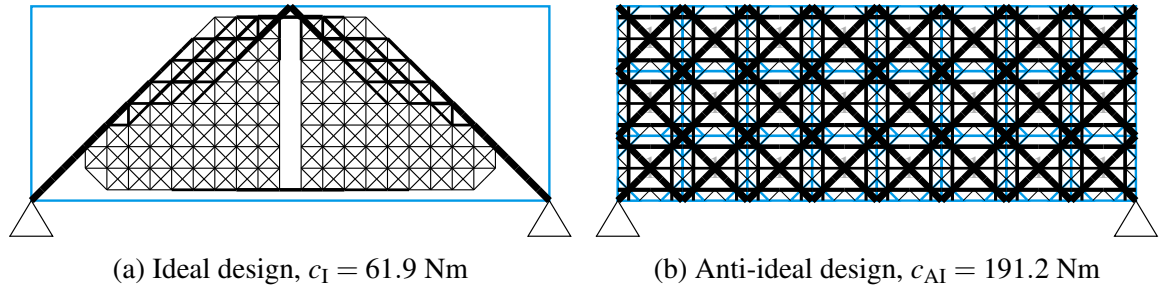


Figure 7.2: Lower-bound (a) and upper-bound (b) solutions to c^* .

Analogously, the upper-bound anti-ideal compliance is obtained through the topology optimization of the design domain assembled from the anti-ideal tiles, recall Eqs. (5.10) and (5.12). In our case, in which the ground structure Fig 5.2c is common to all tiles, the anti-ideal design directly corresponds to the worst-case assembly from only one tile, indicated by the connectivity matrix \mathbf{C} containing all-zeros or all-ones. The anti-ideal topology optimization results in the optimal design, depicted in Fig. 7.2b, with compliance $c_{AI} = 191.2$ Nm. Therefore, the compliance of the optimal modular design for the given tile ground structure will be $c^* \in [61.9, 191.2]$ Nm.

7.1.2 Brute-Force Enumeration

As mentioned in the introductory part to this section, the globally optimal connectivity matrix \mathbf{C}^* and the corresponding compliance c^* were produced from the brute-force enumeration, allowing us to assess quality of designs obtained from the proposed bilevel optimization, recall Chapter 6. Note that even the coarse discretization implies 2^{36} possible combinations of connectivity matrices, making it impossible to enumerate them all within a reasonable time. In order to reduce the complexity, we have enforced symmetry of the connectivity matrix \mathbf{C} with respect to the vertical axis of the beam, consequently limiting the number of combinations of feasible assemblies to 2^{20} . Despite decreasing the problem size dramatically, the global optimum can be distinct from the case without enforced symmetry. Also note that the constrained symmetric assembly does not enforce symmetric topology.

Because all tiles are assigned the same tile ground structure, the number of combinations can be further decreased by exploiting the fact that the vertex types do not have any actual physical meaning—topology optimization of any assembly plan denoted by \mathbf{C} yields equal result to the optimization of reversed \mathbf{C} , i.e. \mathbf{C} having interchanged all 0 with 1 and vice-versa. Subsequently, we need to enumerate 2^{19} distinct combinations instead of the original 2^{36} .

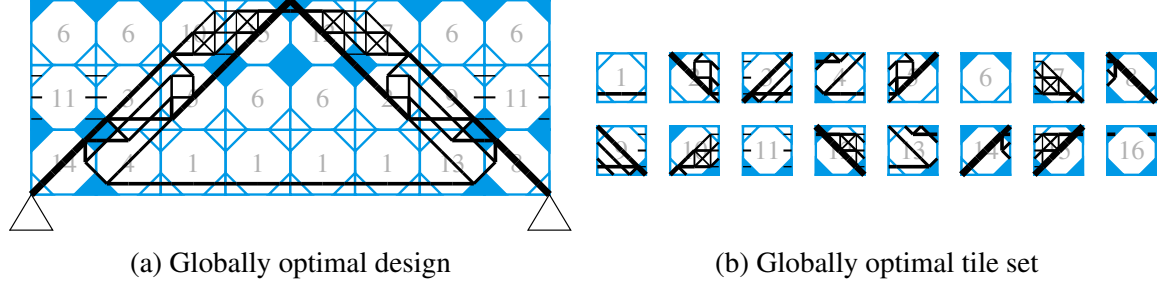


Figure 7.3: (a) Globally optimal design and (b) the corresponding tile set of the coarsely discretized beam of compliance $c^* = 62.7$ Nm.

Optimization of all combinations with the second-order cone programming formulation (5.10) took 9.5 hours. Throughout the enumeration, the globally optimal design of compliance $c^* = 62.7$ Nm was obtained, see Fig. 7.3a. The modular design is only 1.3 % more-compliant compared to the ideal design. The tile set of the globally optimal design, shown in Fig. 7.3b, contains 13 non-empty tiles, the three empty tiles can be thus potentially omitted from the tile set. In overall, the enumerated combinations generate nearly a Gaussian distribution with the mean value of 107.7 Nm and its standard deviation equal to 14.6 Nm, refer to Fig. 7.4.

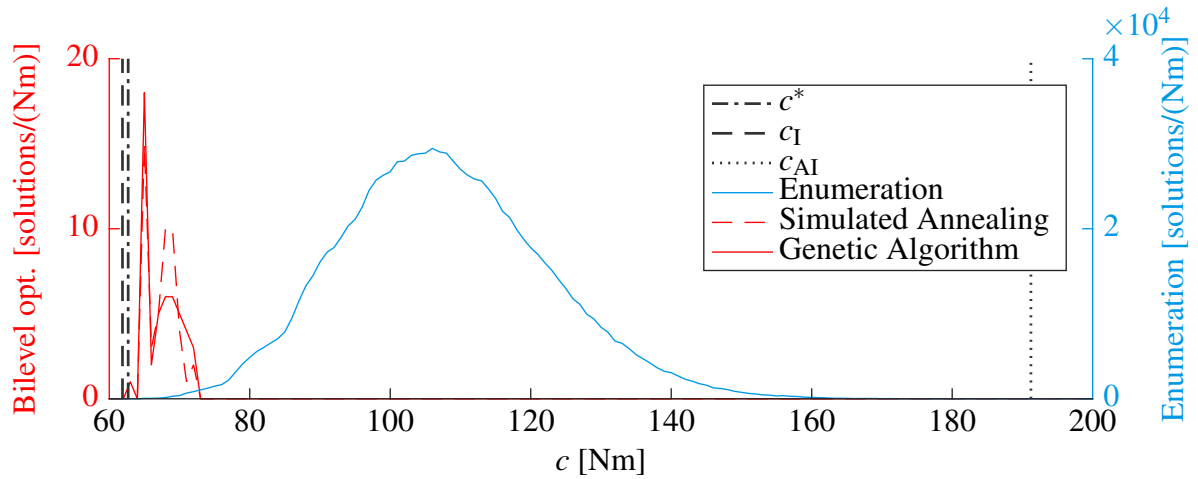


Figure 7.4: Distribution of optimal compliances of all the enumerated combinations, and of 50 independent runs of the bilevel optimization.

7.1.3 Bilevel Optimization

In order to account for the stochastic nature of both the proposed meta-heuristic approaches for solution of the bilevel optimization problems (6.1) and (6.2), the calculations were performed 50 times and statistics of the outputs were compared. Note that both the algorithms are comparable in the count of performed solutions to the inner problem, i.e. topology optimization of modular trusses.

Bilevel Optimization Using Simulated Annealing

The bilevel optimization utilizing the simulated annealing algorithm was run 50 times, each time with a random initial connectivity matrix \mathbf{C} . Convergence of individual optimization runs, as well as the average of all runs, are both shown in Fig. 7.5. On average, the compliance of 105.2 Nm was obtained with an initial random connectivity matrix, closely following the mean value 107.7 Nm of the nearly Gaussian distribution identified with the brute-force enumeration. In the specified 640 iterations of the simulated annealing algorithm, the compliances decreased to the final mean value 67.4 Nm, being 8.9 % higher compared to the ideal solution and 7.5 % higher than the global optimum. Within the 50 performed runs, the global optimum, recall Fig. 7.3, was reached once. Totally, all the achieved compliances lie within the lowest 0.2 % of all attainable compliances, see Fig. 7.4.

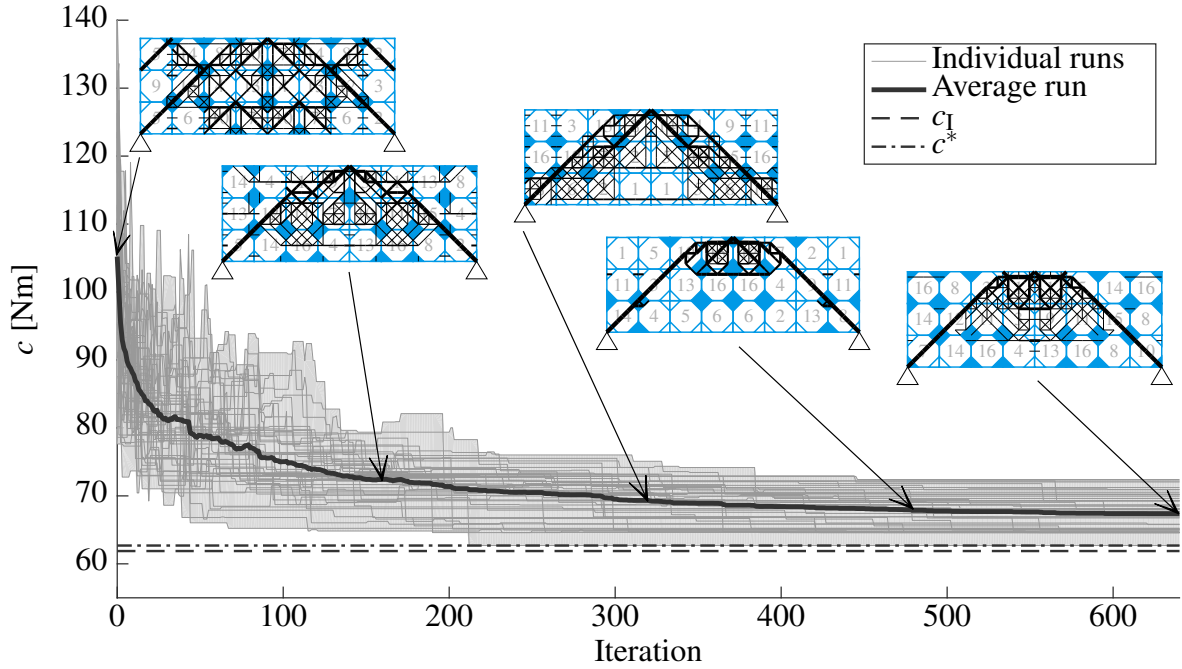


Figure 7.5: Convergence of 50 independent runs of the simulated annealing algorithm. In addition, optimized design samples of a particular connectivity matrix are displayed, proceeding from a random design (the leftmost picture) to the approximate solution to the bilevel optimization problem (the rightmost picture).

Bilevel Optimization Using Genetic Algorithm

As in the case with simulated annealing, genetic algorithm was launched 50 times, starting with a random population of 16 individuals. The effect of evolution on the compliance of the best individual within population is shown in Fig. 7.6.

The initial random populations yielded topologies of a mean compliance 107.4 Nm, corresponding to the mean value 107.7 Nm of the Gaussian distribution. Throughout the prescribed 40 generations of the genetic algorithm, the objective decreased to the final mean value of the best individual 67.4 Nm, being in average 8.9 % higher than the ideal solution and 7.5 % higher than the global optimum. Through the bilevel optimization, the second best design, with compliance 64.6 Nm, was reached, refer to Fig. 7.7. Again, all the achieved objectives are within the lowest 0.2 % of all the combinations.

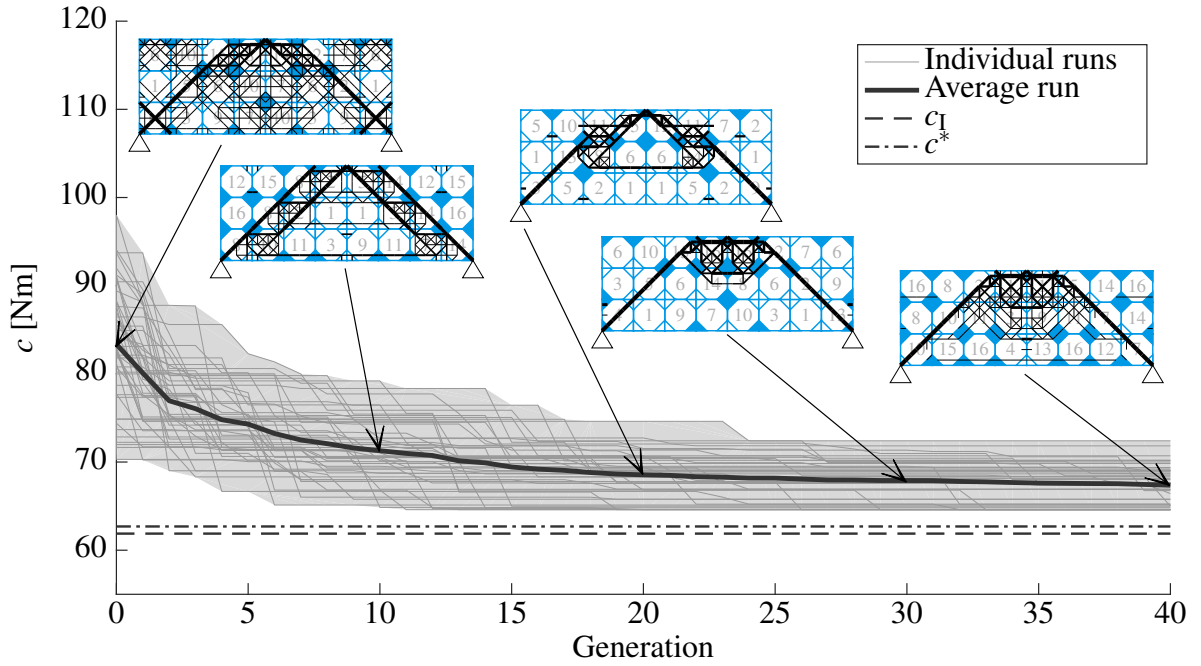


Figure 7.6: Convergence of the best individuals within 50 independent runs of the genetic algorithm. Displayed designs sample the process of evolution through generations.

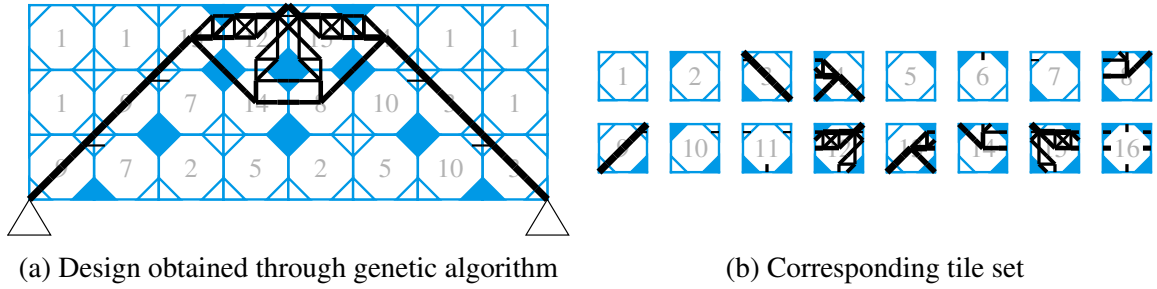


Figure 7.7: The best design of the coarsely discretized beam with compliance $c = 64.6$ Nm obtained through the genetic algorithm (a), and the corresponding tile set (b).

Comparison of Approaches

Concluding the presented results, both the approaches resulted in designs of comparable quality. However, simulated annealing was able to achieve the global optimum, although only once. For overview of the comparison, refer to Table 7.1, showing the best, worst, and mean compliance of all the procedures, and see Fig. 7.4 for the graphical illustration.

Table 7.1: Comparison of the results obtained through the brute-force enumeration, the simulated annealing, and the genetic algorithm.

	Enumeration	Simulated Annealing	Genetic Algorithm
Best compliance	$c^* = 62.7$ Nm	62.7 Nm	64.6 Nm
Worst compliance	$c_{AI} = 191.2$ Nm	72.4 Nm	72.4 Nm
Mean compliance	107.7 Nm	67.4 Nm	67.4 Nm

7.1.4 Relations Between Connectivity Matrix and Design Quality

The brute-force enumeration of all possible designs of the specified problem allowed us to perform a more detailed analysis. The question of the primary interest is the existence of

a relation between quality of designs and connectivity matrices, to permit creation of quality assemblies from scratch.

Firstly, we investigated the influence of a ratio of zero to nonzero elements in the connectivity matrix on the achieved compliance. The boxplot in Fig. 7.8 clearly implies that better designs are obtained when the connectivity matrix comprises nearly equal number of zero and nonzero entries. However, enforcing such assumption a priori to the optimization can lead to missing the global optimum, which is also the case of our example.

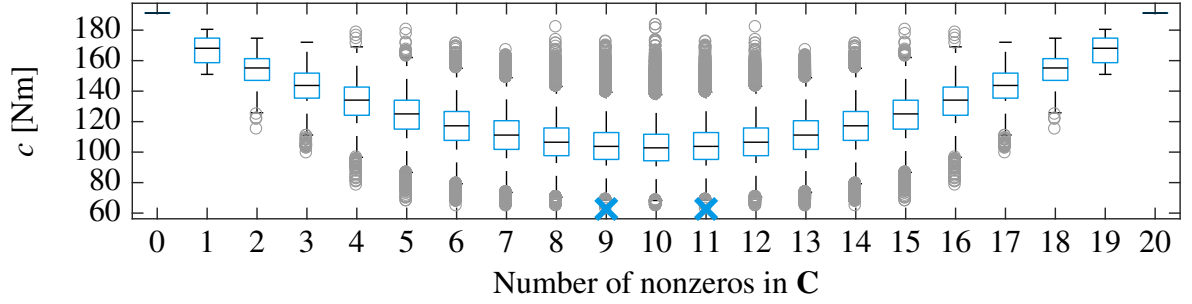


Figure 7.8: Compliance as a functional of the number of nonzero elements in symmetric part of \mathbf{C} of the example beam. The crosses denote global optimum.

Secondly, it is obvious from the anti-ideal design that the quality depends on the number of tiles that are utilized from the complete tile set. Plotting the results of all combinations with respect to the number of tile types appearing in \mathbf{C} , see Fig. 7.9, supports our conclusion that the higher the number of utilized tiles, the better design should we, on average, expect. Again, strictly enforcing such assumption can prevent us from reaching the global optimum.

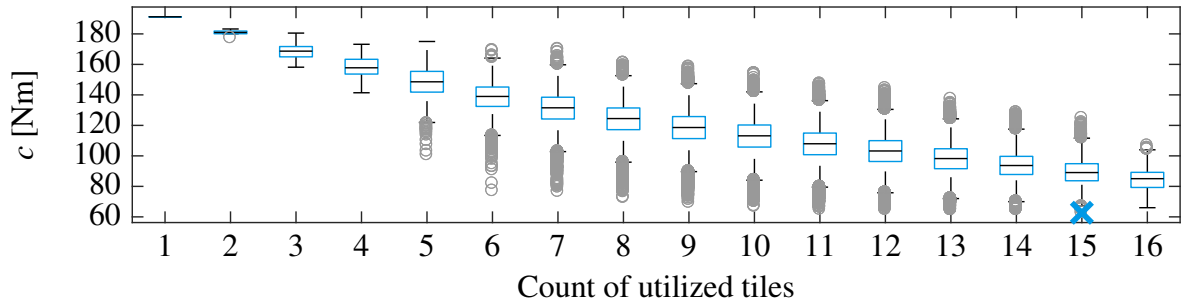


Figure 7.9: Compliance as a functional of the number of utilized tiles in the example beam with enforced symmetry of \mathbf{C} . The cross denotes global optima.

Consequently, we conclude that a connectivity matrix containing similar counts of zero and nonzero elements and resulting in an assembly plan containing all tiles from the tile set is a promising candidate for yielding a low-compliant design.

7.2 Finely Discretized Beam

Let us now consider a beam of the same dimensions and boundary conditions as in the previous example, recall Fig. 7.1, but with refined discretization by 96 tiles of a side length equal to 0.5 m, refer to Fig. 7.10. In order to preserve comparability with the previous case, the connectivity matrix is again enforced to be symmetric along midspan of the beam. Subsequently, the fine discretization permits 2^{62} distinct combinations of assemblies.

This huge number of combinations, pronounced further with increased number of degrees of freedom, makes it impossible to perform brute-force enumeration as in the previous case, leaving us without the knowledge of guaranteed global optimum. However,

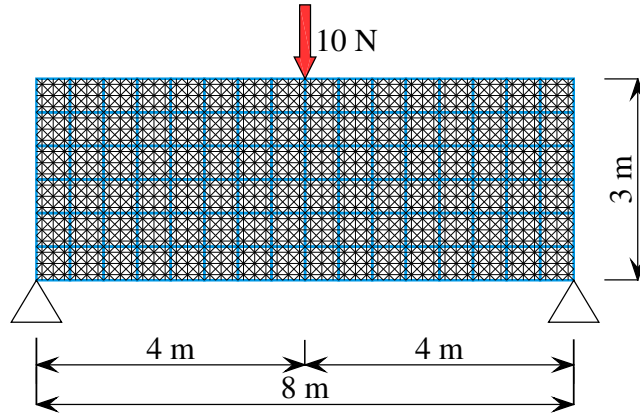


Figure 7.10: Dimensions, discretization, boundary conditions, and ground structure of the evaluated finely discretized beam.

similarly to the previous example, we can straightforwardly obtain the bounds on the optimum: $c_I = 61.1$ Nm, see Fig. 7.11a, and $c_{AI} = 228.7$ Nm, see Fig. 7.11b, implying that $c^* \in [61.1; 228.7]$ Nm.

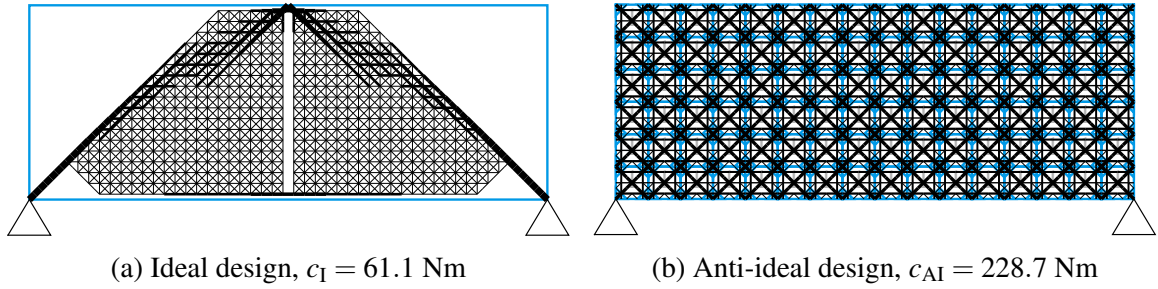


Figure 7.11: (a) Lower-bound and (b) upper-bound (b) solutions to c^* .

Compared to the coarse problem, fine discretization produces a richer ground structure, hence leading to a lower ideal compliance. On the contrary, the anti-ideal compliance noticeably increases, because the total length of bars constrained to have equal cross-sectional areas increases compared to the coarse discretization. Similar consequence of modularity was also reported in (Huang and Xie, 2008).

7.2.1 Bilevel Optimization

The modular-topology optimization of the finely discretized beam was launched 20 times for both of the developed approaches, allowing for direct comparison of the methods. Note that both the approaches involve similar numbers of solutions to the inner problems of (6.1) or (6.2).

Bilevel Optimization Using Simulated Annealing

The mean compliance of the initial 20 random connectivity matrices was 156.2 Nm. Following the observation from the coarse problem, a significantly higher mean value of all connectivity matrices combinations can be expected, compared to the mean value 107.7 Nm of the coarse discretization.

Through the following 2016 iterations, see Fig 7.12, the simulated annealing algorithm converged to the mean compliance 81.9 Nm, i.e. to 34.0 % higher value compared to the ideal design. The best explored design of compliance 72.1 Nm is shown in Fig. 7.13, together with

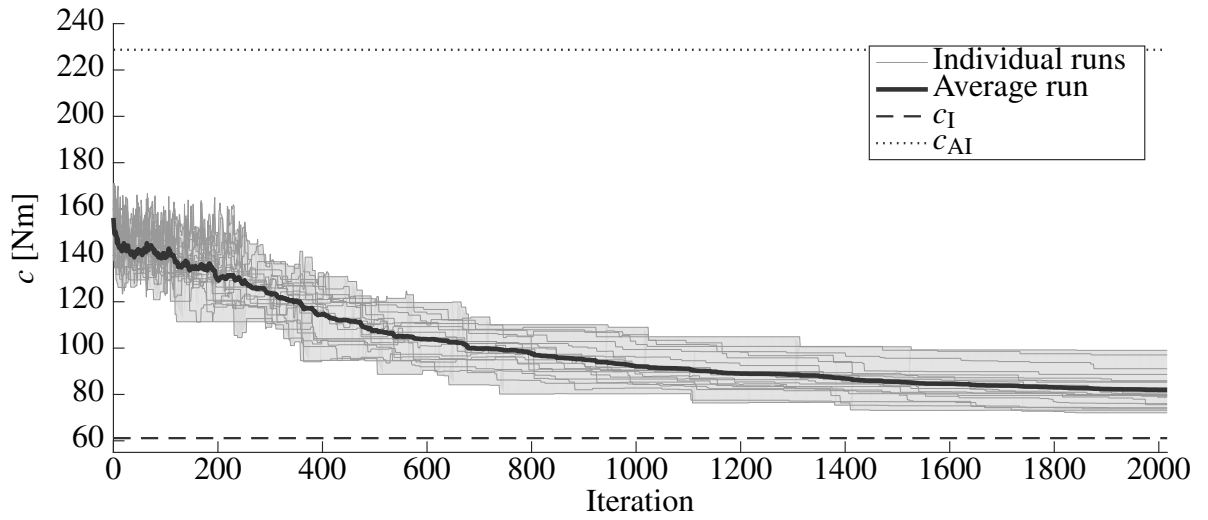


Figure 7.12: Convergence of 20 independent runs of modular-topology optimization of the finely discretized beam using simulated annealing.

the corresponding tile set. Note that the compliance of the reached design is 18.0 % worse than of the ideal design.

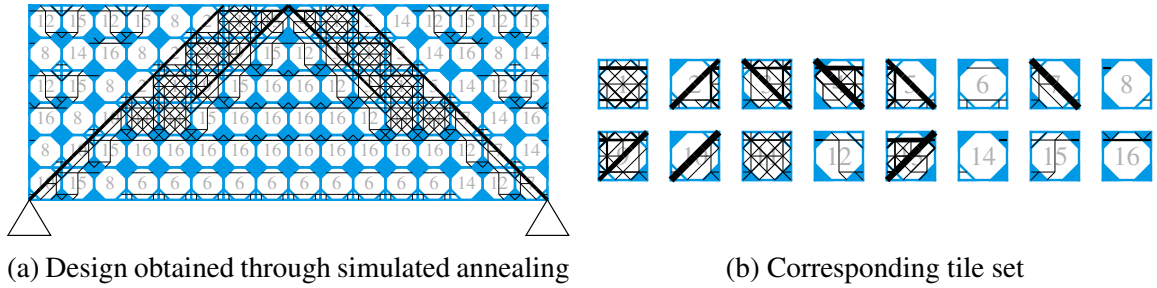


Figure 7.13: The best design of the finely discretized beam with compliance $c = 72.1$ Nm obtained through simulated annealing (a), and the corresponding tile set (b).

Bilevel Optimization Using Genetic Algorithm

The initial random populations of 29 individuals lead to designs of a mean compliance 156.5 Nm, agreeing with the mean compliance obtained in the case of simulated annealing. In the prescribed 70 generations of the bilevel optimization, refer to Fig. 7.15, the algorithm converged to the mean compliance 82.1 Nm, which is 34.4 % higher objective than of the ideal design. The best reached design of compliance 71.6 Nm is shown in Fig. 7.14, being 17.0 % worse than the ideal compliance.

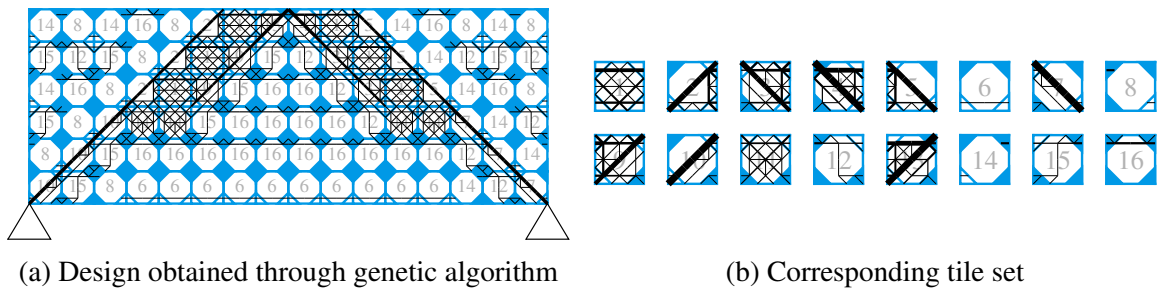


Figure 7.14: The best design of the finely discretized beam with compliance $c = 71.6$ Nm obtained through genetic algorithm (a) and the corresponding tile set (b).

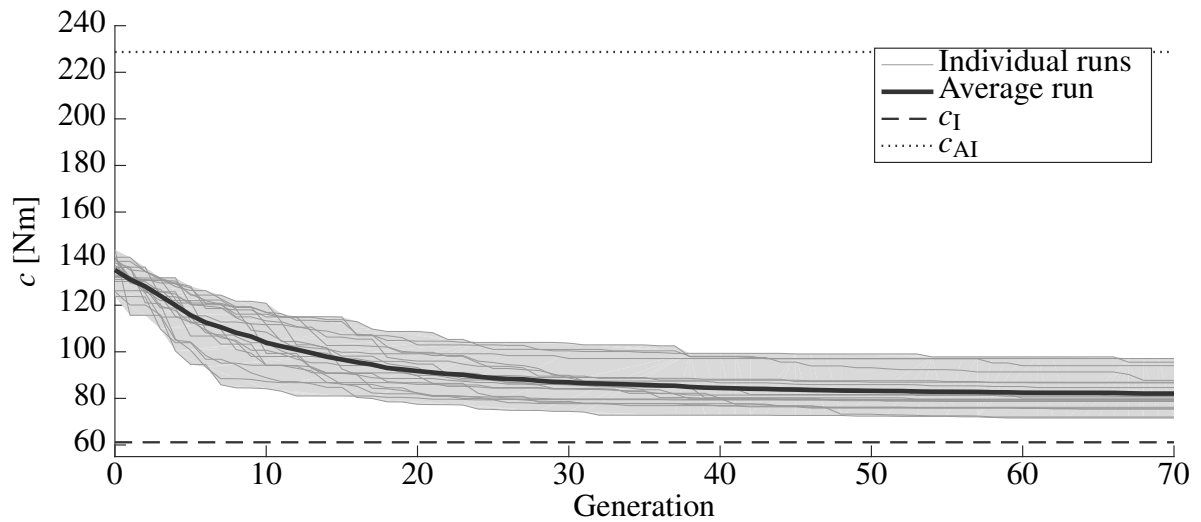


Figure 7.15: Convergence of the best individuals from 20 independent runs of modular-topology optimization of the finely discretized beam using genetic algorithm.

Comparison of Results

Similarly to the coarse discretization, the quality of designs resulting from both the algorithms is very similar also in the case of the finely discretized beam, refer to Table 7.2, and to Fig. 7.16 for an overview.

Table 7.2: Comparison of the results obtained through simulated annealing, and genetic algorithm.

	Simulated Annealing	Genetic Algorithm
Best compliance	72.1 Nm	71.6 Nm
Worst compliance	99.0 Nm	97.1 Nm
Mean compliance	81.9 Nm	82.1 Nm

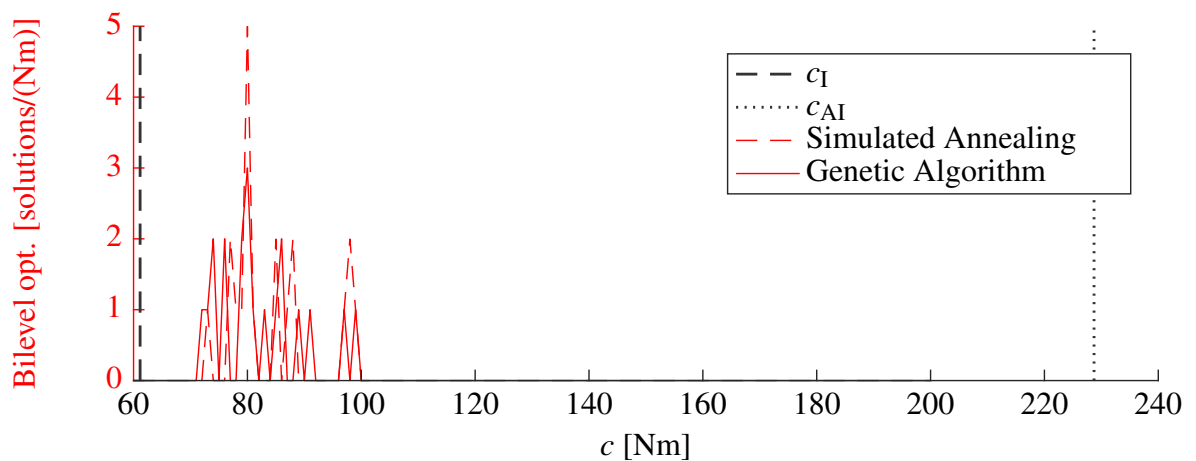


Figure 7.16: Distribution of obtained approximate solutions to the bilevel optimization within 20 independent random runs.

Chapter 8

Summary

In the thesis, a novel *modular-topology optimization* approach was introduced, facilitating simultaneous optimization of topologies of 16 independent truss modules together with their optimal placement within structural macro-scale.

The approach originally utilized the theoretical framework of Wang tiles, particularly their subset of vertex-based Wang tiles, as a suitable formalism for describing aperiodic assemblies of structural modules and maintaining the jigsaw-like compatibility of adjoining modules.

Based on the finite element method, two fundamental approaches leading to the solution of truss structures—direct equilibrium and the principle of minimum potential energy functional—were summarized, served as the basis for the developments in the following chapters.

Next, the well-known elastic minimum-compliance design problem for truss topology optimization was reviewed along with its equivalent convex reformulations, which were derived based on the potential energy function. Specifically, derivation of the quadratic programming formulation was recalled, and its reduction to the classical linear programming plastic design was outlined. Additionally, the equivalence between the aforementioned non-convex formulation with the second-order cone and the semidefinite programs was shown.

Because both the second-order cone and the semidefinite programming formulations involve the compatibility conditions constraints, and the cross-sectional areas serve as primal design variables, the formulations can be directly extended to incorporate structural modularity for a priori specified assembly plan, provided in the form of a valid vertex-based Wang tiling. The extended formulations preserve their convexity.

Although the developed formulations provided a globally optimal design, its quality was mainly influenced by the provided assembly plan. In order to mitigate the dependence, we developed a bilevel modular-topology formulation that couples mathematical programming, optimizing topology of modules through the second-order cone or semidefinite programming, with meta-heuristics, which searches for an optimal assembly plan through simulated annealing or the genetic algorithm.

The developed approach was implemented in MATLAB and its performance was successfully demonstrated on a minimum-compliant design of a simply supported beam, coarsely and finely discretized. The coarse discretization, chosen specifically such that it allowed reaching a globally optimal design by brute-force enumeration, enabled us to assess the quality of the proposed meta-heuristic approaches, concluding that both the approaches led to solutions near the global optimum. The fine discretization then demonstrated possible applicability of the approach to finer and more complex structures.

Numerical results showed that imposing structural modularity does not significantly impair the quality of the optimal design, compared to the non-modular design. Thus, a signifi-

cant savings can be achieved in production of modular trusses or structures with (a)periodic microstructure, composed of truss elements.

8.1 Directions For Future Research

The content of the thesis can be also seen as a proof of concept, establishing ground for following research focused on more complex modular designs. While proving the applicability of the approach, new challenges and topics of further research emerged during the work. Two major directions are listed below.

The first core area of extension considers the bilevel *optimization formulation*. While the developed approach works as intended, it usually requires a high number of solutions to the inner topology optimization problem. In order to return to the purely mathematical structure of the bilevel problem, it is important to reformulate it. A suitable approach might be a single-level mixed-integer program solvable to proven global optimality by a method based on branch-and-bound principles. Such formulation would also avoid direct manipulation with the connectivity matrix and allow subsequent employment of an arbitrary set of Wang tiles. Afterwards, it should be straightforward to relax the problem into a non-convex, yet faster formulation.

Geometry, the second core area of extension, represents a crucial milestone for practical usability of the approach, permitting e.g. 3D printing (Schumacher et al., 2015; Coulais et al., 2016; Alù, 2016). Therefore, the method needs to be generalized to cover 3D design domains by adaptation of Wang cubes. Incorporating complex geometrical constraints, such as prescribed voids, represents another requirement arising in real-world applications that needs to be addressed in future work. Finally, a continuous version of the topology optimization in the spirit of e.g. (Alexandersen and Lazarov, 2015) is a necessary, and represents logical extension of the approach.

Bibliography

- W. Achtziger and M. Kočvara. Structural Topology Optimization with Eigenvalues. *SIAM Journal on Optimization*, 18(4):1129–1164, Jan. 2008. ISSN 1052-6234, 1095-7189. doi: 10.1137/060651446. URL <http://epubs.siam.org/doi/abs/10.1137/060651446>.
- W. Achtziger, M. Bendsøe, A. Ben-Tal, and J. Zowe. Equivalent displacement based formulations for maximum strength truss topology design. *IMPACT of Computing in Science and Engineering*, 4(4):315–345, Dec 1992. ISSN 08998248. doi: 10.1016/0899-8248(92)90005-S. URL <http://linkinghub.elsevier.com/retrieve/pii/089982489290005S>.
- J. Alexandersen and B. S. Lazarov. Topology optimisation of manufacturable microstructural details without length scale separation using a spectral coarse basis preconditioner. *Computer Methods in Applied Mechanics and Engineering*, 290:156–182, 2015. doi: 10.1016/j.cma.2015.02.028.
- M. Alkhader and M. Vural. Mechanical response of cellular solids: Role of cellular topology and microstructural irregularity. *International Journal of Engineering Science*, 46(10): 1035–1051, 2008. ISSN 00207225. doi: 10.1016/j.ijengsci.2008.03.012.
- A. Alù. Metamaterials: Prime time. *Nature Materials*, 15(12):1229–1231, 2016. ISSN 1476-1122. doi: 10.1038/nmat4814. URL <http://www.nature.com/doifinder/10.1038/nmat4814>.
- R. Ammann, B. Grünbaum, and G. C. Shephard. Aperiodic tiles. *Discrete & Computational Geometry*, 8(1):1–25, 1992. ISSN 01795376. doi: 10.1007/BF02293033.
- M. F. Anjos and J. B. Lasserre, editors. *Handbook on Semidefinite, Conic and Polynomial Optimization*, volume 166 of *International Series in Operations Research & Management Science*. Springer US, Boston, MA, 2012. ISBN 978-1-4614-0768-3. doi: 10.1007/978-1-4614-0769-0. URL <http://link.springer.com/10.1007/978-1-4614-0769-0>.
- J. Argyris. Energy theorems and structural analysis: A generalized discourse with applications on energy principles of structural analysis including the effects of temperature and non-linear stress-strain relations. *Aircraft Engineering and Aerospace Technology*, 26(10):347–356, 1954. ISSN 0002-2667. doi: 10.1108/eb032482. URL <http://www.emeraldinsight.com/journals.htm?issn=0002-2667&volume=26&issue=10&articleid=1679779&show=html>.
- A. Asadpoure, J. K. Guest, and L. Valdevit. Incorporating fabrication cost into topology optimization of discrete structures and lattices. *Structural and Multidisciplinary Optimization*, 51(2):385–396, Feb 2015. ISSN 16151488. doi: 10.1007/s00158-014-1133-8. URL <http://link.springer.com/10.1007/s00158-014-1133-8>.

- J. E. Baker. Adaptive selection methods for genetic algorithms. In *Proceedings of an International Conference on Genetic Algorithms and their applications*, pages 101–111. Hillsdale, New Jersey, 1985.
- A. Ben-Tal and M. P. Bendsøe. A new method for optimal truss topology design. *SIAM Journal on Optimization*, 3(2):322–358, 1993.
- A. Ben-Tal and A. Nemirovski. Robust truss topology design via semidefinite programming. *SIAM Journal on Optimization*, 7(4):991–1016, 1997. URL <http://epubs.siam.org/doi/abs/10.1137/S1052623495291951>.
- A. Ben-Tal and A. Nemirovski. *Lectures on Modern Convex Optimization*. Society for Industrial and Applied Mathematics, Jan 2001. ISBN 978-0-89871-491-3. doi: 10.1137/1.9780898718829.
- A. Ben-Tal, F. Jarre, M. Kočvara, A. Nemirovski, and J. Zowe. Optimal design of trusses under a nonconvex global buckling constraint. *Optimization and Engineering*, 1(2):189–213, 2000. URL <http://link.springer.com/article/10.1023/A:1010091831812>.
- M. P. Bendsøe and O. Sigmund. *Topology optimization: Theory, methods and applications*. Springer-Verlag, Berlin, Heidelberg, second edition, 2003. doi: 10.1007/978-3-662-05086-6.
- M. P. Bendsøe, A. Ben-Tal, and R. T. Haftka. *New displacement-based methods for optimal truss topology design*, volume 32, pages 684–696. American Institute of Aeronautics and Astronautics, Apr 1991. ISBN 9788578110796. doi: 10.2514/6.1991-1215. URL <http://arc.aiaa.org/doi/10.2514/6.1991-1215>.
- M. P. Bendsøe, A. Ben-Tal, and J. Zowe. Optimization methods for truss geometry and topology design. *Structural and Multidisciplinary Optimization*, 7(3):141–159, Apr 1994. ISSN 0934-4373. doi: 10.1007/bf01742459. URL <http://link.springer.com/10.1007/BF01742459>.
- M. P. Bendsøe and N. Kikuchi. Generating optimal topologies in structural design using a homogenization method. *Computer Methods in Applied Mechanics and Engineering*, 71(2):197–224, 1988. ISSN 00457825. doi: 10.1016/0045-7825(88)90086-2.
- R. Berger. The undecidability of the domino problem. *Ph.D. Thesis, Division of Engineering and Applied Physics (Applied Mathematics)–Harvard University*, 1964.
- R. Berger. The undecidability of the domino problem. *Memoirs of the American Mathematical Society*, 66(66):0–0, 1966. ISSN 0065-9266. doi: 10.1090/memo/0066. URL <http://www.ams.org/memo/0066>.
- L. Bianchi, M. Dorigo, L. M. Gambardella, and W. J. Gutjahr. A survey on metaheuristics for stochastic combinatorial optimization. *Natural Computing*, 8:239–287, 2009. ISSN 15677818. doi: 10.1007/s11047-008-9098-4.
- S. Boyd and L. Vandenberghe. *Convex Optimization*. Berichte über verteilte messsysteme. Cambridge University Press, 2004. ISBN 9780521833783.
- A. Brindle. Genetic Algorithms for Function Optimization. *Ph.D. Thesis, University of Alberta*, 1981.

- R. E. Burkard. *(Generalized) Convexity and Discrete Optimization*, volume 2, pages 23–37. Kluwer Academic Publishers, 2005. ISBN 978-0-387-23638-4 978-0-387-23639-1. doi: 10.1007/0-387-23639-2_2. URL http://link.springer.com/10.1007/0-387-23639-2_2.
- E. K. Burke and G. Kendall, editors. *Search Methodologies*. Springer US, Boston, MA, 2014. ISBN 978-1-4614-6939-1 978-1-4614-6940-7. URL <http://link.springer.com/10.1007/978-1-4614-6940-7>.
- H. H. Chen, W. G. Hu, D. J. Lai, and S. S. Lin. Nonemptiness problems of wang tiles with three colors. *Theoretical Computer Science*, 547(C):34–45, 2014. ISSN 03043975. doi: 10.1016/j.tcs.2014.06.015. URL www.elsevier.com/locate/tcs.
- P. W. Christensen and A. Klarbring. *An introduction to structural optimization*. Springer, Dordrecht, online-ausg. edition, 2009. ISBN 9781402086663.
- A. Church. An unsolvable problem of elementary number theory. *American Journal of Mathematics*, 58(2):345–363, 1936. ISSN 00029327. doi: 10.2307/2371045. URL <http://links.jstor.org/sici?sici=0002-9327%28193604%2958%3A2%3C345%3AAUPOEN%3E2.0.CO%3B2-1>.
- R. W. Clough. *The finite element method in plane stress analysis*. American Society of Civil Engineers, 1960.
- M. F. Cohen, J. Shade, S. Hiller, and O. Deussen. Wang tiles for image and texture generation. *ACM Transactions on Graphics*, 22(3):287–294, July 2003. ISSN 0730-0301. doi: 10.1145/882262.882265. URL <http://doi.acm.org/10.1145/882262.882265>.
- R. L. Cook. Stochastic sampling in computer graphics. *ACM Transactions on Graphics*, 5(1):51–72, 1986. ISSN 07300301. doi: 10.1145/7529.8927.
- C. Coulais, E. Teomy, K. de Reus, Y. Shokef, and M. van Hecke. Combinatorial design of textured mechanical metamaterials. *Nature*, 535(7613):529–532, 2016. doi: 10.1038/nature18960.
- R. Courant. Variational methods for the solution of problems of equilibrium and vibrations. *Bulletin of the American Mathematical Society*, 49(1):1–24, 1943. ISSN 1539-3755. doi: 10.1090/S0002-9904-1943-07818-4. URL <http://projecteuclid.org/euclid.bams/1183504922>.
- C. Culmann. *Die Graphische Statik*. Meyer & Zeller, Zürich, 1875. URL <https://books.google.cz/books?id=MS74qkfyPhIC>.
- C. Darwin. *On the Origin of the Species*, volume 5. John murray, london, 1859.
- M. Davis. *Computability & unsolvability*. Courier Corporation, 1958.
- K. DeJong. An analysis of the behavior of a class of genetic adaptive systems. *Ph.D. Thesis, University of Michigan*, 1975.
- O. Deussen, P. Hanrahan, B. Lintermann, R. Měch, M. Pharr, and P. Prusinkiewicz. Realistic modeling and rendering of plant ecosystems. In *Proceedings of the 25th Annual Conference on Computer Graphics and Interactive Techniques, SIGGRAPH '98*, pages 275–286, New York, NY, USA, 1998. ACM. ISBN 0-89791-999-8. doi: 10.1145/280814.280898. URL <http://doi.acm.org/10.1145/280814.280898>.

- M. W. Dobbs. Optimization of truss geometry. *Journal of Structural Division Proceedings of the American Society of Civil Engineers*, 95(19):2105–2118, 1969.
- W. S. Dorn, R. E. Gomory, and H. J. Greenberg. Automatic design of optimal structures. *Journal de Mecanique*, 3:25–52, 1964.
- M. Doškář and J. Novák. A jigsaw puzzle framework for homogenization of high porosity foams. *Computers and Structures*, 166:33–41, 2016. ISSN 00457949. doi: 10.1016/j.compstruc.2016.01.003.
- M. Doškář, J. Novák, and J. Zeman. Aperiodic compression and reconstruction of real-world material systems based on wang tiles. *Physical Review E – Statistical, Nonlinear, and Soft Matter Physics*, 90(6):1–8, 2014. ISSN 15502376. doi: 10.1103/PhysRevE.90.062118.
- C. L. Dym and I. H. Shames. *Solid mechanics: a variational approach*. McGraw-Hill, New York, 1973. ISBN 0070185565.
- C. A. Felippa. Introduction to finite element methods, 2014. URL <http://www.colorado.edu/engineering/CAS/courses.d/IFEM.d/IFEM.Ch00.d/>. Accessed: 2016-11-11.
- P. Fleron. Minimum weight of trusses. *Byggningsstatistiske Meddelelser*, 35(3):81, 1964.
- F. Glover. Future paths for integer programming and links to artificial intelligence. *Computers and Operations Research*, 13(5):533–549, 1986. ISSN 03050548. doi: 10.1016/0305-0548(86)90048-1.
- F. Glover and M. Laguna. *Tabu Search*. Springer US, Boston, MA, 1999. ISBN 978-1-4613-0303-9. doi: 10.1007/978-1-4613-0303-9_33. URL http://dx.doi.org/10.1007/978-1-4613-0303-9_33.
- B. Grünbaum and G. C. Shephard. *Tilings and Patterns*. W. H. Freeman & Co., New York, NY, USA, 1986. ISBN 0-716-71193-1.
- J. Guo, D. M. Yan, L. Chen, X. Zhang, O. Deussen, and P. Wonka. Tetrahedral meshing via maximal poisson-disk sampling. *Computer Aided Geometric Design*, 43(12):186–199, 2016. ISSN 01678396. doi: 10.1016/j.cagd.2016.02.004. URL www.elsevier.com/locate/cagd.
- Gurobi Optimization, Inc. Gurobi optimizer reference manual, 2016. URL <http://www.gurobi.com>. Accessed: 2016-11-11.
- H.C.Martin. Finite element analysis of fluid flows. *Proceedings of the Second Conference on Matrix Methods in Structural Mechanics*, pages 517–535, 1969.
- W. Hemp. *Optimum structures*. Oxford engineering science series. Clarendon Press, 1973.
- S. Hiller, O. Deussen, and A. Keller. Tiled blue noise samples. In *Proceedings of the Vision Modeling and Visualization Conference 2001*, VMV '01, pages 265–272. Aka GmbH, 2001. ISBN 3-89838-028-9. URL <http://dl.acm.org/citation.cfm?id=647260.718507>.
- J. H. Holland. *Adaptation in Natural and Artificial Systems: An Introductory Analysis with Applications to Biology, Control and Artificial Intelligence*. MIT Press, Cambridge, MA, USA, 1992. ISBN 0262082136.

- A. Hrennikoff. Solution of problems of elasticity by the framework method. *Journal of applied mechanics*, 8(4):169–175, 1941.
- X. Huang and Y. M. Xie. Optimal design of periodic structures using evolutionary topology optimization. *Structural and Multidisciplinary Optimization*, 36(6):597–606, Nov. 2008. ISSN 1615-147X, 1615-1488. doi: 10.1007/s00158-007-0196-1. URL <http://link.springer.com/10.1007/s00158-007-0196-1>.
- F. Jarre, M. Kočvara, and J. Zowe. Optimal truss design by interior-point methods. *SIAM Journal on Optimization*, 8(4):1084–1107, Nov 1998. ISSN 1052-6234. doi: 10.1137/S1052623496297097. URL <http://link.aip.org/link/SJOPE8/v8/i4/p1084/s1&Agg=doi%5Cnpapers3://publication/doi/10.1137/S1052623496297097>.
- E. Jeandel and M. Rao. An aperiodic set of 11 wang tiles, Jun 2015. URL <http://arxiv.org/abs/1506.06492>.
- A. S. Kahr, E. F. Moore, and H. Wang. Entscheidungsproblem reduced to the $\forall\exists\forall$ case. *Proceedings of the National Academy of Sciences of the United States of America*, 48(3):365–377, 1962.
- Y. Kanno. Global optimization of trusses with constraints on number of different cross-sections: a mixed-integer second-order cone programming approach. *Computational Optimization and Applications*, 63(1):203–236, 2016. ISSN 15732894. doi: 10.1007/s10589-015-9766-0.
- J. Kari. Reversibility of 2d cellular automata is undecidable. *Physica D: Nonlinear Phenomena*, 45(1-3):379–385, 1990.
- J. Kari. A small aperiodic set of wang tiles. *Discrete Mathematics*, 160(1–3):259–264, Nov 1996. ISSN 0012365X. doi: 10.1016/0012-365X(95)00120-L. URL <http://linkinghub.elsevier.com/retrieve/pii/0012365X9500120L>.
- J. Kari. Theory of cellular automata: A survey. *Theoretical Computer Science*, 334(1–3):3–33, 2005. ISSN 03043975. doi: 10.1016/j.tcs.2004.11.021. URL www.elsevier.com/locate/tcs.
- J. Kari and P. Papasoglu. Deterministic aperiodic tile sets. *Geometric And Functional Analysis*, 9:353–369, 1999. ISSN 1016-443X. doi: 10.1007/s000390050090.
- S. Kirkpatrick, C. Gelatt Jr, and M. Vecchi. Optimization by simulated annealing. *Science*, 220(4598):671–680, May 1983. ISSN 0036-8075. doi: 10.1126/science.220.4598.671. URL <http://www.sciencemag.org/cgi/doi/10.1126/science.220.4598.671>.
- U. Kirsch. Optimal topologies of structures. *Applied Mechanics Reviews*, 42(8):223–239, 1989. ISSN 00036900. doi: 10.1115/1.3152429.
- D. E. Knuth. The art of computer programming. vol. 1: Fundamental algorithms. addison-wesley. Reading, Mass, 1968.
- M. Kočvara and J. V. Outrata. Effective reformulations of the truss topology design problem. *Optimization and Engineering*, 7(2):201–219, June 2006. ISSN 1389-4420, 1573-2924. doi: 10.1007/s11081-006-6839-z. URL <http://link.springer.com/10.1007/s11081-006-6839-z>.

- M. Kočvara and J. Zowe. *How mathematics can help in design of mechanical structures*, pages 76–93. D.F. Griffiths and G.A. Watson, eds., Longman, 1996.
- A. Lagae. Tile-based methods in computer graphics. *Ph.D. Thesis, Department of Computer Science, KU Leuven*, 2007. URL http://www.cs.kuleuven.be/publicaties/doctoraten/cw/CW2007_08.abs.html.
- A. Lagae and P. Dutré. An alternative for Wang tiles: Colored edges versus colored corners. *ACM Transactions on Graphics*, 25:1442–1459, 2006. ISSN 0730-0301. doi: 10.1145/1183287.1183296.
- A. Lagae, J. Kari, and P. Dutré. Aperiodic sets of square tiles with colored corners. *Report CW*, 2006. URL <http://graphics.cs.kuleuven.be/publications/LKD06ASSTCC/LKD06ASSTCC.pdf>.
- M. S. Lobo, L. Vandenberghe, S. Boyd, and H. Lebret. Applications of second-order cone programming. *Linear Algebra and its Applications*, 284(1–3):193–228, 1998. ISSN 00243795. doi: 10.1016/S0024-3795(98)10032-0. URL <http://www-isl.stanford.edu/people/>.
- J. Löfberg. Yalmip : a toolbox for modeling and optimization in matlab. In *2004 IEEE International Conference on Robotics and Automation (IEEE Cat. No.04CH37508)*, pages 284–289, Sept 2004. doi: 10.1109/CACSD.2004.1393890.
- D. Logan. *A first course in the finite element method*. Springer International Publishing, 2012. ISBN 9780495668251.
- A. Makrodimopoulos, A. Bhaskar, and A. J. Keane. Second-order cone programming formulations for a class of problems in structural optimization. *Structural and Multidisciplinary Optimization*, 40(1–6):365–380, Jan 2010. ISSN 1615147X. doi: 10.1007/s00158-009-0376-2. URL <http://link.springer.com/10.1007/s00158-009-0376-2>.
- R. J. Melosh. Basis for derivation of matrices for the direct stiffness method. *AIAA Journal*, 1(7):1631–1637, Jul 1963. ISSN 0001-1452. doi: 10.2514/3.1869. URL <http://arc.aiaa.org/doi/10.2514/3.1869>.
- A. G. M. Michell. LVIII. The limits of economy of material in frame-structures. *The London, Edinburgh, and Dublin Philosophical Magazine and Journal of Science*, 8(47):589–597, 1904. URL <http://www.tandfonline.com/doi/pdf/10.1080/14786440409463229>.
- J. H. Mikkola. Managing modularity of product architectures – toward an integrated theory. *204 IEEE TRANSACTIONS ON ENGINEERING MANAGEMENT*, VOL. 50 (2):204–218, May 2003. ISSN 0018-9391. doi: 10.1109/TEM.2003.810826. URL <http://ieeexplore.ieee.org/lpdocs/epic03/wrapper.htm?arnumber=1202983>.
- B. L. Miller and D. E. Goldberg. Genetic algorithms, tournament selection, and the effects of noise. *Complex Systems*, 9:193–212, 1995. ISSN 0891-2513. doi: 10.1.1.30.6625.
- J. Novák, A. Kučerová, and J. Zeman. Compressing random microstructures via stochastic wang tilings. *Physical Review E – Statistical, Nonlinear, and Soft Matter Physics*, 86(4): 4–7, 2012. ISSN 15393755. doi: 10.1103/PhysRevE.86.040104.

- M. Ohsaki. *Optimization of Finite Dimensional Structures*, volume 1. Cambridge University Press, Dec 2011. ISBN 9788578110796. URL <http://ebooks.cambridge.org/ref/id/CB09781107415324A009>.
- M. Ohsaki, K. Fujisawa, N. Katoh, and Y. Kanno. Semi-definite programming for topology optimization of trusses under multiple eigenvalue constraints. *Computer Methods in Applied Mechanics and Engineering*, 180(1–2):203–217, 1999. ISSN 00457825. doi: 10.1016/S0045-7825(99)00056-0.
- M. Osanov and J. K. Guest. Topology optimization for architected materials design. *Annual Review of Materials Research*, 46(1):211–233, July 2016. doi: 10.1146/annurev-matsci-070115-031826.
- A. Pospíšilová and M. Lepš. *Parallel Branch and Bound Method for Size Optimization Benchmarks*, page 1–16. Civil-Comp Press, 2013. doi: 10.4203/ccp.101.20. URL <http://www.ctresources.info/ccp/paper.html?id=7299>.
- W. Prager. A note on discretized Michell structures. *Computer Methods in Applied Mechanics and Engineering*, 3(3):349–355, 1974. ISSN 00457825. doi: 10.1016/0045-7825(74)90019-X.
- A. Radman, X. Huang, and Y. M. Xie. Topology optimization of functionally graded cellular materials. *Journal of Materials Science*, 48(4):1503–1510, 2012. doi: 10.1007/s10853-012-6905-1.
- J. N. Reddy. *Energy principles and variational methods in applied mechanics*. J. Wiley, New York, 2nd edition, 2002. ISBN 047117985X.
- R. Robinson. Seven polygons which permit only nonperiodic tilings of the plane. *Notices Amer. Math. Soc*, 14:835, 1967.
- R. M. Robinson. Undecidability and nonperiodicity for tilings of the plane. *Inventiones Mathematicae*, 12(3):177–209, 1971. ISSN 00209910. doi: 10.1007/BF01418780.
- R. Rockafellar. *Convex Analysis*. Princeton landmarks in mathematics and physics. Princeton University Press, 1997. ISBN 9780691015866. URL <https://books.google.nl/books?id=1Ti0ka9bx3sC>.
- N. Rozvany, I. George, T. Sokół, and V. Pomezanski. Fundamentals of exact multi-load topology optimization – stress-based least-volume trusses (generalized Michell structures) – Part I: Plastic design. *Structural and Multidisciplinary Optimization*, 50(6):1051–1078, Dec. 2014. ISSN 1615-147X, 1615-1488. doi: 10.1007/s00158-014-1118-7. URL <http://link.springer.com/10.1007/s00158-014-1118-7>.
- P. Salamon, P. Sibani, and R. Frost. *Facts, Conjectures, and Improvements for Simulated Annealing*. Society for Industrial and Applied Mathematics, 2002. doi: 10.1137/1.9780898718300. URL <http://epubs.siam.org/doi/abs/10.1137/1.9780898718300>.
- C. Schumacher, B. Bickel, J. Rys, S. Marschner, C. Daraio, and M. Gross. Microstructures to control elasticity in 3D printing. *ACM Trans. Graph.*, 34(4):136:1–136:13, 2015. doi: 10.1145/2766926.

- F. Schury, M. Stingl, and F. Wein. Efficient two-scale optimization of manufacturable graded structures. *SIAM Journal on Scientific Computing*, 34(6):B711–B733, 2012. doi: 10.1137/110850335.
- N. C. Seeman and A. M. Belcher. Emulating biology: building nanostructures from the bottom up. *Proceedings of the National Academy of Sciences of the United States of America*, 99 Suppl 2(90002):6451–5, 2002. ISSN 0027-8424. doi: 10.1073/pnas.221458298. URL http://www.pnas.org/content/99/suppl_2/6451.short.
- J. Shade, M. F. Cohen, and D. P. Mitchell. *Tiling Layered Depth Images*, pages 231–242. Tech. Rep., University of Washington, Department of Computer Science and Engineering, 2000.
- C. Y. Sheu and S. J. L. A. Minimum weight design of elastic redundant trusses under multiple static loading conditions. *AIAA Journal*, 10(2):155–162, 1972. ISSN 00011452. doi: doi:10.2514/6.1971-362.
- O. Sigmund. *Some Inverse Problems in Topology Design of Materials and Mechanisms*, pages 277–284. Springer Netherlands, 1996. doi: 10.1007/978-94-009-0153-7_35. URL http://www.springerlink.com/index/10.1007/978-94-009-0153-7_35.
- H. Spencer. *The Principles of Biology*. Spencer, Herbert: A system of synthetic philosophy. Williams and Norgate, 1864.
- J. Stam. Aperiodic texture mapping, Technical Report, No. R046. *European Research Consortium for Informatics and Mathematics*, 1997.
- M. Stolpe. Truss optimization with discrete design variables: a critical review. *Structural and Multidisciplinary Optimization*, 53(2):349–374, Feb 2016. ISSN 16151488. doi: 10.1007/s00158-015-1333-x. URL <http://link.springer.com/10.1007/s00158-015-1333-x>.
- L. L. Stromberg, A. Beghini, W. F. Baker, and G. H. Paulino. Application of layout and topology optimization using pattern gradation for the conceptual design of buildings. *Structural and Multidisciplinary Optimization*, 43(2):165–180, 2010. doi: 10.1007/s00158-010-0563-1.
- K. Svanberg. On local and global minima in structural optimization. Technical report, DTIC Document, 1981.
- G. Sved. The minimum weight of certain redundant structures. *Australian J. Appl. Sci.*, 5: 1–9, 1954.
- G. Syswerda. Uniform Crossover in Genetic Algorithms. In D. J. Schaffer, editor, *Proceedings of the Third International Conference on Genetic Algorithms*, pages 2–9, San Mateo, California, 1989. Morgan Kaufmann Publishers, Inc.
- B. A. Szabo and G. C. Lee. Derivation of stiffness matrices for problems in plane elasticity by galerkin’s method. *International Journal for Numerical Methods in Engineering*, 1(3):301–310, Jul 1969. ISSN 10970207. doi: 10.1002/nme.1620010308. URL <http://doi.wiley.com/10.1002/nme.1620010308>.
- A. Tugilimana, R. F. Coelho, and A. P. Thrall. Structural optimization of standardized trusses by dynamic grouping of modules. *World Congress on Structural and Multidisciplinary Optimization*, 2015. URL http://web.aeromech.usyd.edu.au/WCSM02015/papers/1071_paper.pdf.

- A. Tugilimana, A. P. Thrall, B. Descamps, and R. F. Coelho. Spatial orientation and topology optimization of modular trusses. *Structural and Multidisciplinary Optimization*, pages 1–18, 2016. doi: 10.1007/s00158-016-1501-7.
- A. M. Turing. On computable numbers, with an application to the entscheidungsproblem. *J. of Math*, 58(345-363):5, 1936.
- M. J. Turner, R. W. Clough, H. C. Martin, and L. J. Topp. Stiffness and deflection analysis of complex structures. *Journal Of The Aeronautical Sciences*, 23(9):805–854, Sep 1956. ISSN 1936-9956. doi: 10.2514/8.3664. URL <http://arc.aiaa.org/doi/10.2514/8.3664>.
- L. Vandenberghe and S. Boyd. Semidefinite programming. *SIAM Review*, 38(1):49–95, 1996. ISSN 0036-1445. doi: 10.1137/1038003. URL <http://epubs.siam.org/doi/abs/10.1137/1038003>.
- H. Wang. Proving theorems by pattern recognition—II. *Bell system technical journal*, 40(1): 1–41, 1961. URL <http://onlinelibrary.wiley.com/doi/10.1002/j.1538-7305.1961.tb03975.x/abstract>.
- H. Wang. Dominoes and the aea case of the decision problem. In *In Proceedings of the Symposium on Mathematical Theory of Automata (New*, pages 23–55, 1962.
- H. Wang. Games, logic and computers. *Scientific American*, 213(5):98–106, 1965. ISSN 0036-8733. doi: 10.1038/scientificamerican1165-98.
- H. Wang. Notes on a class of tiling problems. *Fundamenta Mathematicæ*, 82:295–305, 1975.
- H. Wang. Computer theorem proving and artificial intelligence. In W. W. Bledsoe and D. W. Loveland, editors, *Contemporary Mathematics: Automated Theorem Proving – After 25 Years*, pages 49–71. American Mathematical Society, Providence, RI, 1984.
- Wikimedia Commons. GJV at a magnification of 100:1, 2009. URL https://commons.wikimedia.org/wiki/File:GJV_100e_01_ies.jpg. Accessed: 2016-12-18.
- E. L. Wilson and R. E. Nickell. Application of the finite element method to heat conduction analysis. *Nuclear Engineering and Design*, 4(3):276–286, 1966. ISSN 00295493. doi: 10.1016/0029-5493(66)90051-3. URL <http://www.sciencedirect.com/science/article/pii/0029549366900513>.
- E. Winfree, F. Liu, L. A. Wenzler, and N. C. Seeman. Design and self-assembly of two-dimensional dna crystals. *Nature*, 394(6693):539–544, 1998. ISSN 0028-0836. doi: 10.1038/28998. URL <http://dx.doi.org/10.1038/28998>.
- L. Xia and P. Breitkopf. Recent advances on topology optimization of multiscale nonlinear structures. *Archives of Computational Methods in Engineering*, pages 1–23, 2016. doi: 10.1007/s11831-016-9170-7.
- M. Yamashita, K. Fujisawa, and M. Kojima. Implementation and evaluation of SDPA 6.0 (semidefinite programming algorithm 6.0). *Optimization Methods and Software*, 18(4): 491–505, 2003.
- J. I. Yellott. Spectral analysis of spatial sampling by photoreceptors: Topological disorder prevents aliasing. *Vision Research*, 22(9):1205–1210, 1982. ISSN 00426989. doi: 10.1016/0042-6989(82)90086-4.

- M. Zawidzki and K. Nishinari. Modular truss-z system for self-supporting skeletal free-form pedestrian networks. *Advances in Engineering Software*, 47(1):147–159, May 2012. ISSN 09659978. doi: 10.1016/j.advengsoft.2011.12.012. URL <http://linkinghub.elsevier.com/retrieve/pii/S0965997812000026>.
- W. H. Zhang and S. P. Sun. Scale-related topology optimization of cellular materials and structures. *International Journal for Numerical Methods in Engineering*, 68(9):993–1011, Nov 2006. ISSN 00295981. doi: 10.1002/nme.1743. URL <http://doi.wiley.com/10.1002/nme.1743>.
- O. C. Zienkiewicz, R. L. Taylor, and J. Z. Zhu. *The finite element method*. Elsevier Butterworth-Heinemann, Amsterdam, 6th ed. edition, 2005. ISBN 0750663200.
- O. C. Zienkiewicz, R. L. Taylor, and D. D. Fox. *The finite element method for solid & structural mechanics*. Elsevier/Butterworth-Heinemann, Amsterdam, 7th edition, 2014. ISBN 9780080951362.
- A. Öchsner. *Computational Statics and Dynamics: An Introduction Based on the Finite Element Method*. Springer, 2016. ISBN 978-981-10-0733-0.
- V. Černý. Thermodynamical approach to the traveling salesman problem: An efficient simulation algorithm. *Journal of Optimization Theory and Applications*, 45(1):41–51, 1985. ISSN 00223239. doi: 10.1007/BF00940812.
- K. Čulík. An aperiodic set of 13 wang tiles. *Discrete Mathematics*, 160(1–3):245–251, Nov 1996. ISSN 0012365X. doi: 10.1016/S0012-365X(96)00118-5. URL <http://linkinghub.elsevier.com/retrieve/pii/S0012365X96001185>.
- K. Čulík and J. Kari. *On Aperiodic Sets of Wang Tiles*, pages 153–162. Springer-Verlag, London, UK, UK, 1997. ISBN 3-540-63746-X. URL <http://dl.acm.org/citation.cfm?id=646007.673899>.